NRL Report 6729

Topics in Electron Scattering and Nuclear Models

Notes on lectures given at NRL in the Fall of 1966

H. ÜBERALL

Department of Physics
The Catholic University of America
(Consultant to NRL Linac Branch
Nuclear Physics Division)

July 31, 1968

NAVAL RESEARCH LABORATORY
Washington, D.C.

This document has been approved for public release and sale; its distribution is unlimited.

CONTENTS

Foreword	ii
Abstract	iii
Problem Status	iii
Authorization	iii
GENERAL INTRODUCTION	1
Kinematics of Photoexcitation and Electron Scattering	1
Calculation of Cross Sections in Born Approximation	5
Form Factors in Elastic Electron Scattering	16
Quasielastic Scattering	17
EXCITATION OF LEVELS BELOW THE GIANT RESONANCE	20
Nondynamic Analysis	20
Dynamic Analysis	24
THE GOLDHABER-TELLER AND STEINWEDEL-JENSEN MODELS FOR THE GIANT RESONANCE	28
The Goldhaber-Teller Model	34
The Steinwedel-Jensen Model	44
The Steinwedel-Jensen Model for a Deformed Nucleus	49
COUPLING OF GIANT RESONANCE AND SURFACE VIBRATIONS	52
PARTICLE-HOLE MODEL OF THE GIANT RESONANCES	55
PHENOMENOLOGICAL MODELS	61
Helm's Model and its Generalization	63
Tassie's Model	68
CONCLUSION	71
REFERENCES	71

FOREWORD

The following material was presented in a series of lectures to the staff of the NRL Linac Branch, Nuclear Physics Division, in the Fall Semester of 1966/1967. I thank Dr. T. F. Godlove, Head, Linac Branch and Dr. L. W. Fagg, Head, Electron Interactions Section, for inviting me to hold these lectures as an aid to the experimental work on electron scattering and photonuclear reactions which is presently being carried out at the NRL 60-MeV electron linac.

ABSTRACT

We present a review of the basic theory of electron scattering from nuclei and of photonuclear processes, as well as a discussion of the analysis of electron scattering experiments. This includes cross sections in Born approximation, elastic scattering from nuclei for the study of nuclear moments, and continuum scattering. Particular attention is given to inelastic electron scattering with excitation of nuclear levels, both below and in the giant resonance region. Various theoretical models are discussed that describe excitations of nuclear states.

PROBLEM STATUS

This is an interim report on a continuing problem.

AUTHORIZATION

NRL Problem H01-09
Project RR 002-06-41-5005

Manuscript submitted April 3, 1968.

TOPICS IN ELECTRON SCATTERING AND NUCLEAR MODELS: NOTES ON LECTURES GIVEN AT NRL IN THE FALL OF 1966

GENERAL INTRODUCTION

Kinematics of Photoexcitation and Electron Scattering

Electron scattering is only recently proving itself an important tool for the study of nuclear structure, both for exploring ground state properties, and for excitation of nuclear levels. The main advantage consists in the possibility of varying the momentum transfer q, and thus obtaining nuclear form factors as functions of q. This contrasts with photoexcitation in which the momentum transfer is fixed. In the following introductory discussion we shall consider the kinematics of both reactions.

Photoexcitation — The absorption of an incident photon by a nucleus lifts the nucleus from its ground state to an excited state,

$$\gamma + A_Z \rightarrow A_Z^* , \tag{1a}$$

where the excited state has excitation energy ω if the center-of-mass (CM) energy of the photon is equal to ω. The excited nucleus A^* will decay with the emission of a photon or a particle,

$$A_Z^* \rightarrow A_Z' + \gamma \tag{1b}$$

or

$$A_Z^* \rightarrow (A-1)_Z' + N , \tag{1c}$$

depending on the respective thresholds, etc. Considering only the excitation part of the process, we have

$$\text{momentum conservation:} \quad \mathbf{k} = \mathbf{q} \tag{2a}$$

where $\mathbf{k}$ = photon momentum, $\mathbf{q}$ = nuclear recoil momentum and (using units with $c = 1$)

$$\text{energy conservation:} \quad k = \omega \tag{2b}$$

(the nucleus is assumed heavy). This shows that the recoil q is fixed and equal to

$$q = \omega . \tag{3}$$

Thus, photoexcitation will measure for factors of excited states at one value of q only.

Electron Scattering — Elastic or inelastic electron scattering imparts a recoil momentum $\mathbf{q}$ to the nucleus, in the latter case also raising the nucleus to an excited state (of energy ω):

$$A_Z + e \rightarrow A_Z^* + e' . \tag{4a}$$

The excited nucleus will subsequently decay:

$$A_Z^* \rightarrow A_Z' + \gamma \tag{4b}$$

or

$$A_Z^* \rightarrow (A-1)_Z' + N, \tag{4c}$$

etc. The electron scattering angle will be called θ. The rest mass of the electrons, assumed to have an energy of more than several MeV, shall be neglected; i.e., we assume for their energy

$$E = (k^2 + m_e^2)^{1/2} \approx k \tag{5}$$

The kinematics, sketched below (calling $\boldsymbol{k}_1$ the momentum of the incident electron and $\boldsymbol{k}_2$ the momentum of the scattered electron),

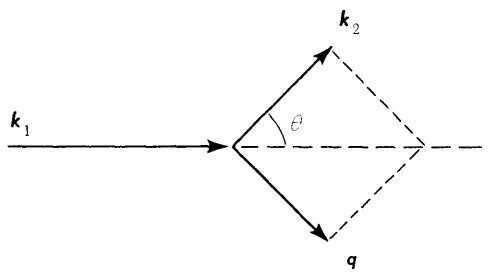

leads to

$$\text{momentum conservation:} \quad \boldsymbol{k}_1 = \boldsymbol{q} + \boldsymbol{k}_2 \tag{6a}$$

and

$$\text{energy conservation:} \quad k_1 = \omega + k_2 . \tag{6b}$$

Experimentally, one may use a fixed incident energy k_1 and may change θ, but for each given θ obtain one energy spectrum (as a function of k_2) of the scattered electrons. Instead of θ and k_2, one may introduce the variables

$$\omega = k_1 - k_2 \tag{7a}$$

and

$$q = (k_1^2 + k_2^2 - 2k_1 k_2 \cos \theta)^{1/2} , \tag{7b}$$

in terms of which the theoretical results usually are given. For forward scattering ($\theta = 0°$) one has $q = k_1 - k_2 = \omega$ as in photoexcitation. For 180° scattering, a geometry used in the NRL linac experiments, one has $q = k_1 + k_2 = 2k_1 - \omega$, which for a given level ω can be varied by varying the incident energy k_1, and which can be made quite large. For example, with the 60-MeV NRL linac, the excitation of nuclear giant resonances ($\omega \approx 20$ MeV) can be explored up to $q \approx 100$ MeV/c.

In any scattering problem, a characteristic quantity is qR, where R is the dimension of the scattering object; for $qR \approx 1$, diffraction effects will appear. Taking the radius of the ^{16}O nucleus, $R \approx 3$ fm (1 fermi = 10^{-13} cm), as an example, Table 1 shows that this value of qR can easily be reached with the 60-MeV NRL linac. It also demonstrates that the usual replacement of the retardation factors $\exp(i\,\boldsymbol{q}\cdot\boldsymbol{r})$ or $j_L(qr)$ in the multipole matrix elements by 1 or $(qr)^L/(2L+1)!!$, respectively, which is fairly well justified for photoabsorption ($\omega R \approx 0.30$ in the same example), cannot be made in electron scattering.

Figure 1 gives a sketch of the general features of a photoexcitation curve σ_γ as a function of q, and of spectra of scattered electrons as functions of q and ω. The figure illustrates that electron scattering can explore a two-dimensional surface of the cross section, whereas the photoabsorption cross section σ_γ is confined to the one particular curve on this surface determined by $q = \omega$. The electron scattering cross section,

Table 1
Values of qR for Different Incident Energies k_1 in 180° Electron Scattering from ^{16}O Giant Resonance States

k_1 (MeV)	q (MeV/c)	q (fm^{-1})	qR
40	60	0.30	0.90
60	100	0.50	1.50

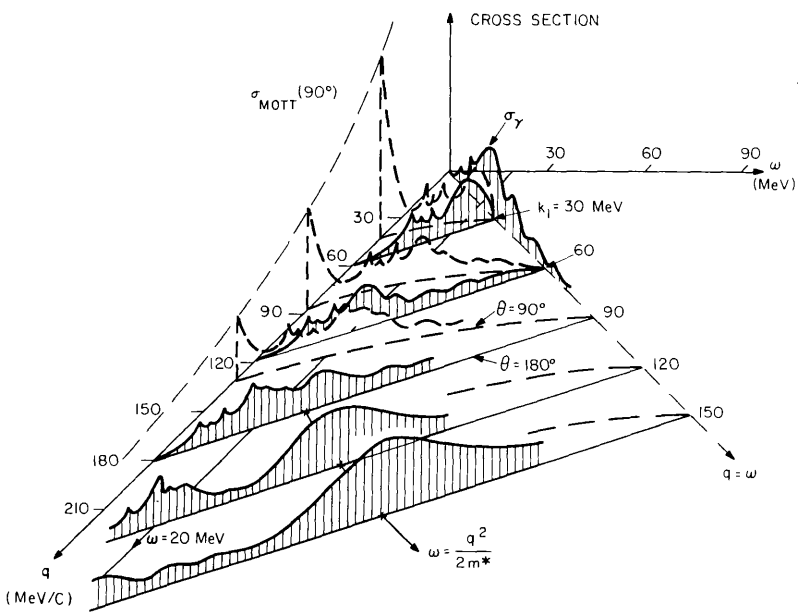

Fig. 1 - Three-dimensional plot of spectra of inelastically scattered electrons, as functions of excitation energy ω (right scale) and of momentum transfer q (forward scale). The electron spectra are drawn as solid, shaded curves above the lines θ = const = 180° in the (ω, q) plane, where $q = 2k_1 - \omega$ (k_1 = incident electron energy), and as dashed curves above the lines θ = const = 90° in the (ω, q) plane. Also indicated as traces in the (ω, q) plane are the lines ω = 20 MeV (peak of the giant resonance), and $\omega = q^2/2m^*$ (peak of the quasielastic scattering), where m^* is the effective nucleon mass inside nuclear matter. The following features are indicated: (a) disappearance of the large Mott elastic scattering cross section as θ goes from 90° to 180° (valid for spinless nuclei), (b) changes in the giant resonance region (emergence of spin-isospin collection levels, decline of isospin levels with increasing q), and (c) emergence of the quasielastic peak for increasing q. Also shown is the photonuclear cross section σ_γ above its trace $q = \omega$ in the (ω, q) plane, indicating the giant resonance. The figure presents the relation between the ways photonuclear excitation curves (measured at $q = \omega$) and scattered electron spectra (measured at k_1 = const and θ = const) are obtained as particular cross sections of the three-dimensional "nuclear excitation strength surface."

differential in q and ω, is plotted over several curves $q = q(\omega, \theta)$ in the (ω, q) plane for $\theta = 90°$ (dashed lines) and $\theta = 180°$ (solid lines), i.e., for $q = [k_1^2 + (k_1 - \omega)^2]^{1/2}$ and $q = 2k_1 - \omega$, respectively, which intersect each other at the photon line $q = \omega$, i.e., at $k_1 = \omega$ and $k_2 = 0$. The various curves correspond to different values of the incident energy k_1, taken as a parameter whose values are shown on the right. Figure 1 emphasizes the following characteristics of the features:

1. The Mott cross section for elastic scattering,

$$\sigma_m = 4k_1^2 \alpha^2 q^{-4} \cos^2 \frac{\theta}{2} \tag{8}$$

with $q = 2k_1 \sin(\theta/2)$ and $\alpha = 1/137$, is nonzero at $\omega = 0$ for $\theta = 90°$, but zero (apart from some small magnetic scattering if the nucleus has spin) for $\theta = 180°$.

2. There are several broad (particle unstable) giant resonance peaks around $\omega \approx 20$ MeV which can be seen both in photoexcitation and in electron scattering, and which change shape as k_1 varies. Note that this change of shape cannot be observed in photoexcitation, since here, only one fixed curve is obtained.

3. Below the giant resonance region, $\omega \approx 20$ MeV, there are excitations of individual levels which are narrow when lying below the particle emission threshold.

4. For higher incident energies, a broad peak appears above the giant resonance region which shifts higher according to

$$\omega = \frac{q^2}{2m^*}, \tag{9a}$$

where m^* is the effective mass (roughly $m/2$, m = proton mass) of the nucleon inside the nuclear matter. This peak is known as the quasielastic peak, and corresponds to the process of knocking off an individual nucleon out of the nucleus (see sketch);

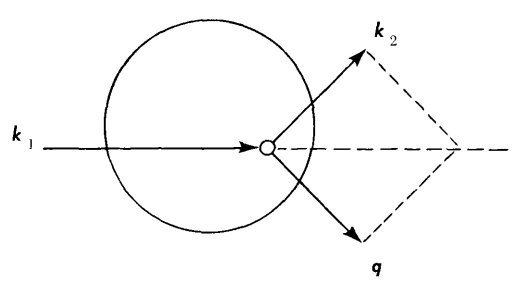

The curves are drawn in Fig. 1 in a way in which the scattered electron spectra are usually presented. One can however also plot the spectra vs ω for fixed q, which can be achieved by varying θ and/or k_1 as we go along the excitation energy ω, using

$$q = \left[k_1^2 + (k_1 - \omega)^2 - 2k_1(k_1 - \omega) \cos \theta\right]^{1/2}, \tag{9b}$$

which for $\theta = 180°$ gives, as before,

$$q = 2k_1 - \omega. \tag{9c}$$

Alternatively, one can plot the cross section of a given level (fixed ω) vs θ for fixed q, by varying the energy k_1 accordingly. Such a procedure has been used to separate longitudinal and transverse contributions to the form factors, as will be seen.

Calculation of Cross Sections in Born Approximation

The calculation of cross sections using the Born approximation is presented in several places in the literature (1-3), and the results are quoted in review articles on the subject (3-6). We shall therefore not repeat the derivation in detail but shall state the important points. The electron, due to its Coulomb field and to the virtual photon field that surrounds it, interacts with the following nuclear quantities: (a) the nuclear (ground state or transition) charge density $e\rho(\mathbf{r})$, where

$$\rho(\mathbf{r}) = \int d^3r_1 \ldots d^3r_A \psi^\dagger \sum_{i=1}^{A} \frac{1+\tau_3^{(i)}}{2} \delta(\mathbf{r}-\mathbf{r}_i)\, \psi_0 , \tag{10a}$$

(b) the nuclear current density $e\mathbf{j}(\mathbf{r})$, where

$$\mathbf{j}(\mathbf{r}) = \frac{1}{m} \int d^3r_1 \ldots d^3r_A \psi^\dagger \sum_{i=1}^{A} \frac{1+\tau_3^{(i)}}{2} \delta(\mathbf{r}-\mathbf{r}_i)\, \mathbf{p}_i\, \psi_0 \tag{10b}$$

(these two quantities being related by

$$\nabla \cdot \mathbf{j} + \dot{\rho} = 0, \tag{10c}$$

the continuity equation), and finally (c) the nuclear magnetization density $e\boldsymbol{\mu}(\mathbf{r})$, where

$$\boldsymbol{\mu}(\mathbf{r}) = \frac{1}{2m} \int d^3r_1 \ldots d^3r_A \psi^\dagger \sum_{i=1}^{A} \delta(\mathbf{r}-\mathbf{r}_i) \left(\mu_p \frac{1+\tau_3^{(i)}}{2} + \mu_n \frac{1-\tau_3^{(i)}}{2} \right) \boldsymbol{\sigma}^{(i)} \psi_0 , \tag{10d}$$

in which m is the nucleon mass (we use units in which $\hbar = c = 1$) and μ_p and μ_n are the proton and neutron magnetic moments, $\mu_p = 2.79$ and $\mu_n = -1.17$. The electromagnetic field (φ = scalar potential, $\mathbf{A}$ = vector potential, and $\mathbf{H} = \nabla \times \mathbf{A}$ = magnetic field) which the electron generates at the nucleus gives rise to an interaction energy

$$H_{\text{int}} = \int d^3r \left[\rho(\mathbf{r})\, \varphi(\mathbf{r}) - \mathbf{j}\cdot\mathbf{A} - \boldsymbol{\mu}\cdot\mathbf{H} \right] . \tag{11}$$

The first term is the Coulomb interaction. The last term accounts for the interaction of the spin magnetic moments, whereas the orbital magnetic moment interaction is contained in the $\mathbf{j} \cdot \mathbf{A}$ term. This point will be demonstrated a little later on.

The interaction Hamiltonian given by Eq. (11) will be used for a Born approximation calculation of the inelastic electron scattering cross section, according to the following Feynman diagram:

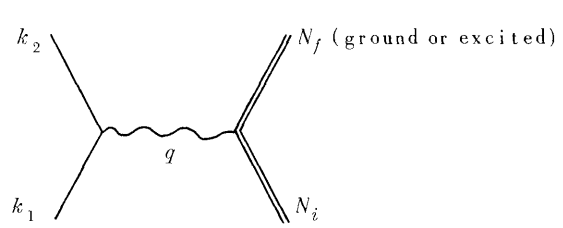

This calculation can be done noncovariantly (2,7,8) or covariantly (3), but the results are the same. Noncovariantly, one has for the electron's scalar potential, e.g.,

$$\varphi(\mathbf{r}) = \int \frac{\rho_e(\mathbf{r}')\, d^3 r'}{|\mathbf{r} - \mathbf{r}'|}\,, \tag{12a}$$

where in the electron transition charge density

$$\rho_e = \psi_f^\dagger\, \psi_i\,, \tag{12b}$$

one uses plane wave states

$$\psi_f = u_f\, e^{i\mathbf{k}_2 \cdot \mathbf{r}} \tag{12c}$$

etc. (Born approximation). The quantities $|\mathbf{r} - \mathbf{r}'|^{-1}$ and $\exp[i(\mathbf{k}_1 - \mathbf{k}_2)\cdot \mathbf{r}]$ one expands in multipoles, while the vector potential $\mathbf{A}$ is expanded in vector spherical harmonics (9).

Before going to the results, let us state what corrections should be (and are) applied to the simple Born approximation and to the experimental data when comparing the two. These are the following:

1. The Schwinger radiative corrections (10) ($\propto \alpha$ effects). The scattered electrons emit many soft photons, all undetected and causing an energy loss of the scattered electron within the experimental resolution. To the following diagrams,

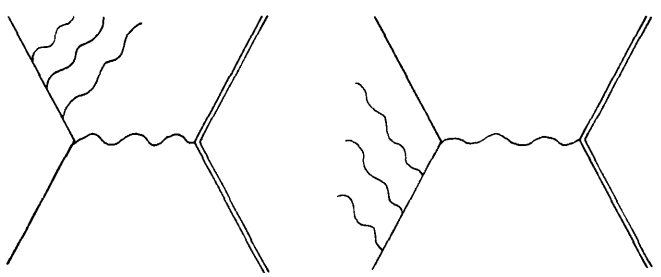

etc.,

one has to add those of virtual photons, i.e., vertex renormalization,

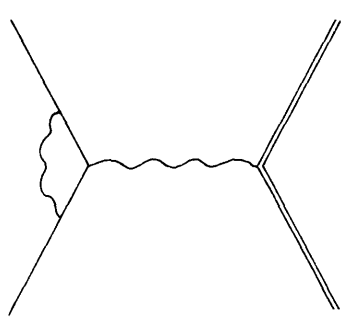

of mass renormalization,

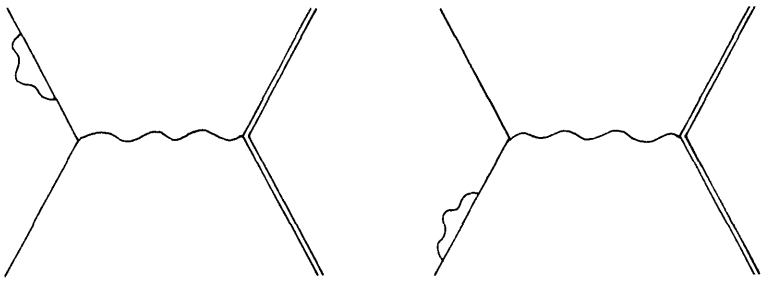

and of vacuum polarization,

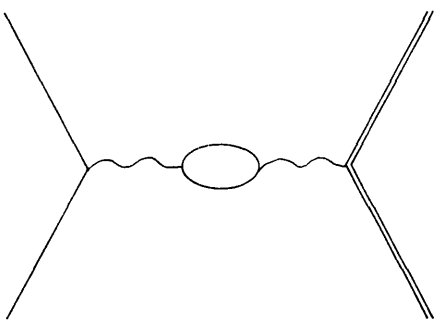

to cancel out the Bloch-Nordsieck infrared divergence inherent in the emission of the soft real photons. The effect of all these processes is to lower and widen the peaks. The necessary corrections to be applied to the measured data were obtained by Tsai (5,11,12). They may lead to considerable corrections of the measured spectrum.

2. The radiative tail (bremsstrahlung tail) ($\propto \alpha$ effects). Real photons are emitted by the electron, either before or after the collision with the nucleus, either while passing the

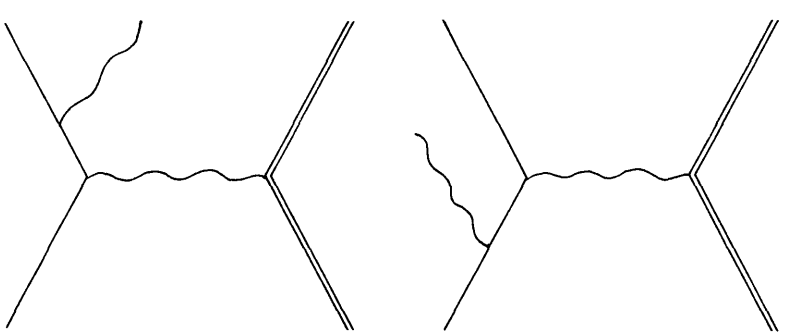

same nucleus on which the electron scatters or while passing another nucleus in the target. A considerable amount of energy may be lost. Another effect included under the heading "radiative tail" is Möller scattering of the electron by an atomic electron, again either before or after the collision with the nucleus. Because of the indistinguishability of the two electrons, the one detected may actually be the recoiling spectator electron.

Finally, straggling losses of the electrons (ionizing collisions) may also play a role. The result of all these effects is to observe in the scattered electron spectrum a broad tail stretching from the elastic peak downward (Fig. 2); this tail actually increases toward very low energies, for two reasons: (a) electrons which emit the photon before they scatter, scatter at a lower energy for which the scattering cross section ($\propto 1/E^2$) is larger, and (b) the spectator electron in Möller scattering (which is symmetric between the incident and the spectator electron) is observed. Each inelastic peak will also have its own radiation tail. The inelastic peaks one wants to study are observed to sit on top of this radiative background, and one has to subtract the latter. The procedure is described in several papers (12-15). Calculations of the bremsstrahlung tail are given by Hand (16), by Ginsberg and Pratt (17), and by Maximon and Isabelle (18), the latter including radiative tails of inelastic peaks.

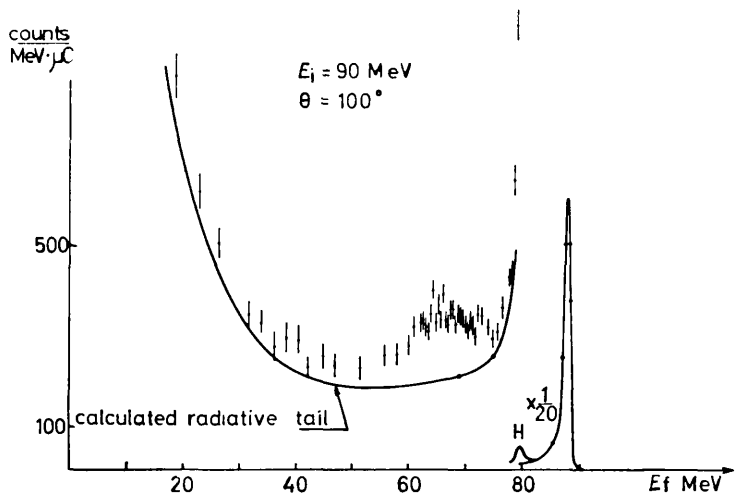

Fig. 2 - Spectrum of electrons inelastically scattered by a water target for $k_1 \equiv E_i$ = 90 MeV and θ = 100°. (The peak labeled H corresponds to elastic scattering on hydrogen.) The outgoing electron energy is $k_2 \equiv E_f$. The calculated radiative tail of the elastic peak for scattering from oxygen (the latter multiplied by 1/20) is shown. (After Isabelle and Bishop (13).)

3. Going beyond the first Born approximations ($\propto Z\alpha$ effects). Only light nuclei (below Ca) can honestly be treated with the Born approximation. For heavier nuclei one must go beyond the first Born approximation, which can be done in two ways. The first way is by phase shift analysis of elastic as well as inelastic scattering. (The initial and final electrons are treated as nonplane waves, distorted by the Coulomb field.) For the latter case, this was done by Biedenharn et al. (19) and by Drechsel (20). The effect of such a calculation is to fill in the diffraction zeros of the Born approximation (Fig. 3) for the cross section plotted vs θ or vs q^2. This figure also shows that beyond the first Born approximation, a difference in the scattering of electrons and of positrons will appear: the lowest order diagram

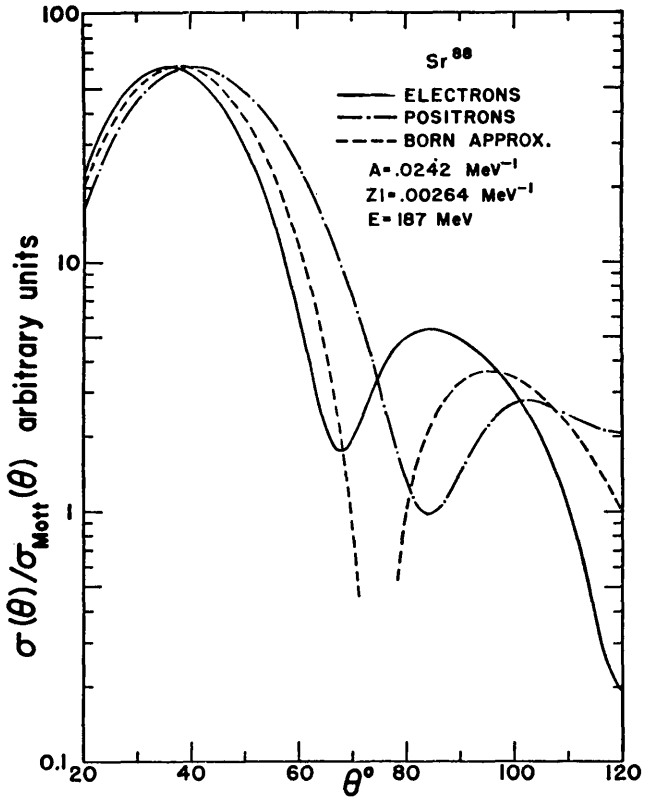

Fig. 3 - Relative cross sections for 187-MeV electrons and positrons scattered from ^{88}Sr with an E2 excitation, compared with the corresponding Born approximation. (After Onley, Reynolds, and Wright (19).)

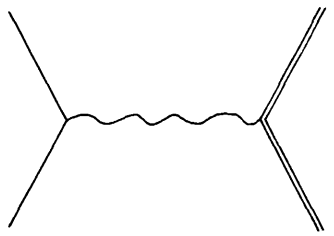

e^+, e^-

is the same for e^+ or e^-, while higher order diagrams such as the following are not.

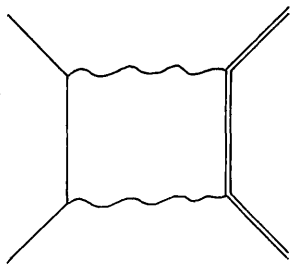

The second way heavier nuclei can be treated is by higher Born approximations. The diagram immediately above refers to this. It also permits the inclusion of dispersion effects (21), i.e., excitation of the intermediate nuclear states:

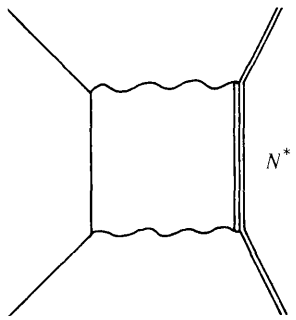

Dispersion effects, for elastic electron scattering, will again deepen the diffraction minima (which had been filled in by non-Born effects) by approximately 10% of the value of the cross section at the minimum.

After this discussion of corrections to be applied, we list the formulas for the cross section of inelastic electron scattering in the Born approximation, with the nucleus making a transition from the ground state of spin J_0 to an excited state of spin J. This includes the elastic scattering also. In the notation borrowed from Lewis and Walecka (22):

$$\frac{d\sigma}{d\Omega} = \frac{k_2}{k_1}\frac{8\pi\alpha^2}{\Delta^4}\left\{V_l(\theta)\sum_{L=0}^{\infty}|F_L^{J_0 J}(q)|^2 + V_t(\theta)\sum_{L=1}^{\infty}\left[|T_L^{eJ_0 J}(q)|^2 + |T_L^{mJ_0 J}(q)|^2\right]\right\}, \tag{13a}$$

in which

$$F_L^{J_0 J}(q) = \hat{J}_0^{-1} \langle J \| M_L(q) \| J_0 \rangle, \tag{13b}$$

$$T_L^{eJ_0 J}(q) = \hat{J}_0^{-1} \langle J \| T_L^e(q) \| J_0 \rangle, \tag{13c}$$

and

$$T_L^{mJ_0 J}(q) = \hat{J}_0^{-1} \langle J \| T_L^m(q) \| J_0 \rangle. \tag{13d}$$

Here, $\alpha = 1/137$ is the fine structure constant; the four-momentum transfer squared is $\Delta^2 = q^2 - \omega^2$; further notation is $\hat{J}_0 = (2J_0 + 1)^{1/2}$. There appear two kinematic factors V_l and V_t (longitudinal and transverse), given by

$$V_l(\theta) = (\Delta^4/q^4)\ 2k_1k_2 \cos^2\frac{\theta}{2} \tag{14a}$$

and

$$V_t(\theta) = \frac{2k_1k_2}{q^2}\sin^2\frac{\theta}{2}\left[(k_1+k_2)^2 - 2k_1k_2\cos^2\frac{\theta}{2}\right]. \tag{14b}$$

They multiply the dynamical quantities called form factors, $F_L^{J_0 J}$ (Coulomb or longitudinal), $T_L^{eJ_0 J}$ (transverse electric) and $T_L^{mJ_0 J}$ (transverse magnetic), which are expressed as the reduced (double-barred) matrix elements of corresponding operators M_L and $T_L^{e,m}$ in Eqs. (13b) to (13d). Reduced matrix elements are defined by the Wigner-Eckart theorem in the form

$$<J_f M_f | M_{LM} | J_i M_i> = \hat{J}_f^{-1} (J_i M_i, LM | J_f M_f) \; <J_f || M_L || J_i> ; \tag{15}$$

i.e., the entire dependence on magnetic quantum numbers of the matrix element $<J_f M_f | M_{LM} | J_i M_i>$ of the spherical tensor operator M_{LM} of rank L is contained in the Clebsch-Gordan coefficient $(J_i M_i, LM | J_f M_f)$. Note that the matrix elements appear in Eq. (13a) as a multipole expansion of multipolarity L, of which only the Coulomb form factor contains a monopole ($L = 0$) (an example of which is the elastic peak), whereas the transverse matrix elements, due to the photon having spin 1, are dipole ($L = 1$) or higher. The operators M_{LM}, T^e_{LM} and T^m_{LM} are

$$M_{LM}(q) = \int d^3r \, \rho(\mathbf{r}) \, j_L(qr) \, Y_{LM}(\hat{r}) , \tag{16a}$$

where $j_L(qr)$ is the spherical Bessel function,

$$T^e_{LM}(q) = T^{ej}_{LM}(q) + T^{e\mu}_{LM}(q) , \tag{16b}$$

and

$$T^m_{LM}(q) = T^{mj}_{LM}(q) + T^{m\mu}_{LM}(q) . \tag{16c}$$

We split the transverse matrix elements into orbital contributions containing $\mathbf{j}(\mathbf{r})$ and spin contributions containing $\boldsymbol{\mu}(\mathbf{r})$:

$$T^{ej}_{LM}(q) = q^{-1} \int d^3r \, \mathbf{j}(\mathbf{r}) \cdot \nabla \times j_L(qr) \, \mathbf{Y}^M_{LL}(\hat{r}) , \tag{16d}$$

$$T^{mj}_{LM}(q) = \int d^3r \, \mathbf{j}(\mathbf{r}) \cdot j_L(qr) \, \mathbf{Y}^M_{LL}(\hat{r}) , \tag{16e}$$

$$T^{e\mu}_{LM}(q) = q \int d^3r \, \boldsymbol{\mu}(\mathbf{r}) \cdot j_L(qr) \, \mathbf{Y}^M_{LL}(\hat{r}) , \tag{16f}$$

and

$$T^{m\mu}_{LM}(q) = \int d^3r \, \boldsymbol{\mu}(\mathbf{r}) \cdot \nabla \times j_L(qr) \, \mathbf{Y}^M_{LL}(\hat{r}) . \tag{16g}$$

We use vector spherical harmonics defined by

$$\mathbf{Y}^M_{Ll}(\hat{r}) = \sum_{mm'} (lm, 1m' | LM) \, Y_{lm}(\hat{r}) \, \hat{e}_{m'} , \tag{17a}$$

with coordinate unit vectors in spherical components (23), $\hat{e}_{m'}$. Only the vector spherical harmonic with $l = L$ appears, which is sometimes written $\mathbf{X}_{LM}(\hat{r})$, and satisfies

$$\mathbf{Y}^M_{LL}(\hat{r}) = \mathbf{X}_{LM}(\hat{r}) = [L(L+1)]^{-1/2} \, \mathbf{L} Y_{LM}(\hat{r}) , \tag{17b}$$

where $\mathbf{L} = -i\mathbf{r} \times \nabla$. Note that Eqs. (13b) to (13d) for the matrix elements, like Eqs. (16) for the operators, are dimensionless.

A different notation for the differential cross section, going back to Alder et al. (2), is (24) (for the Lth multipole):

$$\frac{d\sigma}{d\Omega} = \alpha^2 \frac{q^{2L}}{k_1^2} \frac{4\pi(L+1)}{L[(2L+1)!!]^2} \left\{ \frac{L}{L+1} B(CL, q) v_l(\theta) + [B(EL, q) + B(ML, q)] v_t(\theta) \right\}, \tag{18a}$$

with kinematic factors $v_{l,t}(\theta)$ related to the previous ones by

$$V_{l,t}(\theta) = 2k_1 k_2 (1 - \cos\theta)^2 v_{l,t}(\theta) \tag{18b}$$

and with reduced matrix elements ($i = C, E, M$) defined by

$$B(iL, q) = \sum_{M_L M} \left| \langle JM | M^i_{LM_L} | J_0 M_0 \rangle \right|^2 = J_0^{-2} \left| \langle J \| M^i_L \| J_0 \rangle \right|^2, \tag{18c}$$

i.e., in terms of the operators M^i_{LM}, which are related to the ones we used before by

$$M^C_{LM} = q^{-L} (2L+1)!! \, M_{LM}, \tag{18d}$$

$$M^E_{LM} = q^{-L} \left(\frac{L}{L+1}\right)^{1/2} (2L+1)!! \, T^e_{LM}, \tag{18e}$$

and

$$M^M_{LM} = -i q^{-L} \left(\frac{L}{L+1}\right)^{1/2} (2L+1)!! \, T^m_{LM}. \tag{18f}$$

Hence, we have the connecting relations

$$B(CL, q) = q^{-2L} [(2L+1)!!]^2 \left| F_L^{J_0 J}(q) \right|^2, \tag{19a}$$

$$B(EL, q) = \frac{L}{L+1} q^{-2L} [(2L+1)!!]^2 \left| T_L^{e J_0 J}(q) \right|^2, \tag{19b}$$

and

$$B(ML, q) = \frac{L}{L+1} q^{-2L} [(2L+1)!!]^2 \left| T_2^{m J_0 J}(q) \right|^2. \tag{19c}$$

Probably the simplest notation of the differential cross section known is given in terms of the "Mott cross section of the proton";

$$\sigma_M(\theta) = \frac{\alpha^2}{4k_1^2} \frac{\cos^2 \frac{\theta}{2}}{\sin^4 \frac{\theta}{2}}. \tag{20a}$$

Using

$$\Delta^2 = q^2 - \omega^2 = 4k_1 k_2 \sin^2 \frac{\theta}{2}, \tag{20b}$$

we have that

$$\frac{d\sigma/d\Omega}{4\pi\sigma_M} = \frac{\Delta^4}{q^4} \left[F_l^2 + \frac{V_t}{V_l} F_t^2 \right], \tag{20c}$$

with

$$\frac{V_t}{V_l} = \frac{q^2}{\Delta^2}\left(\frac{1}{2} + \frac{q^2}{\Delta^2}\tan^2\frac{\theta}{2}\right). \tag{20d}$$

We have abbreviated the form factors by

$$F_l^2 = \sum_{L=0}^{\infty}\left|F_L^{J_0 J}(q)\right|^2 \tag{20e}$$

and

$$F_t^2 = \sum_{L=1}^{\infty}\left[\left|T_L^{eJ_0 J}(q)\right|^2 + \left|T_L^{mJ_0 J}(q)\right|^2\right]. \tag{20f}$$

Equations (20c) and (20d) are useful not only because they are simple but also because they show under which condition one can obtain the often encountered approximation

$$\frac{d\sigma/d\Omega}{4\pi\sigma_M} \approx F_l^2 + \left(\frac{1}{2} + \tan^2\frac{\theta}{2}\right)F_t^2. \tag{21}$$

This is the condition $\Delta^2 \approx q^2$, or $\omega^2 << q^2$. For the excitation of an $\omega \approx 20$ MeV level, one has $\omega^2 \approx 10^{-2}$ fm^{-2}, and Eq. (21) will be valid for $q^2 \gtrsim 0.1$ fm^{-2}, which is often the case.

We shall now prove the statement made after Eq. (11), that the $\boldsymbol{j}\cdot\mathbf{A}$ term contributes the orbital magnetic moment interaction energy. The latter gives rise to the magnetic form factor T_{LM}^{mj}, which gets its contribution from the charge current. The entire magnetic form factor can be written

$$T_{LM}^{m}(q) = \int d^3r\, \boldsymbol{\mu}_{tot}(\boldsymbol{r})\cdot\nabla\times j_L(qr)\, \mathbf{Y}_{LL}^{M}(\hat{r}) \tag{22a}$$

(this is, however, true only for ground state form factors, i.e., elastic scattering), where

$$\boldsymbol{\mu}_{tot} = \boldsymbol{\mu} + \boldsymbol{\mu}_{orb}; \tag{22b}$$

here $\boldsymbol{\mu}$ is the spin magnetization density of Eq. (10d), and the orbital magnetization density is given by

$$\boldsymbol{\mu}_{orb} = \frac{1}{2m}\int d^3r_1\ldots d^3r_A\, \psi^\dagger \sum_{i=1}^{A}\delta(\boldsymbol{r}-\boldsymbol{r}_i)\,\frac{1+\tau_3^{(i)}}{2}\,\mathbf{L}^{(i)}\,\psi_0, \tag{22c}$$

with $\mathbf{L} = \boldsymbol{r}\times\boldsymbol{p}$. As a proof, we note that according to Blatt and Weisskopf (9) the nuclear charge current is derived from its magnetization density by

$$\boldsymbol{j}(\boldsymbol{r}) = \nabla\times\boldsymbol{\mu}_{orb}(\boldsymbol{r}). \tag{22d}$$

Inserting this into $T_{LM}^{mj}(q)$ of Eq. (16e) and applying partial integration, we find

$$T_{LM}^{mj}(q) = \int d^3r\, \boldsymbol{\mu}_{orb}\cdot\nabla\times j_L(qr)\, \mathbf{Y}_{LL}^{M}, \tag{22e}$$

i.e., an expression of the form of Eq. (16g), which proves Eq. (22a) and our statement.

The contribution to the cross section equation (Eq. (13a)) of the Coulomb form factor usually is larger than that of the transverse form factor by an order of magnitude. This is true except in the vicinity of $\theta = 0°$ and $\theta = 180°$: at 180° because

$$V_l(180°) = 0 , \tag{23a}$$

and at 0° because

$$\lim_{\theta \to 0}(V_l/\Delta^4) = 2k_1 k_2/\omega^4 , \tag{23b}$$

$$\lim_{\theta \to 0}(V_t/\Delta^4) = (k_1^2 + k_2^2)/2\omega^2\Delta^2 , \tag{23c}$$

and $\Delta^2 = 4k_1 k_2 \sin^2(\theta/2) \to 0$. This makes the contribution of the transverse part go to infinity while that of the longitudinal part remains finite, but this singularity is really due to our neglect of the electron mass. Retaining the latter, we would find (25) a ratio of Coulomb/transverse terms of m_e^2/ω^2, i.e., still a large predominance of the transverse terms.

At all intermediate angles, say $\theta = 30°$ to 120°, the Coulomb terms dominate. It turns out, however, that the transverse terms are more interesting, leading to a greater variety of levels. Experiments at forward angles are difficult, but one now turns increasingly to an investigation of electron scattering at large angles or at 180° outright, so that the transverse form factors are being studied.

One should point out here that photonuclear processes are described by the same transverse matrix elements, Eqs. (16d) through (16g), that enter in inelastic electron scattering. In fact, the photoabsorption cross section integrated over the level width is given by

$$\int \sigma(k)\, dk = (2\pi)^3 \alpha \sum_{L=1}^{\infty} \frac{(L+1)\,\omega^{2L-1}}{L[(2L+1)!!]^2} [B(EL,\omega) + B(ML,\omega)] , \tag{24a}$$

and the gamma decay width of a level J decaying to the ground state J_0 is given by

$$\Gamma = 8\pi\alpha \sum_{L=1}^{\infty} \frac{L+1}{L[(2L+1)!!]^2} \omega^{2L+1} \frac{\hat{J}_0^2}{\hat{J}^2} [B(EL,\omega) + B(ML,\omega)] . \tag{24b}$$

Note that only the matrix elements at $q = \omega$ appear, the momentum transfer for photon reactions being fixed and equal to the energy transfer.

The advantages of the above-mentioned electron scattering experiments at 180° are threefold:

1. By Eq. (23a) the less interesting Coulomb term is removed and the transverse terms that lead to a greater variety of nuclear levels (especially magnetic levels) can be studied in detail.

2. We can reach the largest possible momentum transfers there, namely, $q = 2k_L - \omega$. Thus although at 180° the same (transverse) form factors enter that also describe photonuclear reactions, they generally appear at a much larger momentum transfer than in the photonuclear case (where $q = \omega$) and may then lead to excitation probabilities of certain states that are vastly different from the photoexcitation probabilities.

3. As the elastic peak is removed or much reduced at 180°, so is the disturbing background of the radiation tail.

The selection rules governing the nuclear matrix elements given in Eqs. (13b) to (13d) are the same as the familiar selection rules of the photoexcitation matrix elements which constitute their low-q limits; in particular $F_L(q)$ and $T_L^e(q)$ have the same selection rules. These are, (a) with regard to electric multipoles (for F_L, T_L^e),

$$\text{change of parity} = (-1)^L \tag{25a}$$

and (b) with regard to magnetic multipoles (for T_L^m),

$$\text{change of parity} = (-1)^{L+1} . \tag{25b}$$

Of course, the familiar order-of-magnitude estimate of multipoles in photoexcitation (Ref. 9, p. 592), namely,

$$|T_2^e/T_1^e| \propto \omega R \tag{26a}$$

and

$$|T_1^m/T_1^e| \propto v/c \tag{26b}$$

(with v being the average nucleon velocity in the nucleus), no longer applies in electroexcitation for those values of q where qR is no longer small compared to unity.

However, for Eqs. (24) relating to photon transitions, ωR is small, and it may thus be advantageous to consider the expressions of the operators, Eqs. (16) or Eqs. (19), in the low-q limit. They are obtained simply by using the expansion of the Bessel functions,

$$j_L(qr) \approx \frac{(qr)^L}{(2L+1)!!} , \tag{27}$$

and we find, for example, for the B's, for $q \to \omega << R^{-1}$:

$$B(CL,\omega) \approx \hat{J}_0^{-2} \, |\langle J || \int d^3r \, \rho(\mathbf{r}) \, r^L Y_L(\hat{r}) \, || J_0 \rangle|^2 , \tag{28a}$$

$$B(EL,\omega) \approx \hat{J}_0^{-2} \, \frac{L}{L+1} \, \frac{1}{\omega^2} \, |\langle J || \int d^3r \, \mathbf{j}(\mathbf{r}) \cdot \nabla \times r^L \, \mathbf{Y}_{LL}(\hat{r}) \, || J_0 \rangle|^2 , \tag{28b}$$

and

$$B(ML,\omega) \approx \hat{J}_0^{-2} \, \frac{L}{L+1} \, |\langle J || \int d^3r \left[r^L \, \mathbf{j}(\mathbf{r}) \cdot \mathbf{Y}_{LL}(\hat{r}) + \boldsymbol{\mu}(\mathbf{r}) \cdot \nabla \times r^L \, \mathbf{Y}_{LL}(\hat{r}) \right] || J_0 \rangle|^2 , \tag{28c}$$

the latter two quantities being familiar from the theory of nuclear photon transitions (9). Note that to this order, only the orbital ($\mathbf{j}$) contribution enters in $B(EL,\omega)$. This has the important consequence that in the low-q limit, $B(CL,\omega)$ and $B(EL,\omega)$ may be related to each other by use of the continuity equation, Eq. (10c). Indeed, one finds

$$B(CL,\omega) \approx B(EL,\omega) , \tag{28d}$$

a relation known as the Siegert theorem. Its consequence is that if the matrix element $B(CL,\omega)$ has been found experimentally to vanish or not to vanish, the same will then hold

also for $B(EL, \omega)$, and similarly for $B(CL, q)$ and $B(EL, q)$ with small q, thus implying a connection between transverse and longitudinal form factors.

Note finally that Eq. (28d) is exact (for small q), being based on the exact continuity equation. The latter contains j, which has contributions both from the well-known nucleon currents and from little-known (meson) "exchange currents" in the nucleus. In the low-q limit, by using Eq. (28d) one is able to eliminate $B(EL)$ in favor of $B(CL)$, i.e., to express the effect of the little-known exchange currents in terms of the supposedly better known charge densities, which is remarkable.

Form Factors in Elastic Electron Scattering

In elastic electron scattering, both the initial and final nuclear states are the ground state. Hence, electron scattering can tell us about the nuclear ground state charge distribution and (at 180°) the ground state magnetic moments.

The selection rules for the case of elastic scattering are more stringent than for the general case. We have $J = J_0$; therefore, the multipole order L is limited, for the first and second terms of Eq. (13a), by

$$0 \leq L \leq 2J_0 \text{ (first)}, \qquad 1 \leq L \leq 2J_0 \text{ (second)}, \tag{29a}$$

J_0 being the ground state nuclear spin; further, one has

$$\text{no change of parity.} \tag{29b}$$

From Eqs. (25), one sees that Eq. (29b) eliminates all odd Coulomb and electric multipoles and all even magnetic multipoles, so that in principle CL and EL with L even, and ML with L odd, should contribute. But considering the behavior under time reversal (26), and requiring time reversal invariance, one finds that for the elastic form factors, only even multipoles of CL and odd multipoles of EL and ML should be present. Since these requirements are contradictory for EL, it follows that in elastic scattering, only CL and ML will be present, with even multipoles of CL and odd multipoles of ML. Furthermore, at 180°, the odd multipoles of ML alone are present. The values of L are limited by Eq. (29a). In the Born approximation, one has for the elastic cross section (27) (setting $J = J_0$ in Eqs. (13)):

$$\begin{aligned}\frac{d\sigma}{d\Omega} = \sigma_M \Bigg\{ & Z^2 |F_c(q)|^2 + \frac{q^4}{180} \frac{(J+1)(2J+3)}{J(2J-1)} Q^2 |F_Q(q)|^2 \\ & + \frac{q^2}{4m^2}\left(1 + 2\tan^2\frac{\theta}{2}\right)\left[\frac{1}{3}\frac{J+1}{J}\mu^2 |F_{M1}(q)|^2\right. \\ & \left. + \frac{2q^4}{4725}\frac{(J+1)(J+2)(2J+3)}{J(J-1)(2J-1)}\Omega^2 |F_{M3}(q)|^2\right]\Bigg\},\end{aligned} \tag{30}$$

neglecting higher multipoles. The following static nuclear properties enter:

Z = nuclear charge,

Q = nuclear spectroscopic quadrupole moment (only present for $J \geq 1$),

μ = nuclear magnetic dipole moment (only present for $J \geq 1/2$),

Ω = nuclear magnetic octupole moment (only present for $J \geq 3/2$),

etc.

Each of these terms is multiplied with its appropriate form factor $F(q)$. Two kinds of observations are advantageous:

1. Scattering at small angles. Due to the factor $q^2/4m^2$ (m = proton mass) the magnetic transitions are negligible here (except for heavy nuclei such as lead) and one can measure the charge form factor (as done by Hofstadter) and (for deformed nuclei with spin larger than 1/2) can measure the quadrupole (and higher) moments. These moments, however, are inseparable from the form factors, and due to Eq. (30) also inseparable from each other, so that they can be told apart only by assuming a model. It should be noted, however, that use of an aligned nuclear target would separate the Coulomb moments in a model-independent way (3). Figure 4 presents measurements by Stovall et al. (28) on the charge and quadrupole from factors of ^{11}B. They are fit by a shell model wave function with the choice Q = 3.72 fm^2.

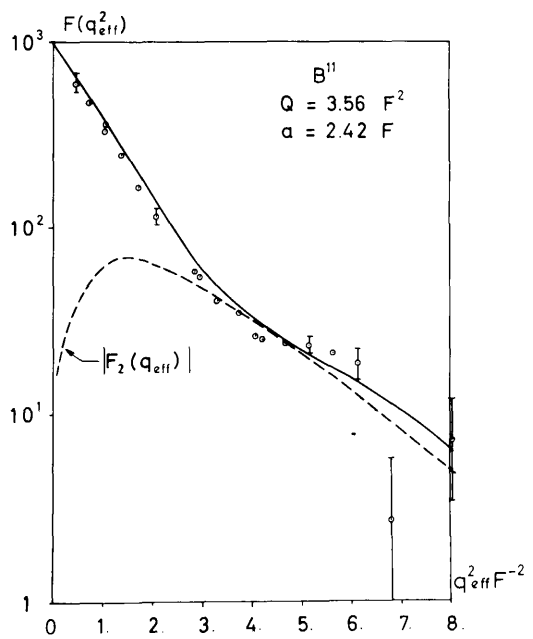

Fig. 4 - Charge and quadrupole form factors of ^{11}B (data from Ref. 28)

2. Scattering at 180°. Since, as before, $\sigma_M \to 0$ but $\sigma_M \tan^2(\theta/2)$ remains finite, one can here observe magnetic dipole, octupole, etc., moments of nuclear ground states. The same remark about the impossibility of model-independent separation of the moments applies. Figure 5 presents measurements of the Orsay group (29) on the magnetic dipole and octupole form factors of ^{11}B, fitted by a shell model.

Quasielastic Scattering

Quasielastic scattering has been mentioned earlier; it gives rise to the broad peak in the cross section above the giant resonances. It could be hoped that due to this process of electron scattering by quasifree nucleons imbedded in nuclear matter, one could study (a) the momentum distribution of a nucleon in the nucleus and (b) the nucleon pair correlation, because the electrons scattered by nucleons located at $\mathbf{r}_i$ and $\mathbf{r}_j$ in the nucleus interfere with a phase difference $\mathbf{q}\cdot(\mathbf{r}_i - \mathbf{r}_j)$; thus the variation of cross section with q should be directly related to the nuclear pair correlation function.

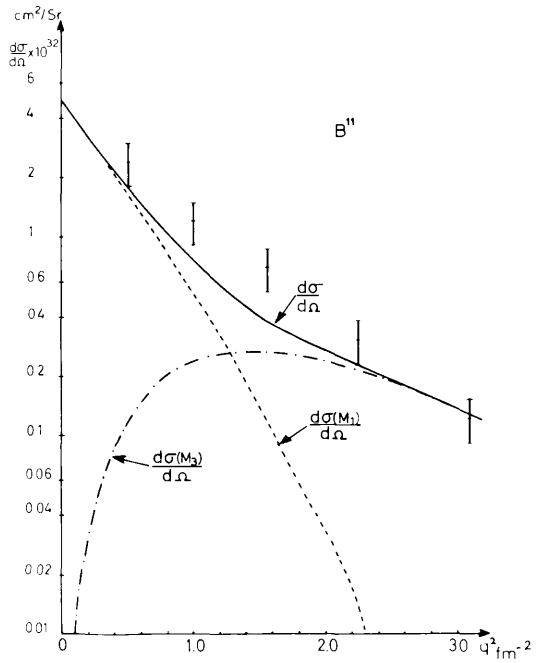

Fig. 5 - Magnetic dipole and octupole form factors of ^{11}B (data from Ref. 29)

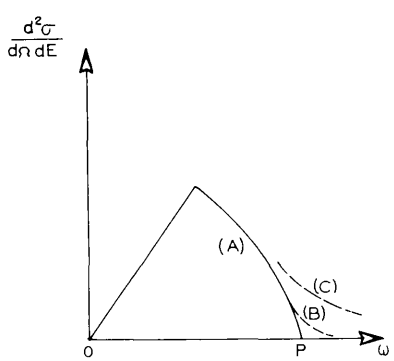

Fig. 6 - Schematic spectra of quasielastically scattered electrons, on the basis of a Fermi gas model. Curve C shows the effect of short-range correlations. (After D. B. Isabelle, University of Paris Report LAL 1152, 1966.)

It turns out, however (30), that the long-range nucleon correlations based on the Pauli principle dominate the quasielastic peak (curve A of Fig. 6) completely (on the basis of a Fermi gas model). With a finite nucleus, the upper limit is smeared out (curve B). Only at this upper limit would short-range correlations modify the picture (curve C), and the smallness of the effect is obvious. Measurements have been made in only one instance (31), and are shown in Fig. 7.

Sum rules for quasielastic scattering, i.e., the integral over the quasielastic peak, have been evaluated by McVoy and Van Hove (32) by summing over all final states and using the closure relation. It can be shown that in this way (5) magnetic moments of nucleons in nuclear matter may be obtained by 180° electron scattering.

Coincidence experiments $(e, e'p)$ have been performed by a group at Frascati (33). Figure 8 shows as an example their results in ^{40}Ca. The scattered electron energy E

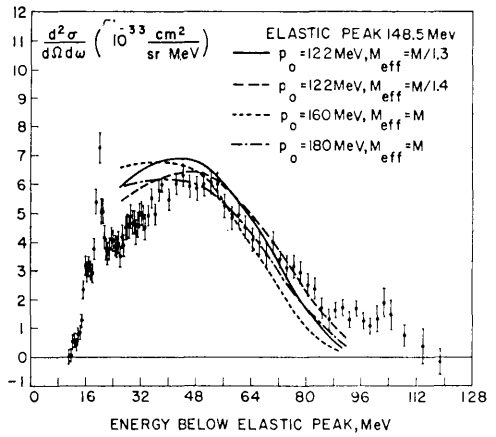

Fig. 7 - Experimental data on the quasielastic peak, obtained by Leiss and Taylor. Calculation by Czyz (Phys. Rev. 131:2141 (1963)).

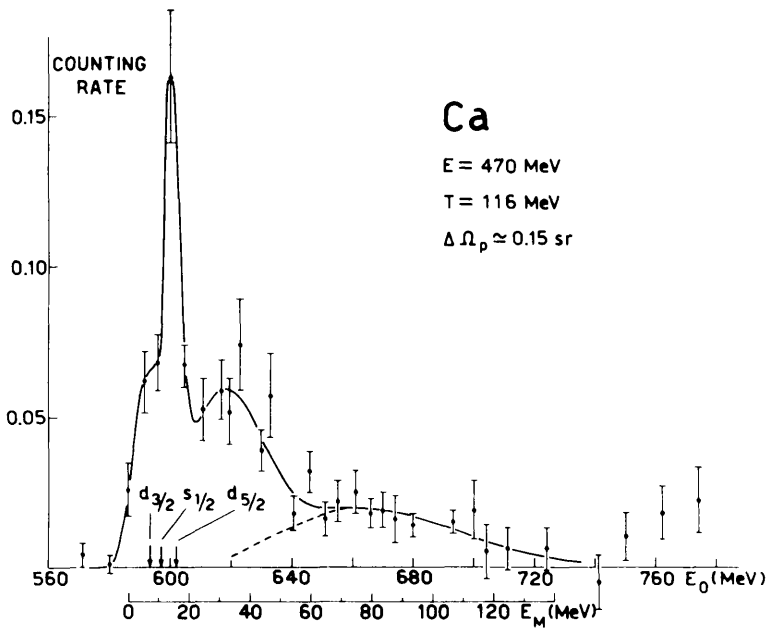

Fig. 8 - Electron-proton coincidence rate in Ca as function of the incoming electron energy E_0 and of the missing energy E_M defined in Eq. (31). (After Amaldi et al. (33).)

and the proton energy T are kept fixed, whereas the incident electron energy E_0 is varied. There appear on such a plot several peaks; their position defines a "missing energy"

$$E_M = E_0 - E - T, \tag{31}$$

which may be interpreted as the binding energy of the proton in the various nuclear shells. One thus obtains binding energies of the $1s$ 1/2 shell equal to approximately 80 MeV, of the $1p$ shell equal to approximately 35 MeV, etc., whereas the width of the peaks indicates the lifetime of a hole in the shell.

EXCITATION OF LEVELS BELOW THE GIANT RESONANCE

Nondynamic Analysis

This subsection on the nondynamic analysis of the excitation of levels below the giant resonance is mainly based on the work of Willey (1) and Spamer (24). Considering the electron scattering cross section in the form of Eq. (18a), the question arises as to how one might best be able to separate experimentally the longitudinal from the transverse contribution and to determine the multipolarity and the character of the transition (and thus the parity). This will be described, but it should be kept in mind that much in our arguments is based on the Born approximation.

We shall first, for a given state of excitation energy ω, vary k_1 and θ in such a way that the momentum transfer q, Eqs. (7), is kept constant. We may rewrite Eq. (18a) in the form

$$X \equiv \frac{d\sigma/d\Omega}{v_t(\theta)/k_1^2} = t_l(L,q)\,\frac{v_l(\theta)}{v_t(\theta)} + t_t(L,q), \tag{32}$$

where t_l contains $B(CL)$ and t_t contains $B(EL)$ or $B(ML)$. The terms t_l and t_t are constant at constant q; but since we vary θ, we may plot the measured quantity X versus the known function of θ, namely, $v_l(\theta)/v_t(\theta)$. Such a plot will yield a straight line, as shown in Fig. 9. In this figure, the quantity X is plotted for the excitation of the 8.56- and 8.93-MeV levels of ^{11}B. For the former, we have a straight line with slope determined by t_l, and an intercept at the origin t_t; for the latter we have a horizontal straight line with intercept t_t (and a slope $t_l = 0$). We remember that t_l contains the Coulomb matrix element M_L and that t_t contains electric form factors $T_L^e = T_L^{ej} + T_L^{e\mu}$ and/or magnetic form factors $T_L^m = T_L^{mj} + T_L^{m\mu}$; both of the latter ones consist of charge current terms T_L^{ij} and spin flip terms $T_L^{i\mu}$. What we can learn from this analysis is as follows.

1. If we find $t_l \neq 0$ but $t_t = 0$, i.e., the zero intercept at the origin, this means $M_L \neq 0$. From the Siegert theorem, Eq. (28d), one would then find $T_L^e \neq 0$, contrary to the fact that $t_t = 0$. The only possibility of this to happen is for monopole transitions, $L = 0$, which occur for M_L only ($L \geq 0$) but not for T_L ($L \geq 1$). Such transitions cannot be seen at 180°, since there, $v_l = 0$. An example of a monopole excitation is discussed by Werntz and Überall (34), who interpret the 20.4-MeV state seen by electroexcitation of the α particle (35) in this way.

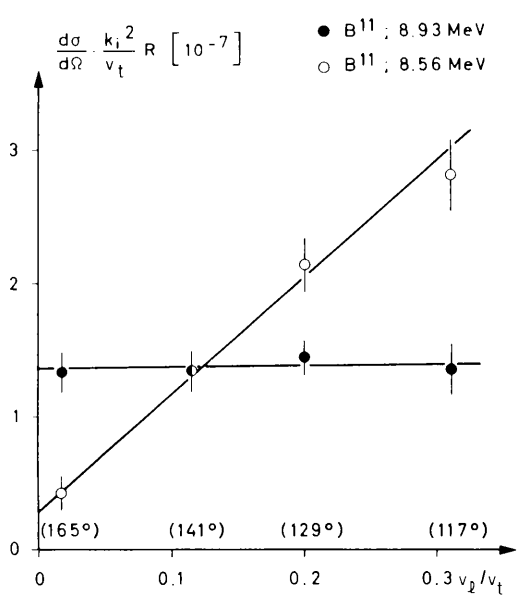

Fig. 9 - Angular dependence of the inelastic electron scattering cross section to the 8.56- and 8.93-MeV levels in ^{11}B. (After Spamer (24).)

2. If we find $t_l \approx 0$ (i.e., X horizontal), this implies $M_L = 0$, and from the Siegert theorem (at small enough q) it follows that $T_L^{ej} = 0$, and the transition is either magnetic, T_L^m, with selection rule $\Delta\pi = (-1)^{L+1}$, or it is a spin-flip electric transition, $T_L^{e\mu}$, with $\Delta\pi = (-1)^L$.

3. If we find $t_l \neq 0$ (X an inclined straight line), then $M_L \neq 0$ and from the Siegert theorem, $T_L^{ej} \neq 0$; i.e., we have an electric transition with $\Delta\pi = (-1)^L$, giving a $t_t \neq 0$ (except at $L = 0$). The transition can thus be seen at $\theta = 180°$, the angle at which the transverse excitations show up best, as mentioned earlier.

4. We see that it is still important to be able to vary the angle θ (away from the preferred position of 180°) so that we may sort out (to some extent) the character and parity of the transitions. It is of course true that putting ourselves at $\theta = 180°$ rids us of the less interesting Coulomb transitions M_L which swamp almost all else at intermediate angles; so we can see more states (namely, those that have only transverse excitation strength), especially magnetic ones, at 180°. But the Darmstadt experiments (24) show that a variation of θ away from 180° is useful, since it gives more information, as was shown, such as whether a transition is completely transverse or not.

We still need means to find out, if possible, (a) the multipole order L and (b) the parities of the observed transitions. For this purpose, it is now necessary to measure the q dependence of the excitation strength. Indeed, plots such as Fig. 9 obtained for a given constant q may be made for several different q's, and the q dependence of t_l and t_t thus obtained along a vertical line, i.e., at constant θ.

By just looking at the scattered electron spectra at a given angle for different incident energies, such as the Darmstadt spectra of Fig. 10, for scattering of 40- or 56-MeV electrons from ^{9}Be, the relative q dependence of different levels is obvious. The strength of the 16.97-MeV level decreases with increasing q relative to the strengths of the 16.65- and 17.50-MeV levels. Theoretically, the q dependence of the B's is involved, but it simplifies greatly if one works at low enough values of q ($\lesssim$ 80-100 MeV/c) so that only the lowest terms in an expansion of powers of q need be retained; indeed, the power of q with which the cross section varies indicates directly the multipole order. Such expansions are given in the literature (1,37); the results are shown in Table 2. Since one wants to compare the different theoretical predictions with the measured q dependence of one given state of given parity, one must compare $ML \pm 1$ to EL, which explains the last two columns. From the column giving the example of $L = 1$, one sees that from parity alone, $M2$ and $E1$ transitions can interfere for one given level, but one may be able to tell which one predominates (if any) from the different q dependence. From the $L = 2$ column, one sees that $E2$, $M1$ interference is possible, with the same q dependence.

Further statements that can be made on the basis of the q dependence of excitation strengths are the following:

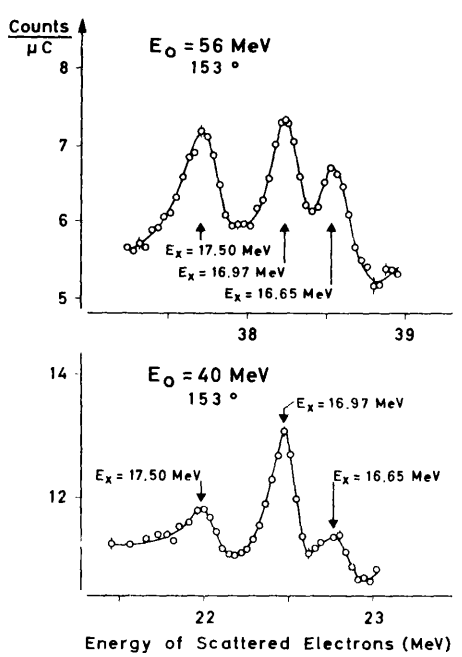

Fig. 10 - Spectrum of inelastically scattered electrons from ^{9}Be. The inelastic momentum transfer is $q = 0.467$ fm^{-1} in the upper part of the figure and $q = 0.310$ fm^{-1} in the lower part of the figure. (After Ref. 36.)

Table 2
The q Dependence of Cross Sections in the Low-q Limit (for Fixed Angle θ)

Cross Section	q Dependence	Examples of q Dependence	
		$L = 1$	$L = 2$
$d\sigma\ (CL)$	$(qR)^{2L}\ v_l(\theta)$	$C1^- \propto q^2$	$C2^+ \propto q^4$
$d\sigma\ (EL)$*	$(\omega/q)^2 (qR)^{2L}\ v_t(\theta)$	$E1^- \propto q^0$	$E2^+ \propto q^2$
$d\sigma\ (M\ L-1)$	$(q/m)^2 (qR)^{2L-4}\ v_t(\theta)$	-	$M1^+ \propto q^2$
$d\sigma\ (M\ L+1)$	$(q/m)^2 (qR)^{2L}\ v_t(\theta)$	$M2^- \propto q^4$	$M3^+ \propto q^6$

*Willey (1) disregards the T_L^{ej} term which is not generally justified, and thus obtains here $(q/m)^2 (qR)^{2L} v_t(\theta)$. Note that the limits shown in Table 2 are valid for general transitions and not just for the single particle transitions considered by Willey.

1. For the case $t_l \neq 0$, the transition has an electric part, whose selection rules are thus known to apply. The q dependence can be measured as was described. Figure 11 shows as an example the excitation of the 4.46-MeV level in ^{11}B. The quantity X has been plotted vs $v_l(\theta)/v_t(\theta)$ for three fixed values of q; three straight lines result. The successive slopes of the three lines measure the q dependence of t_l, whereas the three successive intercepts at the origin give the q dependence of t_t. If we find $t_l(q) \propto q^2$, the transition is $C1^-$, so the state is $J = 1^-$ for a $J_0 = 0^+$ ground state for example; if we find $t_l(q) \propto q^4$, the transition is $C2^+$ (Table 2). The q dependence of $t_t(q)$, obtained from the intercepts, must then agree with the second line of Table 2 for the transverse electric part present, which may serve as a check. But a magnetic admixture may be present in the transverse part, such as $M2^-$ with $E1^-$, or $M1^+$ with $E2^+$ (in the former admixture, the q dependence of t_t would depend on the mixture).

2. For the case $t_l = 0$, t_t consists only of T_L^m, or of an electric spin flip term $T_L^{e\mu}$. Figure 12 presents an example of $t_l = 0$; X is plotted vs v_l/v_t for three values of q for the 5.04-MeV level of ^{11}B. The q dependence can be read off from the ordinate levels of the horizontal lines. From Table 2, if $\propto q^4$ is found, the transition is $M2^-$; $\propto q^2$ may be $M1^+$, or $E2^+$ (spin flip) which cannot be distinguished, so that only the fact that $\Delta\pi = +1$ is established.

The extrapolation of the q dependence of $B(L, q)$ down to $q = \omega$ furnishes the ground state radiative width of the state, given (3) by

$$\Gamma = \frac{8\pi\alpha}{[(2L+1)!!]^2} \frac{L+1}{L} \frac{2J_i+1}{2J_f+1} \omega^{2L+1} B(L, \omega), \tag{33}$$

which can be independently obtained by nuclear resonance scattering (38), thus providing a crosscheck. Γ usually is measured in Weisskopf units (9) Γ_W, which provide a rough single-particle estimate for the EL or ML radiative transition. If we find $\Gamma/\Gamma_W \gg 1$, the transition can be considered collective.

Besides the leading terms in a power series expansion in q as was discussed, one will of course want to measure the q dependence of the matrix elements further out (24).

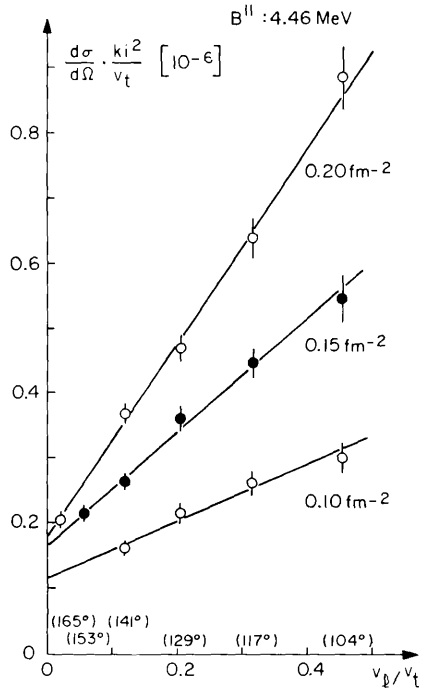

Fig. 11 - Angular distributions at various constant inelastic momentum transfers q (indicated in the diagram) for the 4.46-MeV transition in ^{11}B. The slope of the straight lines gives the longitudinal part, and the intersection with the ordinate scale gives the transverse part of the cross section. (After H. Artus, P. Brix, H. G. Clerc, et al., Proceedings of the International Conference on Nuclear Physics, Gatlinburg, Tenn., Sept. 12-16, 1966.)

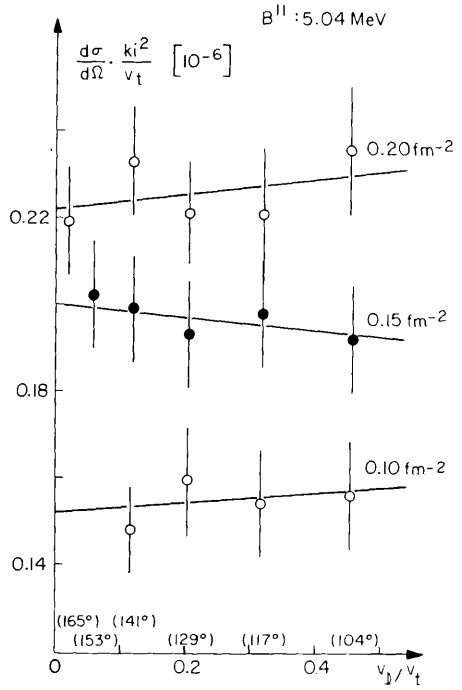

Fig. 12 - Same as Fig. 11, for the 5.04-MeV transition in ^{11}B (same reference)

This provides an additional method of identification for the multipolarity of the transition, besides leading to the measurement of a "transition radius" for the nuclear transition in question. One finds by expansion (24,37):

$$\left[\frac{B(CL,q)}{B(CL,0)}\right]^{1/2} = 1 - \frac{q^2 R_{tr}^2}{2(L+3)} + \dots , \tag{34a}$$

$$\left[\frac{B(EL,q)}{B(EL,0)}\right]^{1/2} = \frac{\omega}{q}\left[1 - \frac{(L+3)\,q^2 R_{tr}^2}{2(L+1)(2L+3)} + \dots\right] , \tag{34b}$$

and

$$\left[\frac{B(ML,q)}{B(ML,0)}\right]^{1/2} = 1 - \frac{(L+3)\,q^2 R_{tr}^2}{2(L+1)(2L+3)} + \dots . \tag{34c}$$

Plotting the measured values for $[B(q)/B(0)]^{1/2}$ vs q^2, one should obtain a descending straight line whose slope determines

$$R_{tr}^2 = \langle r^{L+2}\rangle / \langle r^L\rangle . \tag{35}$$

For example, consider an $M2$ transition. If it had erroneously been assumed to be an $M1$ transition, the "B" thus determined from the measurement of $d\sigma$ is really the quantity

$q^2B(M2, q)$, which leads to an incorrect slope that increases. If it were taken for an $M3$ transition, the "B" really is $q^{-2}B(M2, q)$, which decreases too fast with q^2, thus leading to an unreasonably large R_{tr}. For a concrete example, namely the 8.93-MeV level in ^{11}Be, assuming an $M2$ transition would lead to $R_{tr}^2 = 33$ fm^2, whereas the ground state $\langle r^2 \rangle_0$ is only 5.7 fm^2 (R_{tr}^2 is expected to be close to $\langle r^2 \rangle_0$). This transition therefore must be $M1$, and with a $3/2^-$ ground state, this agrees with the $J = 5/2^-$ assignment of the excited level, as determined by other methods.

This illustrates (24) how, with a small linac limited in energy range (but with excellent resolution), states may be identified and their spin and parities, ground state radiative widths, and transition radii determined from whatever limited range of variation of q is available. The excitation of levels in the region below the giant resonances of ^{24}Mg and ^{26}Mg has been studied, and the character of the transitions determined in this way, by the Darmstadt group (39), as shown in Figs. 13a and 13b. In Figs. 14a, 14b, and 14c we present 180° electron scattering data obtained by the NRL group (L. W. Fagg et al., to be published) for ^{24}Mg, ^{25}Mg, and ^{26}Mg, which include the giant resonance region.

Dynamic Analysis

This subsection, which introduces a dynamic analysis, is based on Kurath's (40) analysis of collective magnetic levels below the giant resonance, using sum rule techniques. Strong $M1$ levels (of collective character) are predicted in even $T = 0$ nuclei.

In our expression for the transverse magnetic matrix element,

$$T^m = T^{mj} + T^{m\mu}, \tag{36}$$

the magnetic spin flip part $T^{m\mu}$ contains the spin magnetic moment operator

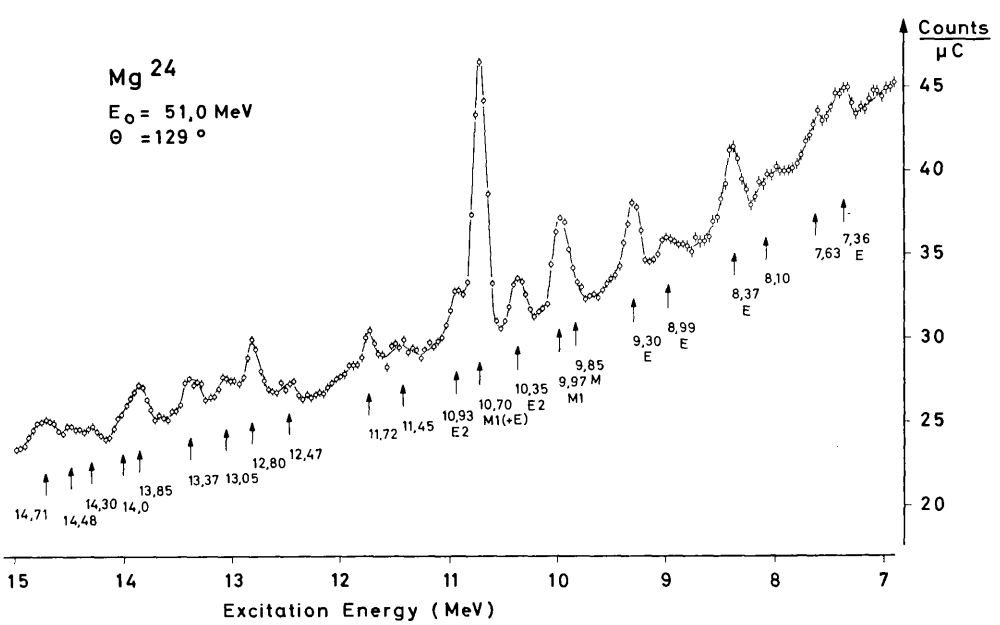

Fig. 13a - Spectrum of inelastically scattered electrons from ^{24}Mg. The arrows indicate the measured excitation energies in MeV. The type of transition, E (electric) or M (magnetic) is indicated. (After O. Titze and E. Spamer, Z. Naturforsch. 21a:1504 (1966).)

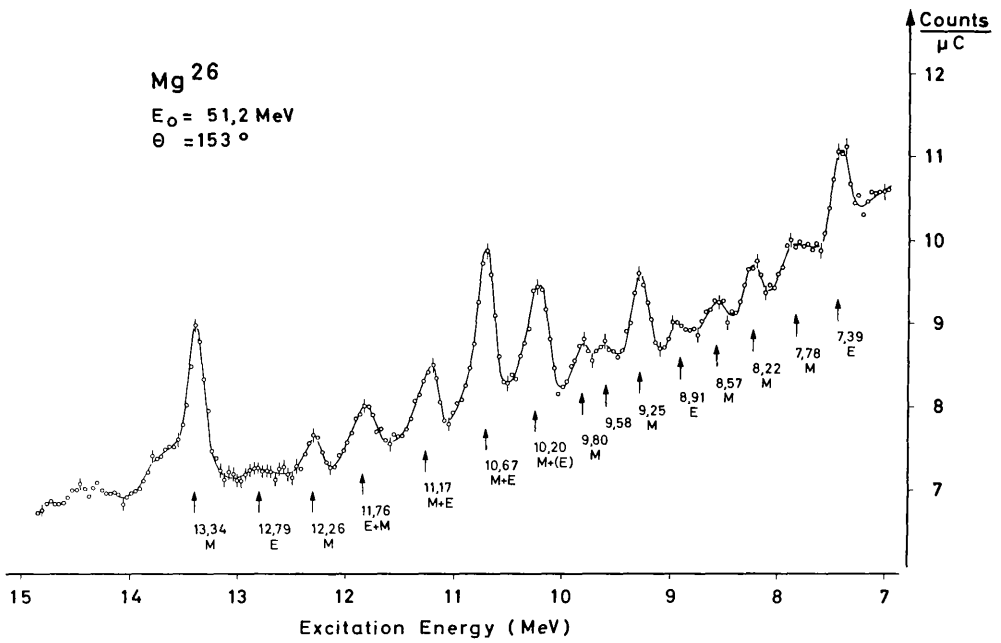

Fig. 13b - Same as Fig. 13a, for ^{26}Mg (same reference)

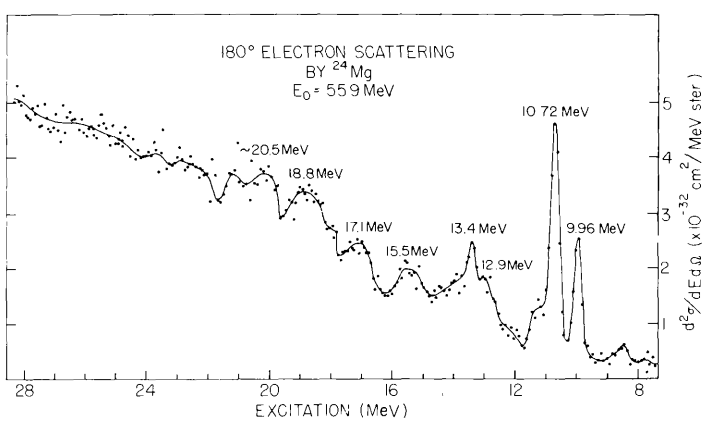

Fig. 14a - Spectrum of inelastically scattered electrons at 180° from ^{24}Mg, including the giant resonance region. (After L. W. Fagg et al., Phys. Rev., to be published.)

$$\boldsymbol{\mu}_s = \frac{1}{2m}\left(\mu_p \sum_p \boldsymbol{\sigma}_p + \mu_n \sum_n \boldsymbol{\sigma}_n\right) , \tag{37a}$$

summed over proton and neutron spins separately, and with proton or neutron magnetic moments $\mu_p = 2.79$ or $\mu_n = 1.91$. This operator can be written as

$$\boldsymbol{\mu}_s = \frac{1}{2m}\left(\mu_p \sum_{i=1}^{A} \frac{1+\tau_3^{(i)}}{2}\boldsymbol{\sigma}_i + \mu_n \sum_{i=1}^{A} \frac{1-\tau_3^{(i)}}{2}\boldsymbol{\sigma}_i\right) \tag{37b}$$

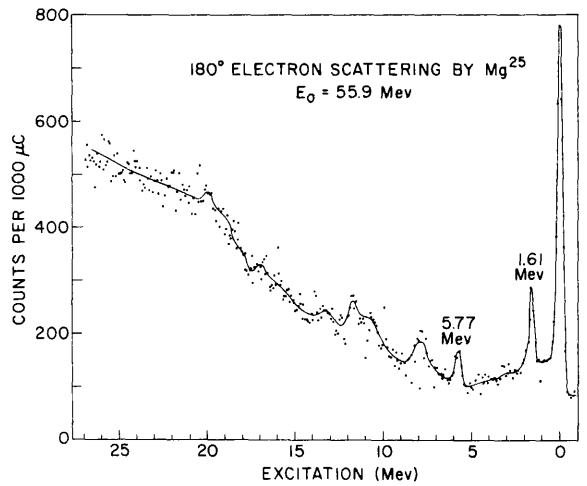

Fig. 14b - Same as Fig. 14a, for ^{25}Mg (same reference)

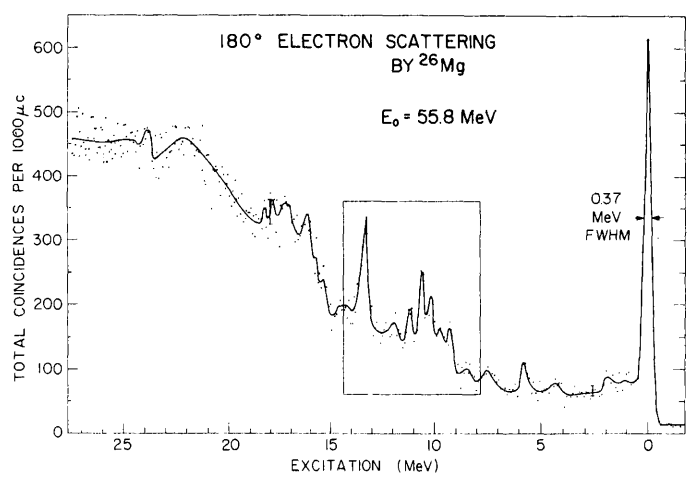

Fig. 14c - Same as Fig. 14a, for ^{26}Mg (same reference)

or

$$\boldsymbol{\mu}_s = \frac{1}{2m}\left(\frac{\mu_p + \mu_n}{2} \sum \boldsymbol{\sigma}_i + \frac{\mu_p - \mu_n}{2} \sum \tau_3^{(i)} \boldsymbol{\sigma}_i\right) , \tag{37c}$$

the first term causing $\Delta T = 0$ transitions, and the second term causing $\Delta T = 0, 1$ transitions. We shall consider even nuclei with a $T = 0$ ground state, so the first term excites $T = 0$ levels and the second term excites $T = 1$ levels. Since $(\mu_p + \mu_n)/2 = 0.44$ and $(\mu_p - \mu_n)/2 = 2.35$, the excitation of the $T = 0$ levels is strongly suppressed (the squares of these terms enter in the probabilities); this is known as Morpurgo's selection rule. The same rule holds for the total magnetic moment operator which governs all of the T_m transitions,

$$\boldsymbol{\mu} = \frac{1}{2m} \frac{\mu_p - \mu_n}{2} \sum_i \tau_3^{(i)} \boldsymbol{\sigma}_i + \frac{1}{2} \sum_i \mathbf{l}_i \tau_3^{(i)} , \quad (37d)$$

since the additional orbital motion term also contains τ_3, i.e., an isovector transition. We shall thus, for the $T = 0$ nuclei, consider only the strong $T = 1$ level excitations. These levels necessarily lie higher in energy, since the two $T = 1$, $T_Z = \pm 1$ neighbors (Fig. 15 shows this isotriplet in ^{12}C) have higher lying ground states.

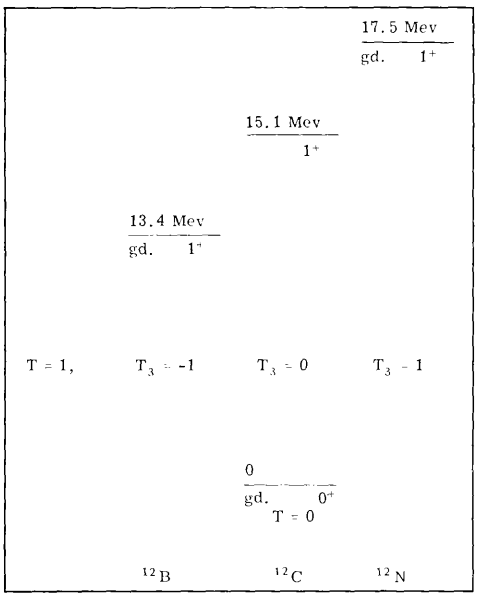

Fig. 15 - Ground state of ^{12}C, and lowest $T = 1$ isotriplet of levels in ^{12}B, ^{12}C, and ^{12}N

Using the shell model for the excited states, such as for the $1p$ shell nuclei, we describe them by various configurations of the $1p\ 3/2$ and $1p\ 1/2$ subshells, both unfilled. The interaction

$$H = \sum_i H_0^i + a \sum_i \mathbf{l}_i \cdot \mathbf{s}_i + \sum_{i>k} V_{ik} \quad (38)$$

including a spin orbit force with strength parameter a produces mixed configurations for the various excited states; parameters are determined by fitting to the lowest few excited levels of some of the nuclei in question. This program has been carried out by Kurath previously (41). With the wave functions thus obtained, we calculate $B(M1, \omega)$, i.e., the low-q approximation. For ^{12}C the values of $B(M1, \omega)$ for the four lowest calculated $M1$ levels (all in the range from about 10 to 15 MeV) are shown in Table 3, for two values of the spin-orbit coupling parameter a/K (K being a representative integral of the two-body interaction). The value $a/K = 4.5$ is the one leading to better agreement between calculated and observed level schemes. One notes that most of the magnetic dipole strength, when the spin-orbit coupling is switched on and mixes the configurations, becomes concentrated in the lowest level, which might then be called a "giant" (or at least, collective) magnetic dipole resonance. The situation is exactly opposite, as we shall see later, to that of the giant electric dipole resonance near 20 MeV, where configuration mixing tends to concentrate the strength in the highest possible level.

Table 3
Values of $B(M1, \omega)$ of the Four Lowest Calculated $M1$ Levels in ^{12}C, for Two Values of the Spin-Orbit Parameter a/K

$M1$ Level	$B(M1, \omega)$	
	$a/K = 1.5$	$a/K = 4.5$
Highest (≈ 15 MeV)	0.2	0.2
—	1.1	0.3
—	1.0	0.4
Lowest (≈ 10 MeV)	1.3	10.0

The $4n + 2$ nuclei of the p shell show a similar picture. In ^6Li, a strong $M1$ state at low energy concentrates 90% of all the $M1$ strength, and in ^{14}N, again 90% of the $M1$ strength lies in a level near 10 MeV (experimentally, there are two levels, at 9.2 and 10.4 MeV).

For $2s$-$1d$ shell nuclei, no such wave functions were available, so Kurath estimated $M1$ strengths by the use of sum rules. The usual way such sum rules are obtained (e.g., Austern and Sachs (42)) is by taking the ground state expectation value of the double commutator of H with μ_z and using closure; then

$$2 \sum_n (E_n - E_0) \, |\langle n | \mu_z | 0 \rangle|^2 = \langle 0 | [\mu_z, (H, \mu_z)] | 0 \rangle . \tag{39a}$$

The left-hand side gives the $B(M1)$ strengths, energy-weighted so as to favor the higher levels; the right-hand side can be evaluated explicitly and is given mainly by the spin-orbit term proportional to a/K. Kurath in this way determined the fraction of the total strength quoted for the individual states of the p shell nuclei. An extrapolation of Eq. (39a) to $2s$-$1d$ shell nuclei can be made by again assuming that the lowest state carries most of the strength, and by setting the right-hand side approximately equal to the result of the spin-orbit term,

$$\sum_n (E_n - E_0) \, B(M1) \approx -a \left(\mu_n - \mu_p + \frac{1}{2}\right)^2 \langle 0 | \Sigma \boldsymbol{l} \cdot \boldsymbol{s} | 0 \rangle . \tag{39b}$$

For a nucleon in the $d\ 5/2$ (or $d\ 3/2$) shell, we have

$$\boldsymbol{l} \cdot \boldsymbol{s} = \frac{1}{2} (j^2 - l^2 - s^2) = 1 \ (\text{or } -1) \tag{39c}$$

(setting $j = 5/2$ or $3/2$, $l = 2$, $s = 1/2$). This shows that as the $1d\ 5/2$ shell fills up, the right-hand side of Eq. (39b) should become largest, and should subsequently drop again as the $1d\ 3/2$ shell fills. The strongest $M1$ levels should thus be found for nuclei around ^{28}Si or ^{32}S, and not for nuclei near ^{16}O or ^{40}Ca.

As for experiments, we mention the famous strong $M1$ levels: 1^+ at 15.1 MeV in ^{12}C and 0^+ at 3.56 MeV in Li^6. Experiments on the ^{12}C level were made by Goldemberg et al. (43) at Stanford, by Dudelzak and Taylor (44) at Orsay, and by Gudden (45) at Darmstadt. Figure 16 presents the Stanford result, showing the peak in the scattered electron spectrum for various electron energies, at 180°. An analysis of Walecka in terms of a jj-coupling shell model, shown in Fig. 17, gave the right shape of the q dependence, but the theoretical absolute magnitude was about four times too high. Kurath (46), using his intermediate-coupling wave functions, got the right magnitude in addition to the right shape (Fig. 18) by adjusting the spin-orbit parameter. The same figure also shows the data and theoretical fits for the 0^+, 3.56-MeV level of ^{6}Li.

THE GOLDHABER-TELLER AND STEINWEDEL-JENSEN MODELS FOR THE GIANT RESONANCE

The so-called giant resonance was first seen in photonuclear reactions such as (γ, n), (γ, p), or in total photon absorption in nuclei (47). The experiments were originally done using a bremsstrahlung spectrum of photons, but the preferable technique of using monochromatic photon beams (from positron annihilation) has now been accomplished (48). Increasing the photon energy (or the bremsstrahlung endpoint, as the case may be), one first observes the relatively weak and narrow magnetic levels described in the preceding section, until at approximately 20 MeV for light nuclei (approximately 15 MeV for heavy ones) the cross section suddenly rises to tens or even hundreds of millibarns and forms a broad hump of width of several MeV which, depending on the nucleus, may show considerable fine structure. Above the giant resonance, the cross section falls off again and shows little structure. Figure 19 presents the giant resonance as seen (49) in the (γ, p) cross section (with varying angles of the emitted proton) for ^{16}O, and Fig. 20 shows total photon absorption cross sections (50) for ^{12}C and ^{16}O.

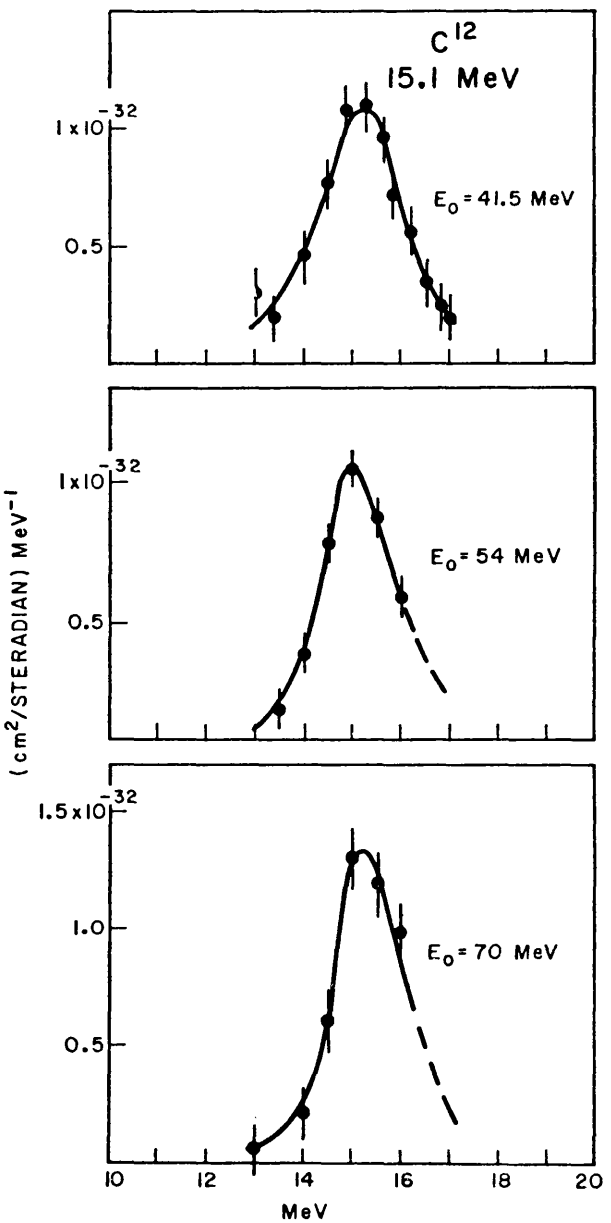

Fig. 16 - Differential cross section for the ^{12}C 15.1-MeV level in inelastic electron scattering at 180° for different incident electron energies E_0 (data from Ref. 43)

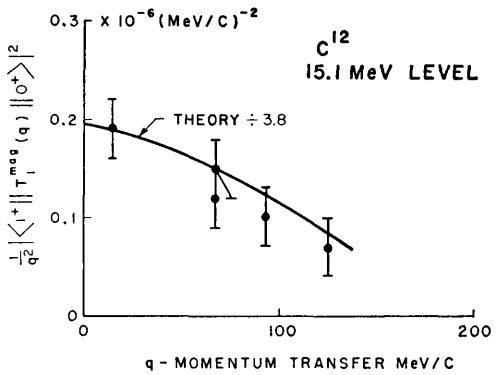

Fig. 17 - The experimental values of the quantity $(1/q^2)\,|\langle 1^+\|T_1^{mag}(q)\|0^+\rangle|^2$ as a function of the momentum transfer (data from Ref. 43). The theoretical curve had to be divided by a factor of 3.8 to fit the data.

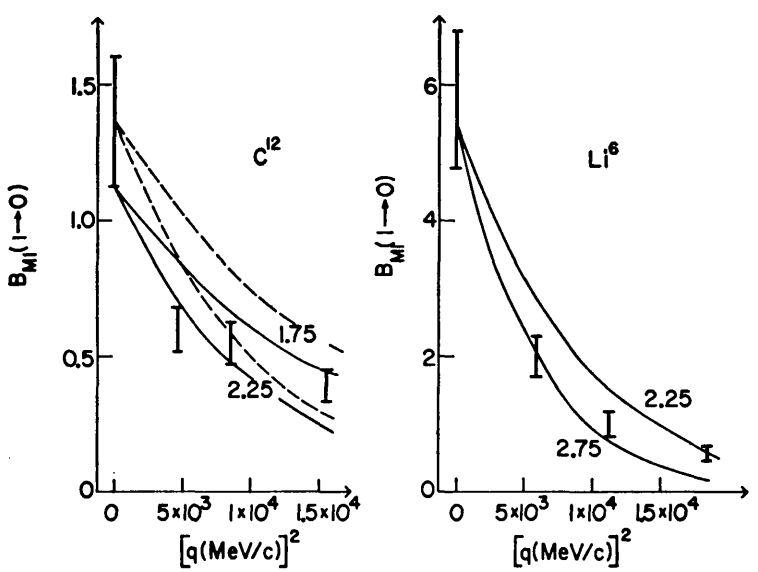

Fig. 18 - The reduced transition probability $B(M1,\ 1\to 0)$ for ^{12}C and ^{6}Li as a function of q^2. The curves are calculated for different values of the harmonic-oscillator parameter $a = (\hbar/m\omega)^{1/2}$, which is given in units of fermis. (After Ref. 46.)

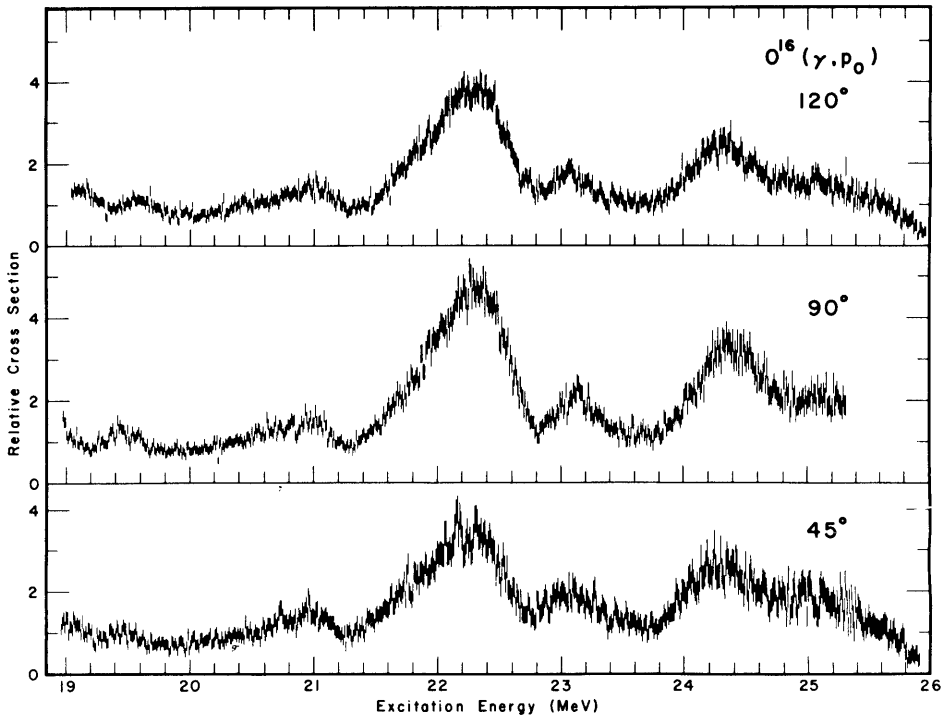

Fig. 19 - Photoproton cross section of ^{16}O obtained at angles of 45°, 90°, and 120° using 26-MeV bremsstrahlung (plots from Ref. 49)

Starting from a 0^+, $T = 0$ ground state such as in ^{12}C or ^{16}O, the giant resonance must be 1^-, $T = 1$, for the following reason: The transition amplitude is given by T^j_{LM} of Eqs. (16), with $q = \omega$ for photons. The order-of-magnitude estimates of Eqs. (26) hold, so only the electric dipole can lead to as large a transition strength as is observed. By the Siegert theorem, Eq. (28d), the $q = \omega$ limit of $T^{ej}_{LM}(q)$ leads to the transition probability

$$B(EL,\omega) \approx \hat{J}_i^{-2} \, |\langle J_f || \int d^3r \, \rho(\mathbf{r}) \, r^L \, Y_L(\mathbf{r}) || J_i \rangle|^2 , \tag{40a}$$

which for $L = 1$ just becomes the familiar matrix element of z

$$B(E1,\omega) \propto |\langle 10| \int d^3r \, \rho(\mathbf{r}) \, z \, |00\rangle|^2 , \tag{40b}$$

and using the transition charge density of Eq. (10a), we have

$$B(E1,\omega) \propto |\langle 10| e \sum_{i=1}^{A} \frac{1+\tau_3^{(i)}}{2} \, z_i \, |00\rangle|^2 \tag{40c}$$

$$= |\langle 10| \frac{e}{2} \sum_{i=1}^{A} z_i \, |00\rangle + \langle 10| \frac{e}{2} \sum_{i=1}^{A} z_i \tau_3^{(i)} \, |00\rangle|^2 . \tag{40d}$$

The first term, which is a $\Delta T = 0$ term, vanishes because

$$\sum_{i=1}^{A} z_i = 0 \tag{41}$$

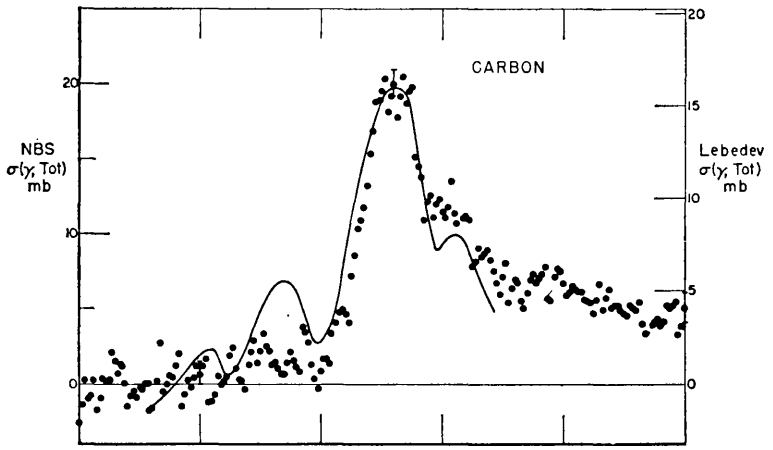

(a) Cross sections for ^{12}C. The solid line is the total photonuclear cross section obtained by the Lebedev group (Burgov et al., Inst. for Theor. and Exp. Physics, Moscow, 1963 (unpublished)), plotted using the right-hand ordinate.

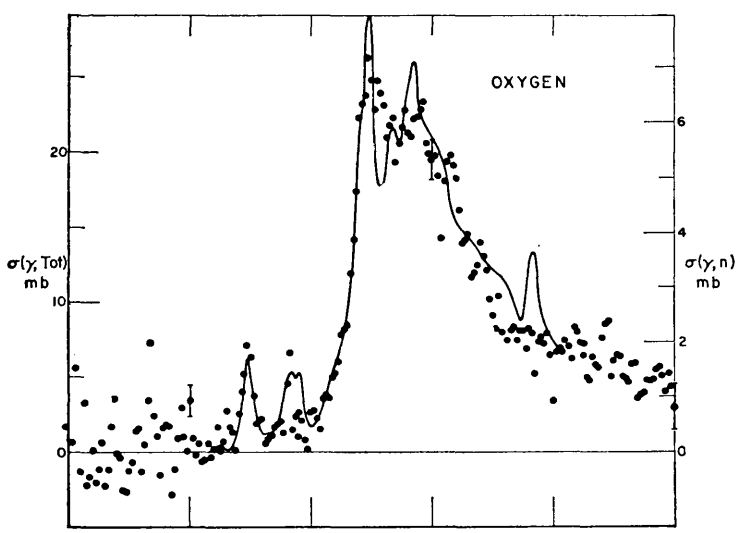

(b) Cross sections for ^{16}O. The solid line is the (γ, n) cross section obtained by the Livermore group (Bramblett et al., Phys. Rev. 133:B869 (1964)).

Fig. 20 - Total photonuclear cross sections for ^{12}C and ^{16}O (points from an experiment at NBS (50))

is the z coordinate of the center of mass. Thus only the second term contributes to the transition, and it implies $\Delta T = 1$. (These and other selection rules were discussed by Gell-Mann and Telegdi (51).) As a consequence, the states excited by dipole photoabsorption have an isospin

$$T_{\text{exc}} = T_{gd}\,,\ T_{gd} + 1 \tag{42a}$$

if $T_{gd} \neq 0$, or

$$T_{\text{exc}} = T_{gd} + 1 \tag{42b}$$

if $T_{gd} = 0$ (for self-conjugate nuclei such as ^{12}C and ^{16}O). Note that in Eq. (42a) the possibility $T_{\text{exc}} = T_{gd} - 1$ does not appear, since for the ground states of stable nuclei, we usually have $|T_{3_{gd}}| = T_{gd}$, and since Eqs. (40) involve only τ_3, we also have $T_{3_{\text{exc}}} = T_{3_{gd}}$.

Since for $T = 0$ nuclei, $T_{\text{exc}} = 1$, the giant dipole resonance forms an isotriplet, whose $T_3 = \pm 1$ components must lie in the neighboring $T = 1$ nuclei. This is shown in Fig. 21 for ^{12}C. Excitation of these "analog" giant resonances can occur by $\Delta T_3 = 1$ processes such as muon or pion capture or neutrino absorption and is discussed in the literature (52). At this point we only remark that from the higher-lying ground states of the neighboring $T_3 = \pm 1$ nuclei, it follows that electric dipole states in the $T = 0$ nucleus will lie only above the ground state energy of the $T = 1$ neighbor, and the states below this region, which are seen strongly in photon transitions, will be magnetic dipole levels.

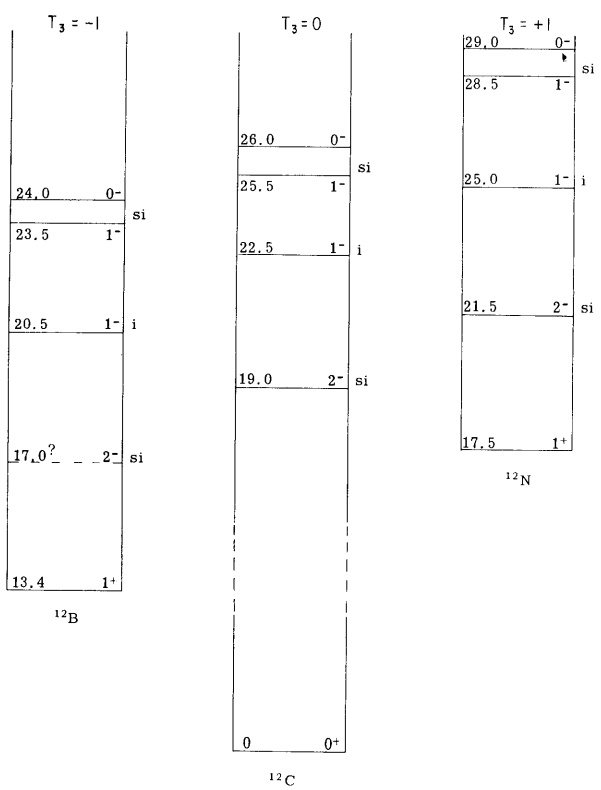

Fig. 21 - $T = 1$ giant resonance levels in ^{12}C, and their $T_3 = \pm 1$ isotopic analogs in ^{12}B and ^{12}N. The terminology is from the generalized Goldhaber-Teller model.

The Goldhaber-Teller Model

The large cross section of the giant resonance leaves no doubt that the excitation comes about by a collective motion of the nucleus, producing as large a dipole moment as possible. In their original paper (53) Goldhaber and Teller therefore suggested that the excited state is a harmonic vibration of the protons of the nucleus as a whole against the neutrons as a whole (Fig. 22a). Assuming that the charge density $\rho_0(r)$ of the ground state, taken to be spherically symmetric, gets displaced rigidly (54), one finds

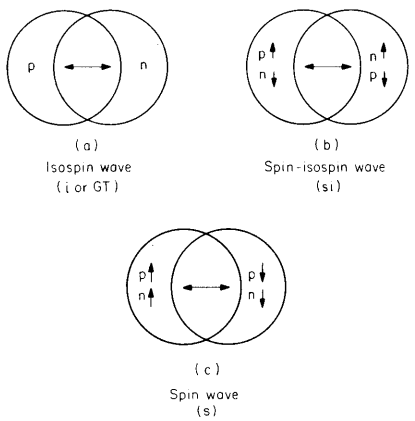

Fig. 22 - Collective dipole vibrations of nuclear matter: modes of the generalized Goldhaber-Teller (GT) model. In mode (a), protons with both spin up ($p\uparrow$) and spin down ($p\downarrow$) move in phase and are indicated collectively as p, whereas in modes (b) and (c) $p\uparrow$ and $p\downarrow$ move out of phase and are indicated separately.

$$\rho_0(r) \to \rho(\boldsymbol{r}) \equiv \rho_0\left(\left|\boldsymbol{r} - \frac{1}{2}\boldsymbol{d}\right|\right)$$

$$\approx \rho_0(r) - \frac{1}{2}\boldsymbol{d}\cdot\nabla\rho_0(r)\,, \tag{43a}$$

where $\boldsymbol{d}$ is the displacement vector between the centers of the neutron sphere and the proton sphere (we assume $Z = N$). Satisfying the continuity equation, $\nabla\cdot\boldsymbol{j} = -\dot{\rho}$, one obtains the charge current

$$\boldsymbol{j}(\boldsymbol{r}) = \frac{1}{2}\dot{\boldsymbol{d}}\rho_0(r)\,. \tag{43b}$$

Now $\boldsymbol{d}$ is considered the coordinate of a harmonic oscillator, with a Hamiltonian

$$H = \frac{1}{2m^*}\boldsymbol{p}^2 + \frac{1}{2}m^*\omega^2\boldsymbol{d}^2\,; \tag{44}$$

its reduced mass is given by $m^* = (1/4)Am$, where m is the nucleon mass, and ω is its eigenfrequency, which we must take from experiment. Quantizing the oscillator, one has in spherical components (with $l = 1$ in the present case)

$$d_{lm} = \left(\frac{\hbar}{2m^*\omega_l}\right)^{1/2}\left[a^\dagger_{lm} + (-1)^m a_{l-m}\right] \tag{45a}$$

and

$$\dot{d}_{lm} = i\left(\frac{\omega_l\hbar}{2m^*}\right)^{1/2}\left[a^\dagger_{lm} - (-1)^m a_{l-m}\right]\,, \tag{45b}$$

and the canonical formalism gives the momentum

$$p_{lm} = m^*\dot{d}^\dagger_{lm}\,. \tag{45c}$$

The Hamiltonian becomes as usual

$$H = \sum_{lm}\left(a^\dagger_{lm}a_{lm} + \frac{1}{2}\right)\hbar\omega_l\,, \tag{46}$$

if one uses the commutation rules

$$[a_{lm}, a_{l'm'}] = [a^\dagger_{lm}, a^\dagger_{l'm'}] = 0 \tag{47a}$$

and

$$[a_{lm}, a^\dagger_{l'm'}] = \delta_{ll'}\,\delta_{mm'} \tag{47b}$$

between creation operators $a^\dagger_{lm}$ and annihilation operators a_{lm}. Thus the part of j that creates one phonon lm, becomes

$$j^{(cr)}_{lm}(\mathbf{r}) = \frac{1}{2}\, i\left(\frac{\omega_l \hbar}{2m^*}\right)^{1/2} a^\dagger_{lm}\rho_0(r)\ , \tag{48a}$$

and the creation part of $\rho(\mathbf{r})$ becomes

$$\rho^{(cr)}(\mathbf{r}) = -\sum_m (-1)^m \frac{1}{2}\left(\frac{\hbar}{2m^*\omega}\right)^{1/2}\left(\frac{4\pi}{3}\right)^{1/2} Y_{1-m}(\hat{r})\, a^\dagger_{1m}\,\rho_0'(r)\,. \tag{48b}$$

Inserting these in Eqs. (16), we obtain the reduced matrix elements

$$\langle 1^- \| M_1 \| 0\rangle = \frac{A}{2}\,\frac{qF(q)}{4\pi}\left(\frac{2\pi}{Am\,\omega_1}\right)^{1/2} \tag{49a}$$

and

$$\langle 1^- \| T_1^{ej} \| 0\rangle = -\frac{A}{2}\,\frac{\omega F(q)}{4\pi}\left(\frac{4\pi}{Am\,\omega_1}\right)^{1/2} \tag{49b}$$

for a creation of a 1^- dipole phonon. It is remarkable that these transition form factors have been expressed by the ground state charge form factor,

$$F(\mathbf{q}) = \int d^3r\, e^{i\mathbf{q}\cdot\mathbf{r}}\,\rho_0(r) = 4\pi\int d^3r\, j_0(qr)\,\rho_0(r)\ , \tag{49c}$$

but this is a consequence of our assumption that the proton distribution as a whole gets displaced rigidly. It should also be mentioned that

$$\langle 1^- \| T_1^{mj} \| 0\rangle = 0 \tag{49d}$$

from parity considerations.

But what about contributions from the nuclear magnetization? For photon transitions at $q = \omega$, Eq. (24b), it is well known that these contributions are small. For electron scattering with large q's, however, spin flip terms may come in strongly. In the collective model with pure charge vibration as described above, there is no possibility for a spin flip; thus it was stated in Ref. 54 that the Goldhaber-Teller model does not lead to a transition magnetization density. This is however correct only for the original version of the model. To give full account of the experiments, the Goldhaber-Teller model must be generalized in such a way that spin flip transitions can occur also in the framework of the giant resonance multiplet. This generalization can be made on the basis of the following consideration. It has been shown that collective vibrations of nuclear matter do not involve two fluids only, those of protons and of neutrons, but involve four fluids (55-57), those of protons with spin up ($p\uparrow$), protons with spin down ($p\downarrow$), neutrons with spin up ($n\uparrow$), and neutrons with spin down ($n\downarrow$), and possible modes of nuclear vibrations are given

by the in-phase displacement of any two of these four fluids, vibrating 180° out of phase against the remaining two fluids. Applied to the Goldhaber-Teller picture, one obtains three possible modes of collective vibrations, shown in Fig. 22. Part (a), the original Goldhaber-Teller (GT) mode, will be called isospin vibration (i), part (b) will be called spin-isospin vibration (si), and part (c) will be called spin vibration (s), for obvious reasons. A mode with all four fluids moving in phase is not possible for the dipole deformations of Fig. 22, since it would not leave the center of mass at rest. Such a mode does occur, however, if nuclear matter gets displaced in a monopole or quadrupole deformation, as will be described.

At this point, we should call attention to the distinction to be observed between the multipolarity of the nuclear matter deformation (described by l, the orbital angular momentum quantum number) and the multipolarity of the electromagnetic transition, L in Eqs. (13). For example, Fig. 22 depicts only nuclear dipole deformations, $l = 1^-$; nevertheless, as we shall see, part (b) of Fig. 22 gives rise, among other transitions, to a magnetic quadrupole giant resonance transition, $L = 2^-$, whereas part (a) leads to the usual electric dipole transition, $L = 1^-$, seen in the photonuclear reactions.

A monopole vibration of nuclear matter, $l = 0^+$, can be described by, for example, introducing an oscillating radial scale factor in the ground state charge distribution analogously to Eq. (43a):

$$\rho_0(r) \rightarrow \rho(r) \equiv N\rho_0\,[r(1+\eta)] \approx N\rho_0(r) + \eta r N\rho_0'(r)\,, \tag{50a}$$

and one has to relax the usual assumption of incompressibility of nuclear matter, which introduces a renormalization factor N to preserve conservation of matter as a whole. One can show that this leads to

$$\rho_0(r) \rightarrow \rho_0(r) = \rho_0(r) + \eta\, r^{-2}\frac{d}{dr}\,[r^3\,\rho_0(r)]\,. \tag{50b}$$

The scale factor η (again considered the coordinate of a linear harmonic oscillator which we quantize) is a scalar and thus corresponds to $l = 0^+$, whereas our previous vector $\boldsymbol{d}$, with spherical components

$$d_{1m} \propto Y_{1m}(\hat{d})\,, \tag{51}$$

corresponds to $l = 1^-$. Figure 23 shows the four possible modes of nuclear monopole vibrations: (a) to (c) are again i, si, and s, respectively, whereas (d) is the mode in which all four nucleon fluids vibrate in phase. Since monopole vibrations depend on the nuclear matter being compressible, the eigenfrequencies ω_0 in general will lie higher than the dipole frequencies ω_1. This effect is less pronounced, however, for lighter nuclei. For example, for ^{4}He the 0^+, 20.4-Mev level seen in inelastic electron scattering (35) (dashed curve, Fig. 24) could therefore be interpreted (34) as a breathing-mode level, with a monopole matrix element obtained by using the transition charge density of Eq. (50b), leading to the cross section

$$\frac{d\sigma}{d\Omega} = \sigma_M\,\frac{Z}{R}\left(\frac{1}{2mA\omega_0}\right)^{1/2} q\,\frac{dF(q)}{dq}\,, \tag{52}$$

given in terms of the derivative of the ground state form factor. Figure 25 shows a comparison of this cross section with experiment; the factor 2 by which the theory is too high is not unusual for the collective model.

Collective quadrupole vibrations of nuclear matter, $l = 2^+$, can be described by a deformation of the ground state charge density according to (58)

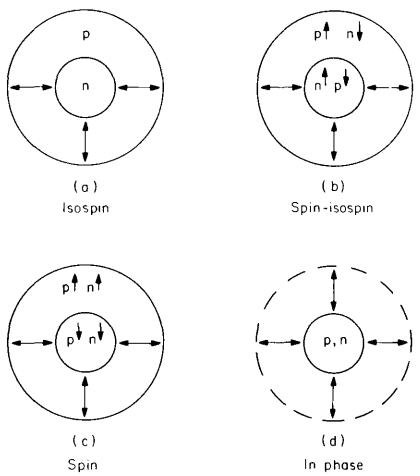

Fig. 23 - Collective monopole vibrations of nuclear matter: modes of the generalized Goldhaber-Teller model

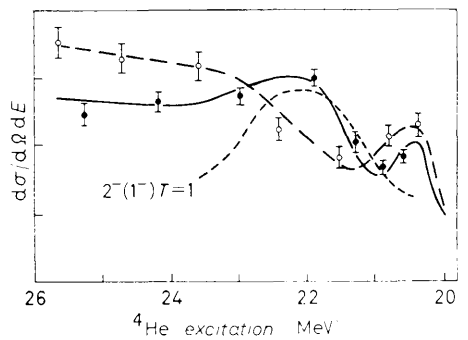

Fig. 24 - Excitation functions of ^{4}He states by inelastic proton scattering (solid curve) and electron scattering (dashed curve). After Ref. 35 (electron scattering) and L. E. Williams, Phys. Rev. Lett. 15:170 (1965) (proton scattering).

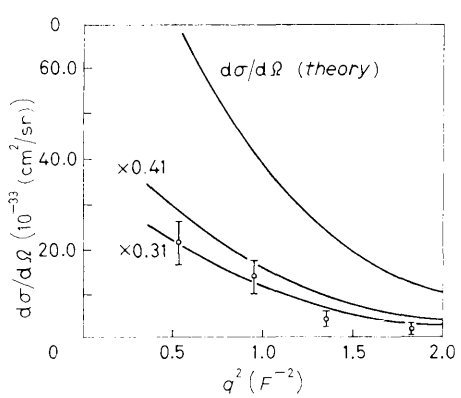

Fig. 25 - Inelastic electron scattering cross section for the 20.4-MeV level in ^{4}He: comparison of experiment with the breathing mode collective model (34)

$$\rho_0(r) \rightarrow \rho_0(\boldsymbol{r}) \equiv \rho_0 \left\{ r \left[1 + \sum_m d_{2m} \, Y_{2m}(\hat{r}) \right] \right\} , \tag{53}$$

expanding again, and using Eqs. (45a) and (45b). The corresponding four modes of collective nuclear vibrations are shown in Fig. 26. We encounter vibrations of ellipsoidal deformations against each other, where for example in the isospin mode (a), the protons prolate at the same time that the neutrons oblate. Again mode (d), where all four fluids prolate and oblate in phase, is possible here.

Going back to the dipole deformation of Eqs. (43) and Fig. 22, we now describe how the Goldhaber-Teller model can be generalized to include spin-isospin vibrations. In quantum mechanics, matrix elements of an operator O can be rewritten in terms of a density matrix ϕ, such that

$$\langle O \rangle = Tr \, \phi \, O . \tag{54}$$

For M_L and T_L^j involving ρ and j, the operator is essentially

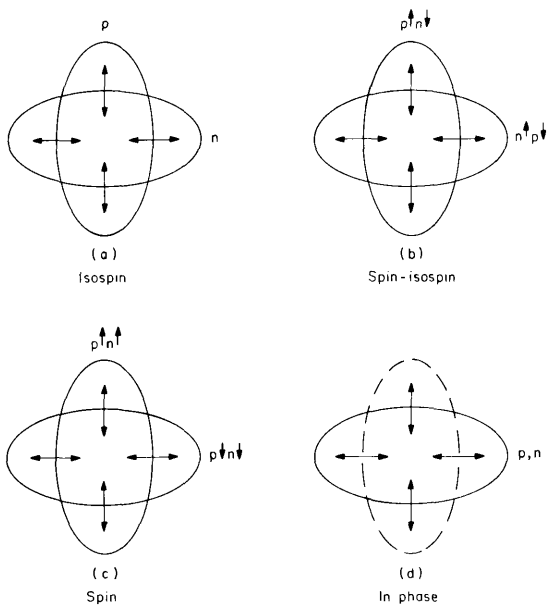

Fig. 26 - Collective quadrupole vibrations of nuclear matter: modes of the generalized Goldhaber-Teller model

$$O \propto \frac{1}{2}(1+\tau_3)\ ; \tag{54a}$$

for T_L^μ, the corresponding operator is, due to Eq. (37c) and Morpurgo's rule, essentially

$$O \propto \tau_3 \boldsymbol{\sigma}\ . \tag{54b}$$

Now we can construct transition density matrices ϕ corresponding to the three dipole modes of Fig. 22. Since $(1+\tau_3)/2$ describes protons, $(1-\tau_3)/2$ describes neutrons, $(1+\sigma_3)/2$ describes nucleons with spin up, and $(1-\sigma_3)/2$ describes nucleons with spin down; then for the isospin mode, the density matrices are simply given by

$$\phi_i = \frac{1}{2}(1+\tau_3)\rho_0\left(\left|\boldsymbol{r} - \frac{1}{2}\boldsymbol{d}\right|\right) + \frac{1}{2}(1-\tau_3)\rho_0\left(\left|\boldsymbol{r} + \frac{1}{2}\boldsymbol{d}\right|\right)\ . \tag{55a}$$

Likewise, for the two other dipole modes, we find

$$\phi_{si} = \left[\frac{1}{2}(1+\tau_3)\frac{1}{2}(1+\sigma_3) + \frac{1}{2}(1-\tau_3)\frac{1}{2}(1-\sigma_3)\right]\rho_0\left(\left|\boldsymbol{r} - \frac{1}{2}\boldsymbol{d}\right|\right) + \left[\frac{1}{2}(1-\tau_3)\frac{1}{2}(1+\sigma_3) + \frac{1}{2}(1+\tau_3)\frac{1}{2}(1-\sigma_3)\right]\rho\left(\left|\boldsymbol{r} + \frac{1}{2}\boldsymbol{d}\right|\right) \tag{55b}$$

and

$$\phi_s = \frac{1}{2}(1+\sigma_3)\rho_0\left(\left|\boldsymbol{r} - \frac{1}{2}\boldsymbol{d}\right|\right) + \frac{1}{2}(1-\sigma_3)\rho_0\left(\left|\boldsymbol{r} + \frac{1}{2}\boldsymbol{d}\right|\right)\ . \tag{55c}$$

Expanding, we get

$$\phi_i \approx -\frac{1}{4}\tau_3\,\boldsymbol{d}\cdot\boldsymbol{\nabla}\rho_0(r)\ , \tag{56a}$$

$$\phi_{si} \approx -\frac{1}{4}\tau_3\sigma_3\,\boldsymbol{d}\cdot\boldsymbol{\nabla}\rho_0(r)\ , \tag{56b}$$

and

$$\phi_s \approx -\frac{1}{4}\sigma_3\,\boldsymbol{d}\cdot\boldsymbol{\nabla}\rho_0(r)\ . \tag{56c}$$

These equations are worth studying. First, we note that the present model is an LS coupling model, since the orbital angular momentum operators $\boldsymbol{d} \propto Y_{1m}(\hat{d})$ and the spin operators σ_3 occur in factorized form. Second, we see that ϕ_i gives rise to $\Delta T = 1$, $\Delta S = 0$ transitions, ϕ_{si} to $\Delta T = 1$, $\Delta S = 1$ transitions, and ϕ_s to $\Delta T = 0$, $\Delta S = 1$ transitions, besides the $\Delta l = 1^-$ transition that is common to all three. The changes in l and S will of course combine to a total angular momentum change ΔL which gives the multipolarity of

the electromagnetic transition. For i, one has therefore $\Delta T = 1$, $\Delta L = 1^-$; for si, one has $\Delta T = 1$, $\Delta L = 0^-, 1^-, 2^-$; and for s, one has $\Delta T = 0$, $\Delta L = 0^-, 1^-, 2^-$. Starting with 0^+, $T = 0$ ground state of a self-conjugate nucleus, one thus arrives at the giant resonance multiplet created by a collective dipole vibration, $l = 1^-$, of the nuclear matter shown in Table 4. Here, L is the multipolarity of the electromagnetic transition, but is also equal to J, the spin of the various giant resonance levels, since $J_0 = 0$. N is the number of states (including the $T_3 = \pm 1$ components in the neighboring nuclei). The entire multiplet of Table 4, which is degenerate in energy to lowest order, is an example (59) of an $SU4$ multiplet of Wigner's theory of nuclear supermultiplets (60). If the nuclear forces are spin and charge independent (which is approximately satisfied in practice), the nuclear Hamiltonian is invariant not only under the $SU2$ subgroups of spin and isospin but under the full Lie group, $SU4$, in which a vector operator has the 15 components

$$T_\alpha = \frac{1}{2} \sum_i \tau_i^\alpha w_i , \tag{57a}$$

$$Y_\lambda^\alpha = \frac{1}{2} \sum_i \tau_i^\alpha \sigma_{\lambda i} w_i , \tag{57b}$$

and

$$S_\lambda = \frac{1}{2} \sum_i \sigma_{\lambda i} w_i . \tag{57c}$$

Table 4
The Giant Resonance Multiplet of a Self-Conjugate Nucleus, Corresponding to Dipole Vibrations of Nuclear Matter (Shown in Fig. 22)

Mode	T	l	S	$L = J$	N
i	1	1^-	0	1^-	3
si	1	1^-	1	$0^- 1^- 2^-$	9
s	0	1^-	1	$0^- 1^- 2^-$	3
Dimension of supermultiplet:					15

(The factor w_i is an arbitrary function of r_i; setting $w = 1$, we obtain the generators of $SU4$.) Our matrix elements of Eqs. (16) are just given by these operators, and the density matrices of the generalized Goldhaber-Teller model, Eqs. (56), are directly related to them. The giant resonance states are generated by an application of Eqs. (57) on the 0^+ ground state, and are thus degenerate; the values of T_α and S_λ can be used for classifying the individual levels in the fashion of Table 4. In practice, the nuclear forces are spin dependent, the symmetry under $SU4$ will only be approximate, and, as a consequence, the levels corresponding to the different modes, and also to different spins J, are split up. The Goldhaber-Teller model does not provide any of the level energies, and these have thus to be taken from experiment, or from a particle-hole calculation as described in a later section.

Similar supermultiplets appear for the monopole or quadrupole vibrations of nuclear matter. They are shown in Tables 5 and 6 respectively. If we now, again for the giant resonance of dipole vibrations, use the density matrices of Eqs. (56) to calculate our matrix elements M_L and T_L, using Eqs. (54), we see immediately that M_L and T_L^j will receive contributions from only the isospin mode (i) and that T_L^μ will receive contributions

Table 5
The Supermultiplets of a Self-Conjugate Nucleus, Corresponding to Monopole Vibrations of Nuclear Matter (Shown in Fig. 23)

Mode	T	l	S	$L = J$	N	Dimension
i	1	0^+	0	0^+	3	
si	1	0^+	1	1^+	9	15
s	0	0^+	1	1^+	3	
(d)	0	0^+	0	0^+	1	1

Table 6
The Supermultiplets of a Self-Conjugate Nucleus, Corresponding to Quadrupole Vibrations of Nuclear Matter (Shown in Fig. 26)

Mode	T	l	S	$L = J$	N	Dimension
i	1	2^+	0	2^+	3	
si	1	2^+	1	$1^+\ 2^+\ 3^+$	9	15
s	0	2^+	1	$1^+\ 2^+\ 3^+$	3	
(d)	0	2^+	0	2^+	1	1

from only the spin-isospin (si) mode. Due to the Gell-Mann-Telegdi and Morpurgo rules, the spin-wave mode (s) will not appreciably contribute to electromagnetic transitions (and neither to muon or radiative pion capture or to neutrino absorption, which all contain $\tau_\pm$, related to τ_3 by the Wigner-Eckart theorem, but this mode will and does contribute to excitations by protons, etc., where no such selection rules apply: cf. the solid curve in Fig. 24 in which the 22.2-MeV level of ^{4}He, excited by protons, but not electrons, can be identified as the $T = 0$, 2^- spin wave level). Calculating the spin-flip reduced matrix elements, we find

$$\begin{aligned} \langle 2^- \| T_2^{m\mu} \| 0 \rangle &= i \langle 1^- \| T_1^{e\mu} \| 0 \rangle \\ &= -i \frac{q^2}{m} \frac{\mu_p - \mu_n}{2} \frac{F(q)}{4\pi} \left(\frac{2\pi}{Am\,\omega_1} \right)^{1/2} \end{aligned} \tag{58}$$

Comparing Eq. (58) with Eqs. (49), we notice the additional factor (q/m). This factor causes the spin-flip transitions to be negligibly small for photon transitions, i.e., a small $q = \omega$. However, for electron scattering at 180° (to remove the dominant Coulomb transition, given by Eq. (49a), which would mask the spin flip transitions), and increasing the momentum transfer q to high values, the spin-flip terms, Eq. (58), will rise up strongly at the same time that the convection-current terms, Eq. (49), actually go down. In fact, it is by this method that the spin-isospin members of the giant resonance supermultiplet have first been identified (61). Figure 27 shows (47) the giant resonance in ^{12}C from photonuclear reactions ($q = \omega \approx 25$ MeV/c), whereas Fig. 28 presents (61) the same states as excited by 65-MeV electrons at 180°, i.e., $q \approx 105$ MeV/c. One notices the new state at approximately 19.5 MeV in electron scattering, and also a relatively higher rising bump at approximately 26 MeV compared to the photonuclear case. The 22.5-MeV

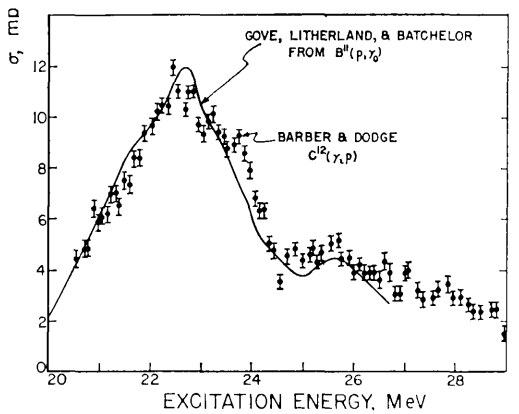

Fig. 27 - The giant resonance in ^{12}C, from (γ, p) and (p, γ_0) photonuclear experiments. (After Hayward (47).) The (γ, p) data are from W. R. Dodge and W. C. Barber, Phys. 127:1746 (1962), and the (p, γ_0) data are from H. E. Gove et al., Nucl. Phys. 26:480 (1961).

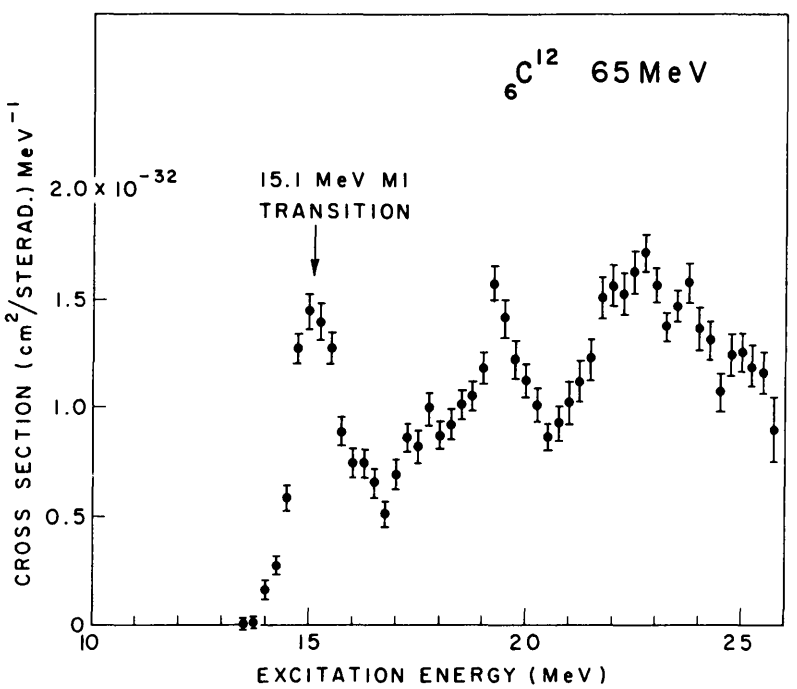

Fig. 28 - The giant resonance in ^{12}C, from inelastic scattering of 65-MeV electrons at 180° (61)

state, practically the only seen in photoexcitation, is thus explained as the $J = 1^-$ isospin state, the Goldhaber-Teller giant dipole resonance. The new states at 19.5 and 26.0 MeV are interpreted as the $J = 2^-$ and 1^- components of the spin-isospin mode of the giant resonance. The Goldhaber-Teller expressions of the cross sections could be fitted to these states nicely (62); see Fig. 29, which shows for 180° electron scattering by ^{12}C the relative decrease of the i state and increase of the si states with increase of primary energy. In this figure the widths of the states were calculated using particle-hole wave functions of the giant resonance states given by Gillet (63); these particle-hole calculations will be described in a later section. Noteworthy here is that the particle-hole model tends to give a similar quantitative picture of the i and si levels in self-conjugate nuclei, and similar behavior under variations of q (except that the theoretical values are generally too high by a factor of 2). The 2^- level at 19.5 MeV in ^{12}C was recently remeasured

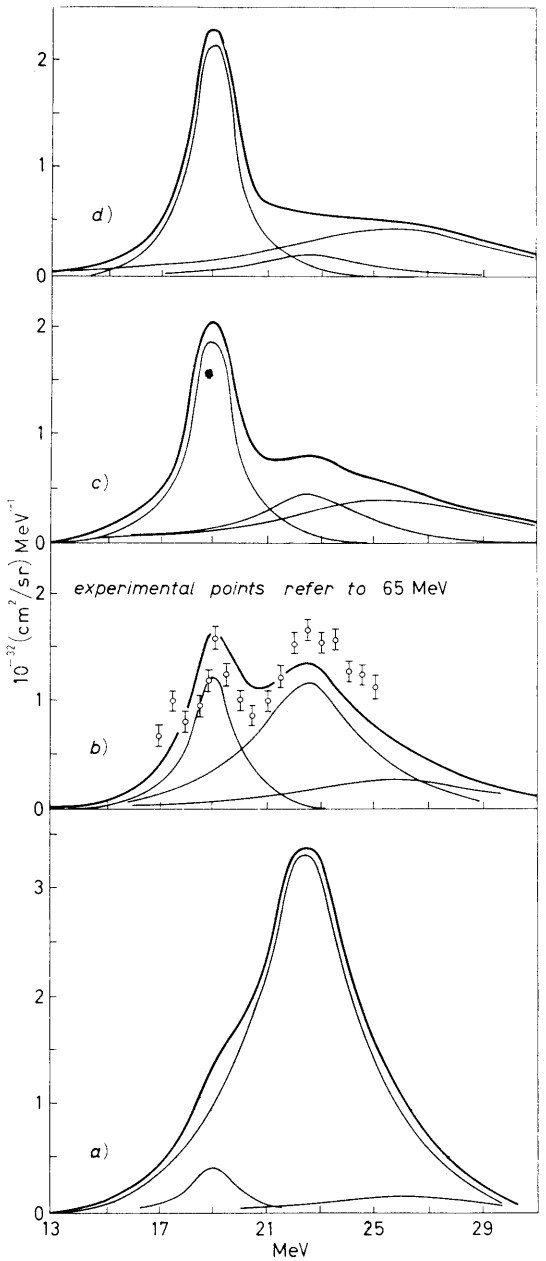

Fig. 29 - Electroexcitation cross sections of the giant resonances in ^{12}C at θ = 180° and for various primary energies: (a) k_1 = 40 MeV, (b) k_1 = 60 MeV, (c) k_1 = 80 MeV, and (d) k_1 = 100 MeV. The curves are from the generalized Goldhaber-Teller model (62); the data points are from Ref. 61.

by the Saskatchewan group, as well as (64) a corresponding 2^- level in ^{16}O; Fig. 30 presents the first matrix element of Eq. (58) for the latter, calculated by a particle-hole model and compared with experiments. One sees the rise of the form factor with q, but a later decline at very high q and a passage through zero (due to the Born approximation).

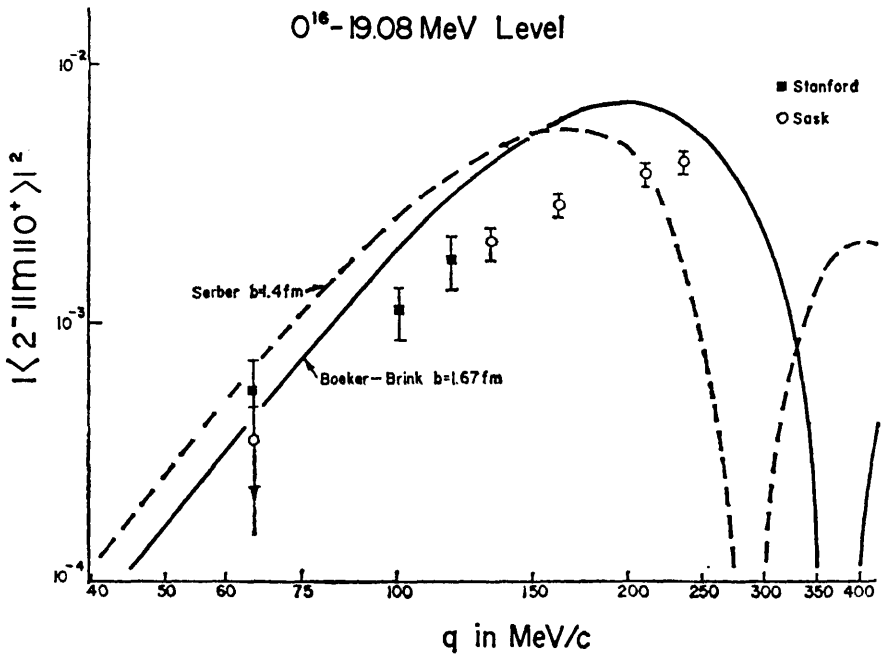

Fig. 30 - Squared matrix element for the transition $0^+ \rightarrow 2^-$ to the 19.08-MeV level in ^{16}O. The data are from Ref. 64, and from Ref. 65 and G. J. Vanpraet and W. C. Barber, Nucl. Phys. 79:550 (1966).

The 1^- si level at 26.0 MeV in ^{12}C (Fig. 27) still seems to be present in photoexcitation ($q = \omega$), although from the Goldhaber-Teller model it should be practically absent. (The corresponding 1^- si level at 25.0 MeV in ^{16}O persists at $q = \omega$ to an even much stronger degree.) The explanation may be the presence of an LS coupling (due to the spin dependence of the nuclear forces) which mixes isospin and spin-isospin levels and thus adds an isospin component to the spin-flip state. The particle-hole calculations which take spin dependence into account, should thus predict a certain photoexcitation strength of the 25- to 26-MeV 1^- levels. For ^{16}O this comes out quite satisfactorily, whereas for ^{12}C, no strength is yet found (63). In this special case, one has invoked (66, 67) the presence of a coupling of the giant resonance vibration to a collective nuclear surface vibration (2^+); the surface vibration by itself produces for example the 4.43-MeV 2^+ first excited state of ^{12}C. A similar 2^+ vibration should sit on top of the 22-MeV 1^- giant dipole (i) level, and thus cause the 26-MeV 1^- state. What is seen in photoexcitation is thus the latter dipole-surface state and not the 1^- si state (which is situated at about the same energy, and does rise with increasing q in electron scattering). Such coupled giant resonance, surface quadrupole states have also been discussed (68) for electron scattering in ^{12}C.

An application of the model of collective quadrupole vibrations corresponding to Fig. 26 has been made (58) for the positive parity states in ^{16}O. The energies of these states were taken from a particle-hole calculation (69). It was shown that these collective

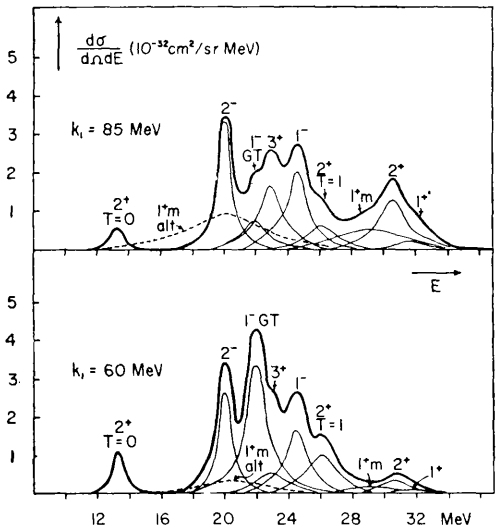

Fig. 31 - Theoretical electroexcitation cross sections of collective dipole (0^-, 1^-, 2^-) and quadrupole (1^+, 2^+, 3^+) states in ^{16}O for primary electron energies of 60 and 85 MeV and θ = 180° (58)

quadrupole states may attain considerable strength (Fig. 31), especially at large q, and may be able to explain the observed fine structure in the giant resonance region of ^{16}O as observed in 180° electron scattering (65) (Fig. 32).

The Steinwedel-Jensen Model

The Steinwedel-Jensen collective model leads to predictions rather similar to those of the Goldhaber-Teller model, although its assumptions are quite different. We should also note that, as in the original Goldhaber-Teller model, only the isospin vibration, Fig. 22a, has been considered so far in this model, but the inclusion of spin and spin-isospin modes should be straightforward, at least for the case $Z = N$.

For the isospin mode, one considers the two fluids of protons and neutrons (and assumes generally that $Z \neq N$). They are

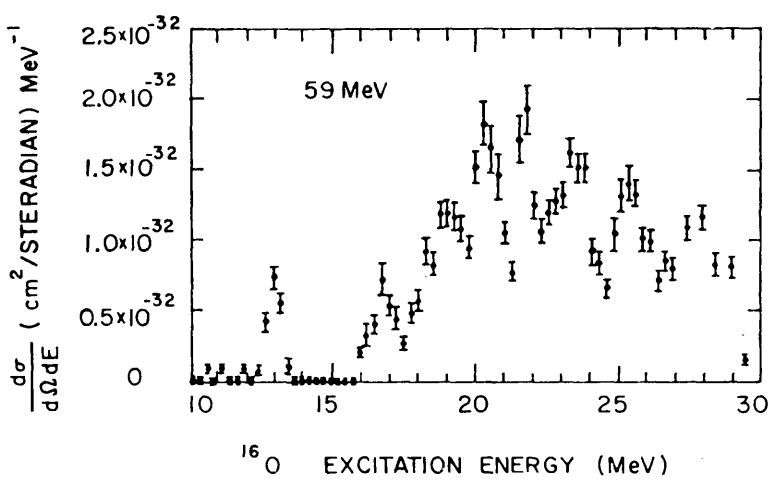

Fig. 32 - Fine structure in the experimental electroexcitation cross section for ^{16}O in the giant resonance region, with an incident electron energy of 59 MeV and θ = 180°. (The data are from Ref. 65.)

allowed to move against each other but within the confines of a rigid spherical nuclear surface (70). The total nucleon density ρ_0 is assumed constant within this sphere (and zero outside); in the ground state we have

$$\rho_p^0 + \rho_n^0 = \rho_0 , \tag{59a}$$

where

$$\rho_p^0 = \frac{Z}{A}\rho_0 \text{ and } \rho_n^0 = \frac{N}{A}\rho_0 . \tag{59b}$$

For the state of collective motion, we write the nucleon densities as

$$\rho_p(\mathbf{r}, t) = \rho_p^0 + \eta(\mathbf{r}, t) \tag{59c}$$

and

$$\rho_n(\mathbf{r}, t) = \rho_n^0 - \eta(\mathbf{r}, t) , \tag{59d}$$

which still makes them add up to ρ_0,

$$\rho_p(\mathbf{r}, t) + \rho_n(\mathbf{r}, t) = \rho_0 , \tag{59e}$$

but we may have proton or neutron enrichment on opposite sides of the nucleus. The total density may be normalized such that

$$\frac{4\pi}{3} r_0^3 \rho_0 = 1 , \qquad r_0 = 1.4 \times 10^{-13} \text{ cm} . \tag{60}$$

The flow velocities of the p and n fluids are $\mathbf{v}_p(\mathbf{r}, t)$ and $\mathbf{v}_n(\mathbf{r}, t)$, and we shall work with the relative flow velocity

$$\mathbf{v}(\mathbf{r}, t) = \mathbf{v}_p(\mathbf{r}, t) - \mathbf{v}_n(\mathbf{r}, t) , \tag{61a}$$

whereas the velocity of the center of mass must vanish:

$$\frac{\rho_n \mathbf{v}_n + \rho_p \mathbf{v}_p}{\rho_0} = 0 . \tag{61b}$$

The usual assumption is to consider the relative velocity to be curl-free, i.e.,

$$\nabla \times \mathbf{v} = 0 , \qquad \mathbf{v} = -\nabla \phi(\mathbf{r}, t) , \tag{61c}$$

introducing a velocity potential $\phi(\mathbf{r}, t)$. A reduced density may also be considered,

$$\rho_r = \frac{\rho_p \rho_n}{\rho_0} \approx \frac{\rho_p^0 \rho_n^0}{\rho_0} , \tag{61d}$$

since we have introduced relative and center-of-mass variables. Then the kinetic energy of the collective motion is given by

$$T = \int d^3r \left(\frac{1}{2} m \rho_0 \mathbf{V}^2 + \frac{1}{2} m \rho_r \mathbf{v}^2 \right) = \int d^3r \, \frac{1}{2} m \rho_r \mathbf{v}^2 , \tag{62}$$

m being the nucleon mass. A potential energy U, whose minimum is given when the proton and neutron fluids interpenetrate uniformly, may be obtained from the nuclear symmetry energy (9)

$$E_s = K \left(\frac{N - Z}{A} \right)^2 \tag{63a}$$

with an empirically obtained constant $K \approx 24$ MeV. This indicates that finite nuclei tend to have $N = Z$; however, we assume that it is also true for the nucleon densities to tend toward $\rho_n = \rho_p$, so that a symmetry energy density is obtained:

$$K\left(\frac{\rho_n - \rho_p}{\rho_0}\right)^2 \rho_0 , \tag{63b}$$

with an equilibrium value $K(\rho_n^0 - \rho_p^0)^2/\rho_0$. The Lagrangian $L = U - T$ then becomes

$$L = \int d^3r \left[K \frac{(\rho_p - \rho_n)^2}{\rho_0} - \frac{1}{2} m \rho_r \mathbf{v}^2\right] . \tag{64}$$

Using Eq. (61c), Steinwedel and Jensen (70) show that one can express

$$\frac{\rho_p - \rho_n}{\rho_0} = \frac{m}{4K} \dot{\phi} , \tag{65}$$

so that the Lagrangian

$$L = \int d^3r \left[\frac{\rho_0 m^2}{16K} \dot{\phi}^2 - \frac{m}{2} \rho_r (\nabla\phi)^2\right] \tag{66a}$$

is now expressed in terms of the variables ϕ and $\dot{\phi}$. A subsidiary condition is provided by the equation of continuity, which we can write as

$$\frac{\partial\eta}{\partial t} + \rho_r \nabla \cdot \mathbf{v} = 0 . \tag{66b}$$

The equation of motion for the collective vibration is obtained by subjecting L to the Euler-Lagrange equation,

$$\frac{\partial L}{\partial \phi} - \frac{d}{dt} \frac{\partial L}{\partial \dot{\phi}} = 0 . \tag{67a}$$

We have

$$\frac{\partial L}{\partial \phi} = \frac{m}{2} \rho_r \frac{\partial}{\partial \phi} \int \phi \nabla^2 \phi \, d^3r = m\rho_r \int \nabla^2 \phi \, d^3r , \tag{67b}$$

and

$$\frac{d}{dt} \frac{\partial L}{\partial \dot{\phi}} = \int \frac{\rho_0 m^2}{8K} \ddot{\phi} \, d^3r , \tag{67c}$$

so that Eq. (67a) gives

$$\ddot{\phi} - \frac{8K}{m} \frac{\rho_r}{\rho_0} \nabla^2 \phi = 0 . \tag{67d}$$

Using $\rho_r/\rho_0 = NZ/A^2$ and the continuity equation, we find

$$\left(\frac{\partial^2}{\partial t^2} - \frac{8K}{m} \frac{NZ}{A^2} \nabla^2\right) \eta(\mathbf{r}, t) = 0 , \tag{68}$$

which is a wave equation for the excess density $\eta(\mathbf{r}, t)$. Assuming a harmonic solution

$$\eta(\mathbf{r}, t) = \psi(\mathbf{r}) e^{i\omega t} , \tag{69}$$

and using the boundary condition $v_r = 0$ at $r = R \equiv r_0 A^{1/3}$ (since there should be no outflow through the rigid spherical nuclear surface), i.e.,

$$\left.\frac{\partial \eta}{\partial r}\right|_{r=R} = 0 , \tag{70}$$

one finds the set of normal mode solutions labeled by lmn:

$$\eta_{lmn}(\mathbf{r}, t) = e^{i\omega_{ln}t} \psi_{lmn}(\mathbf{r}) \tag{71a}$$

and

$$\psi_{lmn} = A_{lmn}\, j_l(k_{ln} r)\, Y_{lm}(\hat{r}), \tag{71b}$$

with a normalization factor

$$A_{lmn} = \frac{1}{j_l(k_{ln}R)} \left[\frac{1}{2} R^3 \left(1 - \frac{l(l+1)}{k_{ln}^2 R^2}\right)\right]^{-1/2} \tag{71c}$$

This set of solutions was obtained by setting $\omega_{ln} = k_{ln} u$ in Eq. (69) and inserting it in Eq. (68), which becomes

$$(\nabla^2 + k_{ln}^2)\, \psi_{lmn} = 0 . \tag{71d}$$

We then have

$$u^2 = \frac{8K}{m} \frac{NZ}{A^2} , \tag{71e}$$

where, from the definition $u = \omega_{ln}/k_{ln}$, u may be called the velocity of sound in nuclear matter. The eigenvalues k_{ln} are fixed by the boundary condition,

$$\frac{d}{dr}\, j_l(k_{ln} r)\,|_{r=R} = 0 , \tag{72}$$

which for a given l has roots labeled by $n = 0, 1, 2, \ldots$. The complete set of functions, Eqs. (71), now may be used to quantize the model. We expand the generalized coordinate ϕ in terms of normal modes,

$$\phi(\mathbf{r}) = \sum_{mn} q_{lmn} \psi_{lmn}(\mathbf{r}), \tag{73a}$$

and likewise, we expand the canonically conjugate momenta

$$\pi(\mathbf{r}) = \frac{\partial \mathfrak{L}}{\partial \dot{\phi}} = \frac{\rho_0 m^2}{8K} \dot{\phi} \tag{73b}$$

(where $L = \int \mathfrak{L}\, d^3r$):

$$\pi(\mathbf{r}) = \sum_{lmn} p_{lmn} \psi^*_{lmn}(\mathbf{r}). \tag{73c}$$

The Hamiltonian is given by

$$H = \int (\pi\dot{\phi} - \mathfrak{L})\, d^3r = \int d^3r \left[\frac{4K}{\rho_0 m^2} \pi^2 + \frac{m\rho_r}{2} (\nabla\phi)^2\right] . \tag{74}$$

The quantization proceeds by postulating the commutation properties

$$[\phi(\mathbf{r}), \phi(\mathbf{r}')] = [\pi(\mathbf{r}), \pi(\mathbf{r}')] = 0$$

and (75)

$$[\phi(\mathbf{r}), \pi(\mathbf{r}')] = i\hbar\,\delta(\mathbf{r} - \mathbf{r}') .$$

If we introduce creation and annihilation operators $a^\dagger_{lmn}$ and a_{lmn} in the usual way, namely,

$$q_{lmn} = \left(\frac{\hbar}{2\mu\,\omega_{ln}}\right)^{1/2} \left[a_{lmn} + (-1)^m a^\dagger_{l-mn}\right]$$

and (76a)

$$p_{lmn} = i\left(\frac{\mu\hbar\,\omega_{ln}}{2}\right)^{1/2} \left[a^\dagger_{lmn} - (-1)^m a_{l-mn}\right] ,$$

with

$$\mu = \rho_0 m^2/8K , \tag{76b}$$

we find that they satisfy the usual commutation rules

$$\left[a_{lmn}, a_{l'm'n'}\right] = \left[a^\dagger_{lmn}, a^\dagger_{l'm'n'}\right] = 0$$

and (76c)

$$\left[a_{lmn}, a^\dagger_{l'm'n'}\right] = \delta_{ll'}\,\delta_{mm'}\,\delta_{nn'} .$$

and the Hamiltonian becomes as usual

$$H = \sum_{mn} \hbar\,\omega_{ln} \left[a^\dagger_{lmn}\, a_{lmn} + \frac{1}{2}\right] . \tag{77}$$

We introduce a complete system of state vectors on which the a_{lmn} operate; the ground state is designated by $|0\rangle$, and the excited states are given by

$$|lmn\rangle = a^\dagger_{lmn}|0\rangle . \tag{78a}$$

The giant dipole state is represented by one collective phonon in the lowest state of excitation, $n = 0$:

$$|1m0\rangle = a^\dagger_{1m0}|0\rangle , \tag{78b}$$

having (orbital) angular momentum $l = 1^-$. Its energy is given by the first node, $n = 0$, of Eq. (72) with $l = 0$:

$$\hbar\,\omega_{10} = \frac{\hbar u}{R}\,(k_{10}R) , \qquad k_{10}R = 2.08 ; \tag{79a}$$

thus

$$\hbar\,\omega_{10} = 2.08\,\frac{\hbar}{R}\left(\frac{8K}{m}\,\frac{NZ}{A^2}\right)^{1/2} . \tag{79b}$$

Using $K \approx 24$ MeV from the nuclear symmetry energy, Eq. (79b) checks reasonably well with experimental energies of giant resonances. Note that $\hbar\omega_{10}$ behaves like $A^{-1/3}$ as a

function of nuclear mass number. A recent theory of Werntz and Bach (71), which replaces the sharp nuclear radius of the Steinwedel-Jensen model by a gradual density falloff, arrives at $\hbar\omega_{10} \propto A^{-1/6}$, however, a behavior which seems to fit the experimental giant dipole resonance energies throughout the entire periodic system.

One may now calculate (72) $T_{1M}^{ej}(q)$, the transverse matrix element that governs 180° electron scattering, using

$$\boldsymbol{j} = \rho_p \mathbf{v}_p \approx -\rho_r \nabla\phi , \tag{80}$$

with the result

$$|\langle 1-| \; |T_1^{ej}(q)| \; |0\rangle|^2 = 24\left(\frac{\hbar}{mc}\right)^2 \rho_0 R^2 K \left(\frac{NZ}{A^2}\right)^2 \frac{1}{\hbar\omega_{10}} \left[\frac{A_{100}}{q} j_1(qR) \; j_1(k_{10}R)\right]^2 . \tag{81}$$

This gives the q dependence of the excitation strength of the 1^- giant dipole state (isospin mode), as it may be measured in 180° electron scattering. One finds a decreasing function of q, quite similar to the result of the Goldhaber-Teller mode (isospin mode), Eq. (49b), and only about 20% lower than the latter. Both curves will be plotted later in the report, together with the results of the particle-hole model. It is remarkable that the two collective models, based on rather different assumptions, lead to similar results.

We wish to repeat that the existing version of the Steinwedel-Jensen model includes the isospin mode of collective vibrations only. An extension of the model to include spin-isospin and spin modes in the same way as this was done in the Goldhaber-Teller model is probably quite straightforward for $Z = N$, but seems difficult for $Z \neq N$. However, only in the latter case, namely for heavy nuclei, would this make any sense, since due to the assumption of a sharp nuclear surface made in the Steinwedel-Jensen model the applicability of this model to light nuclei seems questionable.

The Steinwedel-Jensen Model for a Deformed Nucleus

The Steinwedel-Jensen model was generalized to the case of deformed nuclei by Danos (73). The result is that the (isospin) giant resonance gets split into two components. One may again solve the wave equation,

$$(\nabla^2 + k^2)\psi = 0 , \tag{82a}$$

and one may, for the sake of greater generality, introduce friction into the collective motion via a damping constant Γ:

$$k^2 = \frac{u^2}{\omega^2}\left(1 - \frac{i\Gamma}{\omega}\right) . \tag{82b}$$

The boundary condition on the nuclear surface is again

$$\boldsymbol{n} \cdot \nabla\psi(\boldsymbol{r})\,|_{\mathrm{surf}} = 0 , \tag{82c}$$

which leads again to the eigenvalues of k. As we saw before, for a spherical surface the eigenvalue for the lowest dipole mode is $kR = 2.08$. If Eq. (82c) is applied to a spheroidal surface, however, described by the equation

$$R = R_0\left[1 + \Sigma\alpha_m Y_{2m}^*(\hat{r})\right] , \tag{82d}$$

the eigenvalues will change, and they will also differ among themselves depending on whether $m = 0$ or $m = \pm 1$. Geometrically, this means the collective oscillation takes place along the major, or along a minor, axis. As a function of the deformation parameter

$$\epsilon = \frac{a^2 - b^2}{R^2} , \tag{83}$$

where a and b are the half axes and R is the radius of a sphere with equal volume, ($R^3 = ab^2$), Danos finds the eigenvalues ka or kb as shown in Figs. 33 and 34. For $\epsilon = 0$, both eigenvalues start out at 2.08, of course. They can be approximated by the equation

$$\frac{\omega_b}{\omega_a} \approx 0.911 \frac{a}{b} + 0.089 . \tag{84}$$

The splitting between ω_b and ω_a is thus positive ($\omega_b > \omega_a$) for $a > b$, i.e., for a prolate spheroid, and negative for an oblate spheroid. This means that in the direction of a longer axis, the oscillation proceeds more slowly. If the resonance is excited by incident photons polarized along the a axis, one will see only one peak at the frequency ω_a; similarly for polarization parallel to the b axis, a peak at ω_b is seen. For randomly oriented nuclei, however, the total cross section is given by

$$\sigma(E) = \frac{1}{3} \sigma_a(E) + \frac{2}{3} \sigma_b(E) , \tag{85a}$$

which shows that the b peak contains about twice the area of the a peak; the ratio of the peak heights are given by

$$\frac{(\sigma_a)_{max}}{(\sigma_b)_{max}} = \frac{\Gamma_a}{2\Gamma_b} . \tag{85b}$$

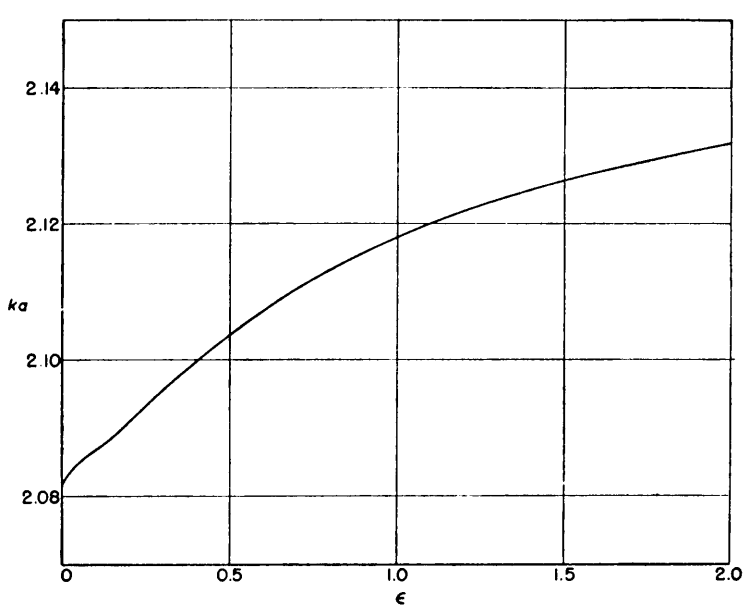

Fig. 33 - Eigenvalue ka in the deformed Steinwedel-Jensen model as a function of the deformation ϵ (73)

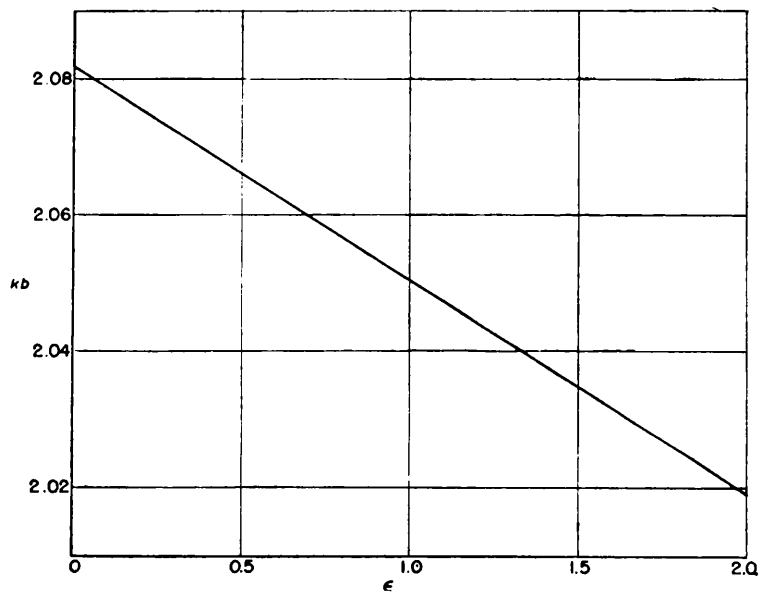

Fig. 34 - Eigenvalue kb in the deformed Steinwedel-Jensen model as a function of the deformation ϵ (73)

If therefore the peak with the larger area is found to lie in energy above the other peak, the nucleus has the form of a prolate spheroid.

An example of the (γ, n) cross section for deformed nuclei is shown in Fig. 35, for the nuclei of holmium and erbium.

In many cases, however, the situation becomes more complicated due to the coupling between giant resonance and surface collective vibrations as will be discussed in the next section.

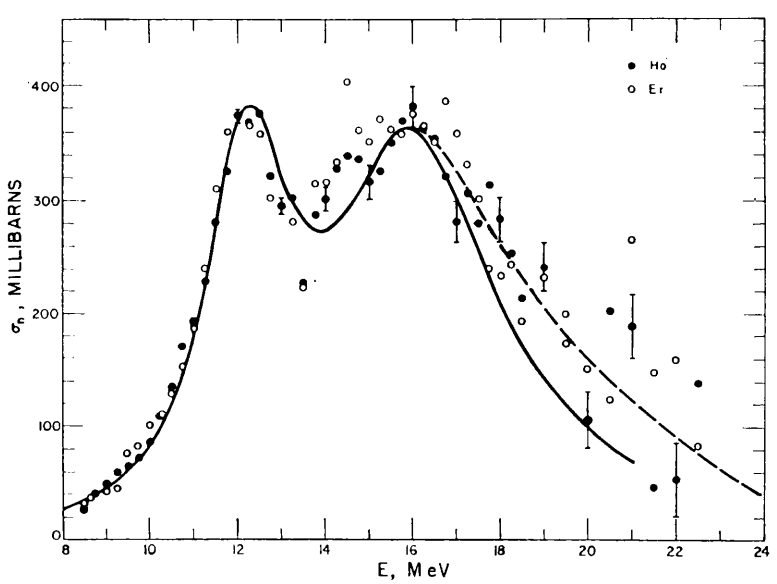

Fig. 35 - Neutron yield data for the (γ, n) reaction in the deformed nuclei of holmium and erbium. The solid curve is the sum of two Lorentz lines, the dashed curve is a fit-by-eye drawn through the data. (After Ref. 85.)

COUPLING OF GIANT RESONANCE AND SURFACE VIBRATIONS

Le Tourneux (74), as well as Greiner and collaborators (75,76) generalized the Steinwedel-Jensen model further by assuming that the nuclear surface which encloses the nucleon fluids is not rigid but may undergo (slow) vibrations itself while the nucleon fluids carry out the giant dipole oscillations. A coupling between the surface and the dipole oscillations results which often considerably influences the shape of the giant resonance curves. Greiner et al. call this the "dynamic collective theory." Later on (65), to treat light nuclei to which the Steinwedel-Jensen model does not apply, they describe the giant resonances by the particle-hole model while they still treat the surface vibrations collectively. This procedure they termed "collective correlations." Initially deformed (75) and spherical (76) nuclei have to be treated separately, and we shall here only sketch the dynamic collective theory for spherical nuclei (76).

It is well-known that many low-lying states of spherical nuclei (≈ 100 to 1000 keV) can be described by collective nuclear surface vibrations (77) in which the originally spherical nuclear surface becomes

$$R = R_0 \left[1 + \sum_{\lambda\mu} \alpha_{\lambda\mu} Y^*_{\lambda\mu}(\hat{r}) \right] ; \tag{86a}$$

in the main, these are quadrupole vibrations with $\lambda = 2$. The displacement coordinates $\alpha_{\lambda\mu}$ are, in the classical case, harmonic functions of time. Bohr and Mottelson expand the Hamiltonian in powers of $\alpha_{\lambda\mu}$ and get

$$H_{\text{surf}} = \frac{1}{2} \sum_{\lambda\mu} \left(B_\lambda |\dot{\alpha}_{\lambda\mu}|^2 + C_\lambda |\alpha_{\lambda\mu}|^2 \right) , \tag{86b}$$

since the restoring force is proportional to the deformation and hence to $\alpha_{\lambda\mu}$, while the kinetic energy gives us the square of the velocity, i.e., $\dot{\alpha}^2_{\lambda\mu}$. If $\alpha_{\lambda\mu}$ is taken as a generalized coordinate, the canonically conjugate momentum is given by

$$\pi_{\lambda\mu} = B_\lambda \dot{\alpha}^*_{\lambda\mu} , \tag{86c}$$

so that we can also write

$$H_{\text{surf}} = \frac{1}{2} \sum_{\lambda\mu} \left(\frac{1}{B_\lambda} |\pi_{\lambda\mu}|^2 + C_\lambda |\alpha_{\lambda\mu}|^2 \right) . \tag{86d}$$

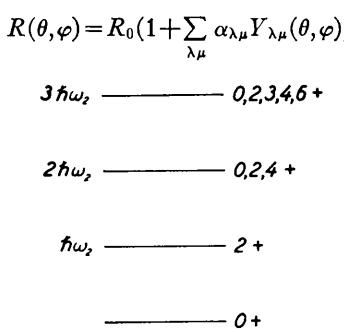

Fig. 36 - Quadrupole vibrational spectrum for even-even nuclei with a spherical equilibrium shape (2)

This system may be quantized by postulating commutation relations between $\pi_{\lambda\mu}$ and $\alpha_{\lambda\mu}$, and the energy of the harmonic oscillator is given by

$$\hbar\omega_\lambda = \hbar(C_\lambda/B_\lambda)^{1/2} . \tag{86e}$$

Figure 36 shows the possible spectrum. Two phonons with $\lambda = 2^+$ each can couple to 0^+, 2^+, and 4^+ only, since in the principal axis system (78), $\alpha_{\lambda\pm1} = 0$ (no off-diagonal moments of inertia exist). In practice, the levels will not be equally spaced, and the degeneracies will be removed.

Since $\omega_{\text{surf}} \lesssim$ some MeV and $\omega_{\text{gi. dip.}} \approx 20$ MeV, we see that the giant dipole vibrations proceed at least

20 times faster than the surface vibrations, and one may make the approximation that effectively the dipole vibrations proceed in a deformed nucleus whose deformation changes adiabatically. Using this approximation, one may use a dipole Hamiltonian of a deformed nucleus, such as in the model of Danos, whose deformation depends on the amplitude of the surface vibrations, $\alpha_{2\mu}$. Thus, in the Hamiltonian, one will have terms that depend both on the Steinwedel-Jensen amplitudes a_{lmn} (with $l = 1$) of the giant dipole vibrations, and the $\alpha_{2\mu}$ of the surface quadrupole vibrations, i.e., coupling or "surface-dipole interaction" terms. The total Hamiltonian is given by

$$H = H_{\mathrm{dip}} + H_{\mathrm{surf}} + H_{\mathrm{int}}, \tag{87a}$$

where H_{dip} describes the free (spherical) dipole oscillations, H_{surf} describes the free surface oscillations, and H_{int} describes the surface-dipole interaction. The interaction term was worked out by Urbas and Greiner (79); its general form (not in lowest order in the phonon creation operators!) is fixed by rotational symmetry and parity conservation, and we have

$$H_{\mathrm{int}} = K_1 \left(\alpha_2 a_1 a_1\right)_0 + K_0 \left(\alpha_2 \alpha_2\right)_0 \left(a_1 a_1\right)_0 + K_2 \left[\left(\alpha_2 \alpha_2\right)_2 \left(a_1 a_1\right)_2\right]_0 , \tag{87b}$$

the subscripts on the parenthesis indicating coupling to these angular momenta. The constants were found to be

$$K_0 = -0.708\ C_1 , \tag{87c}$$

$$K_1 = -1.588\ C_1 , \tag{87d}$$

and

$$K_2 = -0.936\ C_1 , \tag{87e}$$

in terms of the parameter C_1 of the free dipole vibrations,

$$H_{\mathrm{dip}} = -\frac{\sqrt{3}}{2}\left[\frac{1}{B_1}\left(\pi_1 \pi_1\right)_0 + C_1 \left(\alpha_1 \alpha_1\right)_0\right] . \tag{87f}$$

There are essentially no free parameters, since we use

$$\hbar\omega_1 = \hbar(C_1/B_1)^{1/2} \approx 80\ A^{-1/3}\ \mathrm{MeV}, \tag{88a}$$

$$\hbar\omega_2 = \hbar(C_2/B_2)^{1/2} = \text{energy of first } 2^+ \text{ level}, \tag{88b}$$

and

$$B(E2) = (5\hbar\omega_2/2C_2)^{1/2}. \tag{88c}$$

The only exception is the use of an effective nucleon mass $m \to m^* < m$ in the Steinwedel-Jensen expression for the dipole operator, and of empirical line widths, Γ.

If the dipole and the quadrupole vibrations were uncoupled, our nuclear states would be of the form

$$|N_1 l_1;\ N_2 v l_2;\ JM\rangle, \tag{89a}$$

where

N_1, N_2 = number of dipole, quadrupole phonons,

l_1, l_2 = total angular momentum of dipole, quadrupole phonons, and

v = seniority (= number of quadrupole phonons that do not couple pairwise to zero).

However, the states of Eq. (89a), may be taken as basis states for a diagonalization of the energy matrix,

$$\langle N_1' l_1' \ldots | H | N_1 l_1 \ldots \rangle , \tag{89b}$$

which has off-diagonal elements due to H_{int}. This matrix was calculated up to six surface phonons, $N_2 = 6$, superimposed on the dipole phonon, $N_1 = 1$. It was diagonalized by the method of Householder, and the dipole matrix elements T_{1M}^{ej} for photon absorption were calculated. For a "rigid" nuclear surface, one expects to find the original giant resonance level and, above it, regularly spaced (by about the same energy as that of the first 2+ excited state) and rapidly decreasing in amplitude, a series of satellites corresponding to N_2 = 1, 2, 3, . . . ; for a "soft" nuclear surface, this picture will no longer hold, dipole and various numbers of quadrupole phonons becoming more and more mixed. Figure 37 bears this out: dipole strengths are shown for increasing values of $\beta_0 \equiv B(E2)$. Figures 38 and 39 show some comparisons with experimental results. One notices that the fine structure of the giant resonance is quite well described by the dynamic collective theory, and the remarkable fact is that this fine structure is determined by the parameters which have been obtained from the low-energy spectrum of the same nucleus.

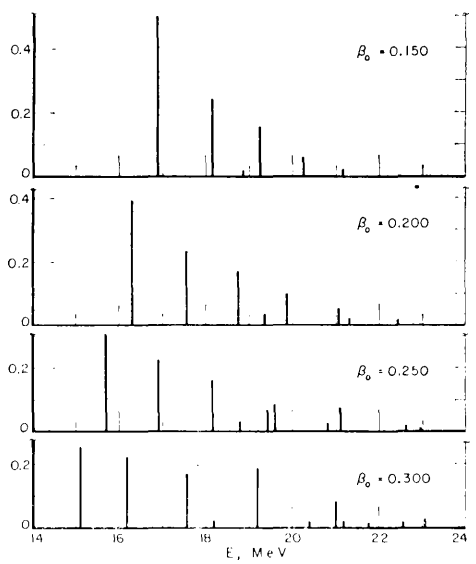

Fig. 37 - Dipole strengths given by the dynamic collective model. After M. G. Huber et al., Phys. Rev. 155:1073 (1967). The main giant dipole state and satellites are shown for different values of $\beta_0 \equiv B(E2)$.

For a deformed nucleus (75), the coupling with surface vibrations causes the two vibrations along the b axes to be no longer degenerate, and provides satellites to each of the three main peaks.

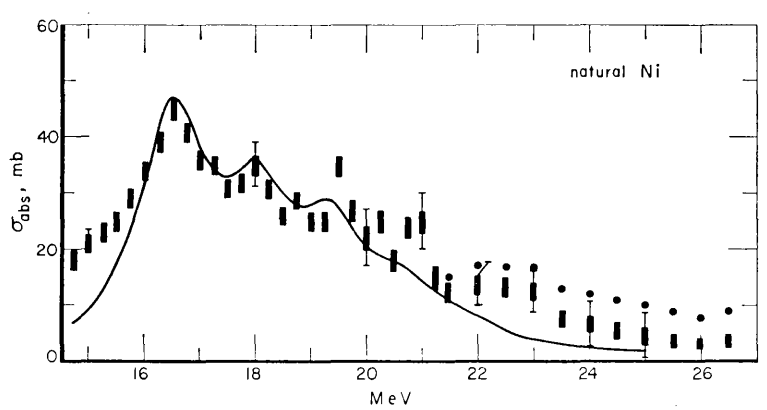

Fig. 38 - Comparison of the dynamic collective theory (Fig. 37) with experimental data on photonuclear giant dipole excitation in natural nickel. (The data are taken from G. Baciu et al., Nucl. Phys. 67:178 (1965).)

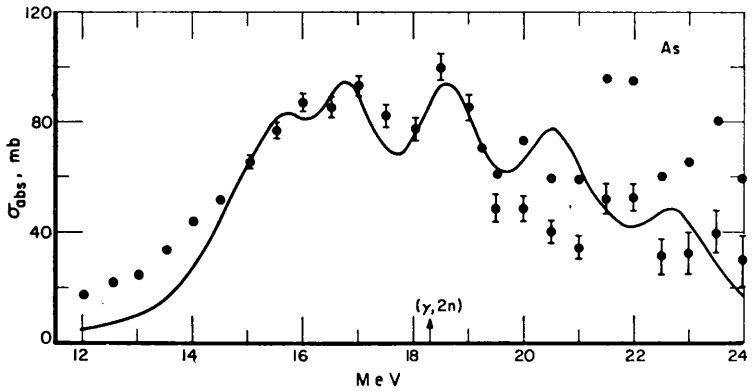

Fig. 39 - Comparison of the dynamic collective theory (Fig. 37) with experimental data on photonuclear giant dipole excitation in ^{75}As. (Data are taken from D. S. Fielder et al., Phys. Rev. Letters 15:33 (1965).)

PARTICLE-HOLE MODEL OF THE GIANT RESONANCES

We will now discuss a description of the giant resonances based on the shell model. Although superficially such a description seems almost diametrically opposed to that offered by the collective model, the results again are very similar. However, the shell model does provide a much more detailed picture; in particular it furnishes the energies of the states, predicts a greater variety of states, and allows a calculation of the widths of the states from the wave functions using R matrix theory.

The first version of the particle-hole model was given by Elliott and Flowers (80), with later more detailed versions published by Gillet (63) and by Lewis and Walecka (72). So far, only closed-shell nuclei have been treated, or those near closed shells.

Prime examples of the application of this model have been the light closed-shell nuclei ^{16}O and ^{40}Ca, and the closed-subshell nuclei ^{12}C, ^{28}Si, and ^{32}S, among others, treated with a spherical shell model. The latter nuclei should perhaps more appropriately be described by a deformed shell model such as the Nilsson model, but this procedure (81,82) applied to ^{24}Mg produced notably bad results.

The independent-particle-model picture of the giant resonance states in closed-shell nuclei, as originally used by Wilkinson (83), Brown and Bolsterli (84), and Elliott and Flowers (80), describes the $T = 1$, $J = 1^-$ giant dipole states being created by removing a nucleon from a filled shell and raising it to a higher unfilled shell of opposite parity, so that a hole stays behind. Depending on which nucleus we consider, and its configurations, a nucleon can be raised in a variety of ways, as will be discussed below for the example of ^{16}O. The relevant shell-model states are shown in Fig. 40. The neutrons and protons occupying them may be treated in a completely charge-symmetric fashion, but this is not a necessary assumption and is sometimes relaxed, as in ^{40}Ca.

It may be noted that for such a shell model with pure configurations as used originally (83), the total transition probability (integrated photon absorption cross section) satisfies the classical sum rule of the nuclear photoeffect. For a single-particle transition at energy E_k, the absorption cross section is given (85) by

$$\int \sigma_k \, dE = (2\pi)^2 \, E_k \, D_k^2 \, , \tag{90a}$$

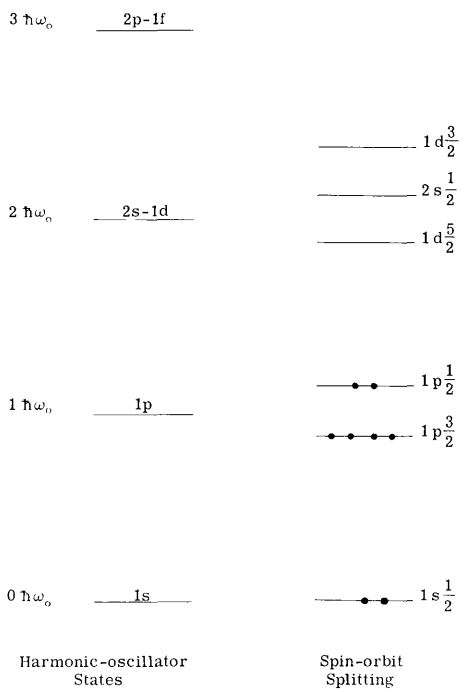

Fig. 40 - Harmonic-oscillator single-particle shell-model states, and spin-orbit splitting. Occupied levels for the ^{16}O ground state are indicated.

with a (squared) dipole strength

$$D^2 = q^2 \left| \int \psi_2^* \, z \, \psi_1 \, d\tau \right|^2 \tag{90b}$$

(the $q \to 0$ limit of our transverse matrix element T_{1M}^{ej}), q being the effective charge (Ne/A for proton and $-Ze/A$ for a neutron), introduced for taking into account nuclear recoil effects (85). The simple shell model leads to

$$\sum_k D_k^2 = \frac{e^2}{2} \frac{NZ}{A} \frac{1}{m\omega_0} , \tag{90c}$$

so that the integrated absorption cross section becomes

$$\int \sigma \, dE = \frac{2\pi^2 e^2}{m} \frac{NZ}{A} = 0.06 \frac{NZ}{A} \text{ MeV-barns.} \tag{90d}$$

This is precisely the classical dipole sum rule. It has also been shown (52) that the sum rule is satisfied (in the limit $q \to 0$) by the generalized Goldhaber-Teller model.

In Eqs. (90), all the transition energies have been taken as those of the harmonic oscillator, $\hbar\omega_0 = 41 \, A^{-1/3}$ MeV. This energy is approximately 15 MeV in O^{16}, whereas the observed giant resonance lies at approximately 22 MeV. (For heavy nuclei, the giant resonance is at approximately $80 A^{-1/3}$ MeV.) Elliott and Flowers (80) were able to improve the shell model picture by the following procedure: (a) the single-particle energies are taken from the observed ground and low excited states of the neighboring closed shell ±1 nuclei, and (b) a "residual interaction" between the raised particle in the higher shell, and the hole it left behind in the filled shell, is assumed, determined by the empirical nucleon-nucleon force as obtained from scattering experiments. This interaction mixes the pure configurations, and by diagonalization of the energy matrix, one obtains new mixed configurations and correspondingly shifted energy levels.

Part (a) of this procedure immediately raises the energies of some of the 1^- states into the observed giant resonance region. The dipole strengths, however, remain considerable even for lower lying states, contrary to observation. Part (b), however, remedies this by not only moving the states somewhat farther up again, but mainly by concentrating the dipole strength into the highest levels exclusively, providing a picture that checks with experiment semiquantitatively. This is illustrated below for ^{16}O.

The energy levels of ^{15}O and ^{17}O, from which the single-particle (and hole) levels for part (a) of our formalism are obtained, are shown in Fig. 41 as given by Gillet (85, 86) (who made extensive applications of the particle-hole model to ^{12}C, ^{16}O, ^{40}Ca, and ^{208}Pb). A variety of particle-hole configurations may be obtained by promoting one particle, and coupling it with the remaining hole to $T = 1$ and $J = 1^-$ (or $J = 0^-$, $J = 2^-$); e.g., 1^- can be obtained by the five configurations shown in Table 7, column 1. The "unperturbed" particle-hole energies $E_0^{(i)}$, taken from Fig. 41, are given in the second column, the squared dipole strengths D_0^2, Eq. (90b), based on the corresponding pure configurations are shown in the third column. One observes that at this stage, the main dipole strengths are still located at 16 to 18 MeV, too low compared to the experiments,

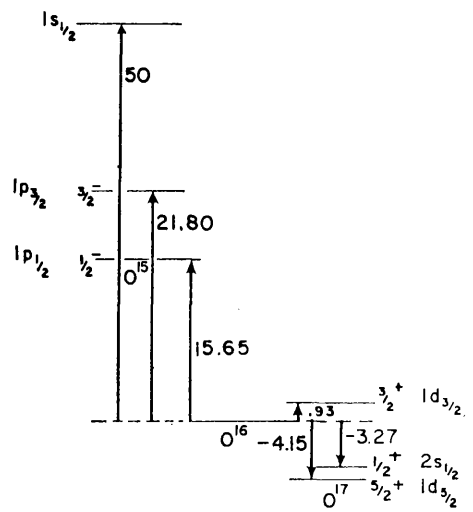

Fig. 41 - The energy levels (MeV) in ^{15}O and ^{17}O from which the independent-particle shell model levels are calculated (86)

Table 7
Giant Dipole States $T = 1$, $J = 1^-$ in ^{16}O, Particle-Hole Model (85)

Configuration	E_0 (MeV)	D_0^2 (%)	E (MeV)	D^2 (%)
$\left(1p\,\frac{3}{2}\right)^-\left(2s\,\frac{1}{2}\right)$	18.53	11	19.6	2
$\left(1p\,\frac{3}{2}\right)^-\left(1d\,\frac{5}{2}\right)$	17.65	50	22.2	73
$\left(1p\,\frac{1}{2}\right)^-\left(1d\,\frac{3}{2}\right)$	16.58	28	18.1	1
$\left(1p\,\frac{1}{2}\right)^-\left(1s\,\frac{1}{2}\right)$	12.38	5.5	13.5	4
$\left(1p\,\frac{3}{2}\right)^-\left(1d\,\frac{3}{2}\right)$	22.73	5.5	25.2	20

which give a large peak at approximately 22 MeV (1^- GT in the Goldhaber-Teller model), and a second sizable peak at approximately 25 MeV (1^- si).

If the nuclear wave functions using the pure configurations of Table 7, column 1, are designated as Φ_i, the actual wave functions of the different states may be written as linear combinations,

$$\psi_i = \sum_j c_j^{(i)} \Phi_j \,. \tag{91a}$$

Using these, the energy matrix

$$\langle \psi_k | H | \psi_j \rangle \tag{91b}$$

may be calculated, where the interaction is simply

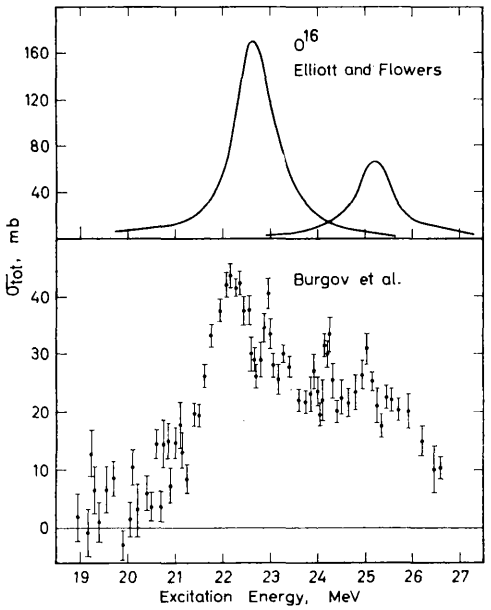

Fig. 42 - A comparison of the results of the particle-hole calculations of Elliott and Flowers (80) with the measured (N. A. Burgov et al., Zhur. Eksptl. i Teor. Fiz. 43:70 (1963); Soviet Phys. JETP 16:50 (1963)) total photoabsorption cross section for ^{16}O. (After Hayward (47).)

$$H = E_0^{(i)} + \sum V_{res}, \qquad (91c)$$

where the residual particle-hole two-body interaction V_{res} is taken from the nucleon-nucleon scattering experiments. It leads to off-diagonal terms in the energy matrix, Eq. (91b), which matrix is then diagonalized. This diagonalization leads to new energy levels $E^{(i)}$ given in the fourth column of Table 7, moved up farther from the unperturbed values $E_0^{(i)}$. It also determines the configuration-mixing coefficients $c_j^{(i)}$ in Eq. (91a), which turn out to be quite small, except for the previously pure main configuration. However, in spite of this small configuration mixing, the amplitudes of the admixed configurations add coherently in such a way that an important change in the dipole strengths is produced (Table 7, last column): the state at 22.2 MeV now has 73% of the dipole strength, and the state at 25.2 MeV has 20%. This agrees very well with experiment (Fig. 42). The upper part of the figure shows these two states (with arbitrary widths), the lower part the experimental total absorption cross section (87).

Due to the coherent addition of configurations, these states may be considered collective states. They may be identified with the two prominent 1^- states of the Goldhaber-Teller model, 1^- GT (22.2 MeV) and 1^- *si* (25.2 MeV), the latter being justified since the configuration $(1p\ 3/2)^-\ (1d\ 3/2)$ involves a spin flip. That the 1^- *si* state is excited by photons in the particle-hole model, whereas such an excitation is negligible in the Goldhaber-Teller model, is because the latter model is based on the assumption of spin independence of nuclear forces, whereas the residual nuclear force V_{res} employed in the particle-hole model is usually assumed spin dependent (although weakly); this leads to some mixing of the 1^- GT and *si* states in the particle-hole model, and thus to a certain excitation strength of the spin-flip state even for photons. In the Goldhaber-Teller model, such a mixing could also be produced by phenomenologically introducing an L-S spin-orbit coupling interaction.

It should be noted that in the preceding example we restricted ourselves to one particle, one hole configuration only, and excitation energies of one oscillator quantum, $1\ \hbar\omega_0$. This is known as the "Tamm-Dancoff approximation." Going a step further, the introduction of more than one particle-hole pair, together with ground state correlations, can be done by a Green's function expansion ("Random Phase approximation"), cf. Gillet (63). This procedure leads to little new, and its value has been questioned.

Total absorption cross sections obtained by the particle-hole model surpass the experimental ones by about a factor 2 in magnitude: first, the classical sum rule is satisfied to 50 to 75% only for light nuclei (85), and further, the configuration mixing increases the value of $\int \sigma\, dE$ beyond that given by the sum rule, Eq. (90d). Such a factor-2 discrepancy is not uncommon in the collective models also. The reason is that both shell models and collective models describe only long-range correlations between nucleons, not short-range ones. The latter are present, however, and roughly speaking lead to the

presence of "quasi-deuterons" in nuclear matter, which produce a considerable amount of dipole strength in photoabsorption at higher energies ($\gtrsim$ 30 MeV); this strength is thus sapped away from the giant resonance at approximately 20 to 25 MeV, in such a way that the total dipole strength exhausts the sum rule.

The particle-hole model was applied to giant resonance excitation in inelastic electron scattering by Lewis and Walecka (72) and deForest (88) for ^{12}C and ^{16}O. The first reference obtained the T = 1, 1^- GT, and 1^- si states; the second reference added the 2^- si state. As a function of momentum transfer q, it is found that just as the 1^- GT state decreases in the generalized Goldhaber-Teller model, the 1^- and 2^- si states increase with q. If (in spite of their energy separation) one superposes the contributions of these states (as must have been suggested by the poor energy resolution in the early experiments), one obtains a curve with a minimum. This is shown in Figs. 43 and 44, which plot the squared matrix elements T_1^e and T_2^m (Fig. 44 adds the contribution of the 2^- si state to that of the 1^- states of Fig. 43, for ^{12}C). The minimum, and the important effect of the 2^- state, are clearly visible. In Fig. 43, curves for the squared matrix elements of T_1^e for the Goldhaber-Teller and Steinwedel-Jensen model are also shown. It should be pointed out, however, that these curves include only the charge vibrations (GT or isospin), since it was not realized at the time that the Goldhaber-Teller (as well as the Steinwedel-Jensen) model was amenable to a generalization (as was carried out in the subsection "The Goldhaber-Teller Model") which included the spin-isospin vibrations. Indeed such a generalization must be carried out, and then the collective models do describe electron scattering correctly, in particular predicting the rise of the spin- isospin state cross section with rising q, as discussed in Ref. 62, and herein. Indeed, such a rise occurs for all models, as has been shown by Czyz et al. (89) in a model-independent way, using sum rules.

The fact that in Fig. 43 the particle-hole model curve lies as low as the experiments, and the collective-model curves are higher by a factor 2, has its origin in the fact that the particle-hole matrix elements used by Lewis and Walecka (72) contain a multiplicative factor $\hbar\omega_{osc}$, the energy parameter of the oscillator potential. In the limit $q \to 0$, however, it is shown (Ref. 72, Eqs. (52) and (53)) that the Siegert

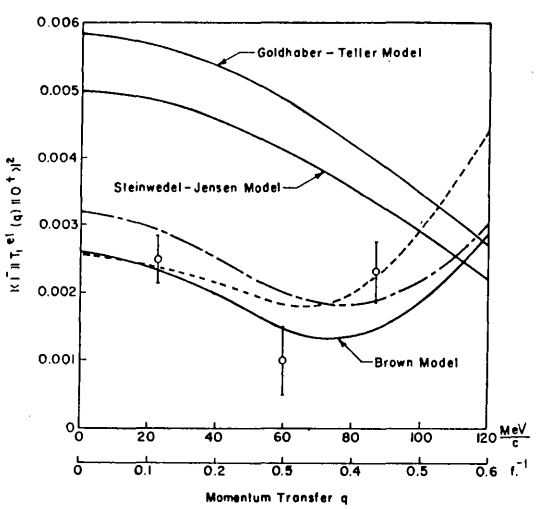

Fig. 43 - Sum of squared transverse matrix elements for the transition $0^+ \to 1^-$ (giant resonance) in ^{12}C, plotted vs momentum transfer q. The curves labeled Brown model represent results of the particle-hole model with various residual interactions. The Goldhaber-Teller and Steinwedel-Jensen curves were calculated for charge vibrations only. After Ref. 72.

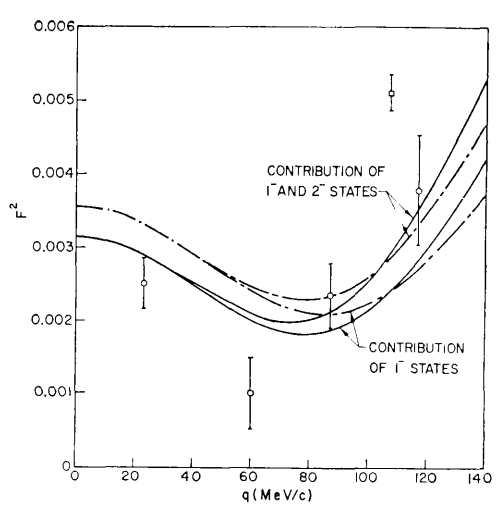

Fig. 44 - Same as Fig. 43, but with the added contribution of the $0^+ \to 2^-$ transition (88)

theorem is satisfied only if instead of $\hbar\omega_{osc}$ the energy of the dipole levels $E^{(i)}$ had been used. Since the Siegert theorem, an exact relation, must be satisfied, the particle-hole curves in Fig. 43 should have been multiplied by $(E^{(i)}/\hbar\omega_{osc})^2 \approx 2$, which makes them lie as high up as the collective model results. The fact that all models then lie above the experiments by a factor 2 need not worry us particularly, since, as was pointed out, this discrepancy is explained by short-range correlations which none of the models contain. Unfortunately, Fig. 43 has been reprinted (5,90) in later review articles, without noting the above objections attached to it.

Similar calculations have been carried out (91-93) for the giant resonance states in ^{12}C, ^{16}O, ^{28}Si, ^{32}S, and ^{40}Ca. Figures 45 and 46 present, as functions of q, the squared matrix elements for electroexcitation of the 1^- and 2^- states in ^{28}Si; Figs. 47 and 48 present the corresponding quantities for ^{32}S; and Figs. 49 and 50 present those for ^{40}Ca. The energies of the states (found by diagonalization) are labeled along the curves. It is seen that in all these cases, there is a prominent 1^- state which decreases with q and may be interpreted as the collective 1^- GT state; another 1^- state that increases with q, representing the collective 1^- si state; and also a prominent 2^- si state. The latter, for ^{12}C and ^{16}O situated at 19 to 20 MeV (see Fig. 28), now moves down for the nuclei in question: to 14.3 MeV in ^{28}Si (Fig. 46), 13.5 MeV in ^{32}S (Fig. 48), and 16.35 MeV in ^{40}Ca (Fig. 50). These states could be found if looked for in 180° electron scattering with

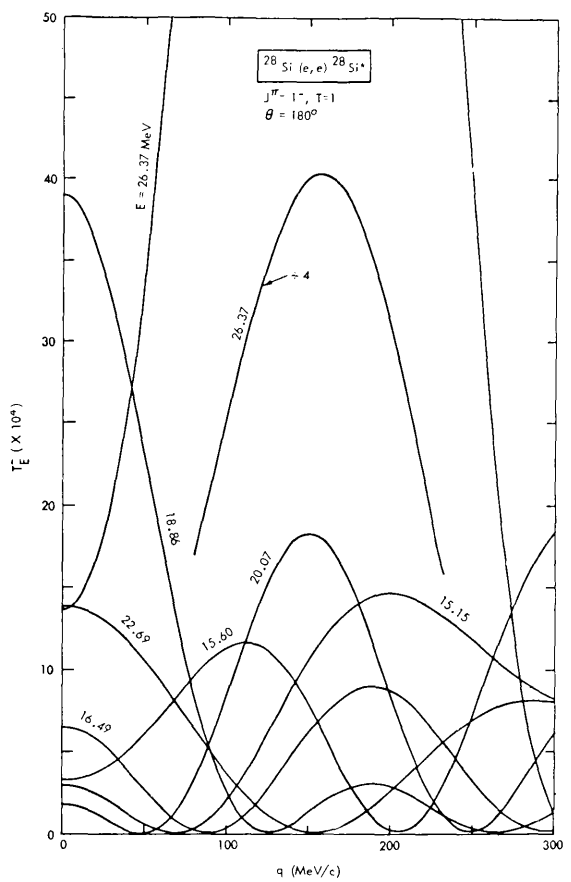

Fig. 45 - Transverse electric form factors (squared) vs momentum transfer, for the $0^+ \rightarrow 1^-$ giant dipole transitions in ^{28}Si, based on the particle-hole model (93)

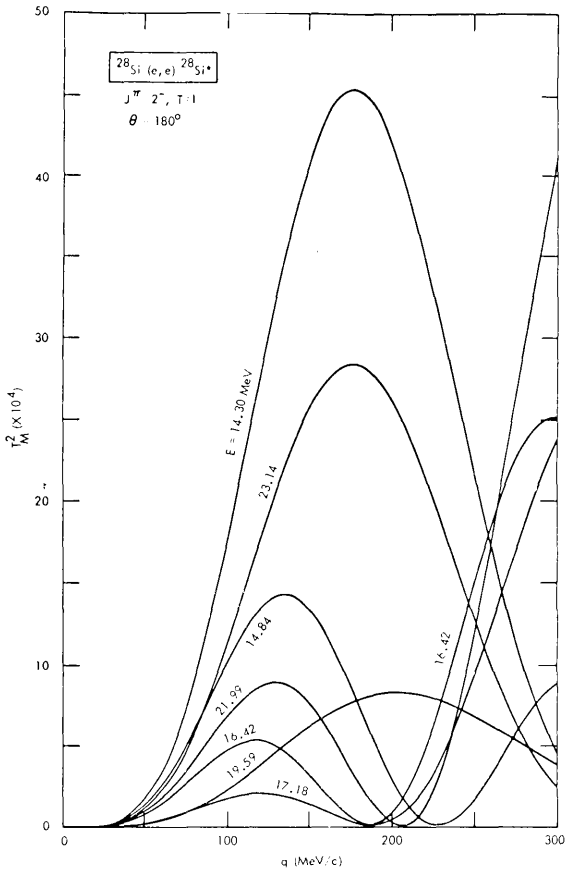

Fig. 46 - Transverse magnetic form factors (squared) vs momentum transfer, for the $0^+ \rightarrow 2^-$ giant resonance transitions in ^{28}Si, based on the particle-hole model (93)

momentum transfers extending to $q \approx 100$ to 150 MeV/c, and there are indications (94) that such a 2^- state at approximately 14 MeV has been seen in ^{28}Si. Recent spectra of inelastically scattered electrons at 180° from ^{28}Si in which a state at 14.6 MeV shows up have been obtained by the NRL group Fagg, Bendel, Tobin, and Kaiser (Fig. 51).

PHENOMENOLOGICAL MODELS

The great variety of levels below the giant resonance, both charge-type and magnetic, which are seen in electron scattering at 180° and at other angles, cannot possibly all be described by a detailed model such as the shell model. The amount of labor involved in such a description is warranted only if the level has special significance (e.g., in the case of the giant resonance levels, or prominent $M1$ levels such as the one at 15.1 MeV in ^{12}C). Simple phenomenological models are needed which describe the q dependence of the excitation strength, and can be used by the experimenter to fit his curves without excessive labor, providing him at the same time with a meaningful result such as a transition radius, and perhaps a surface thickness. Two such models will be briefly described.

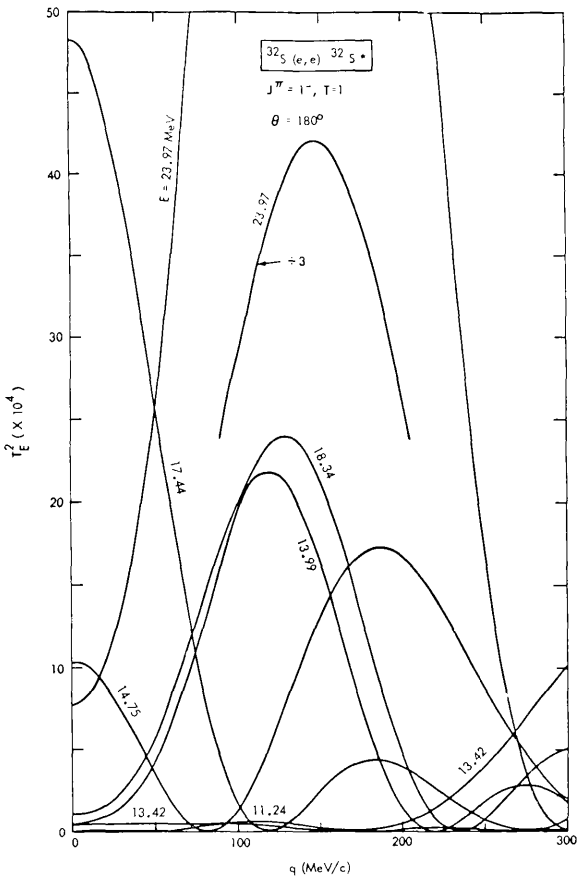

Fig. 47 - Transverse electric form factors (squared) vs momentum transfer, for the $0^+ \rightarrow 1^-$ giant dipole transitions in ^{32}S, based on the particle-hole model (91)

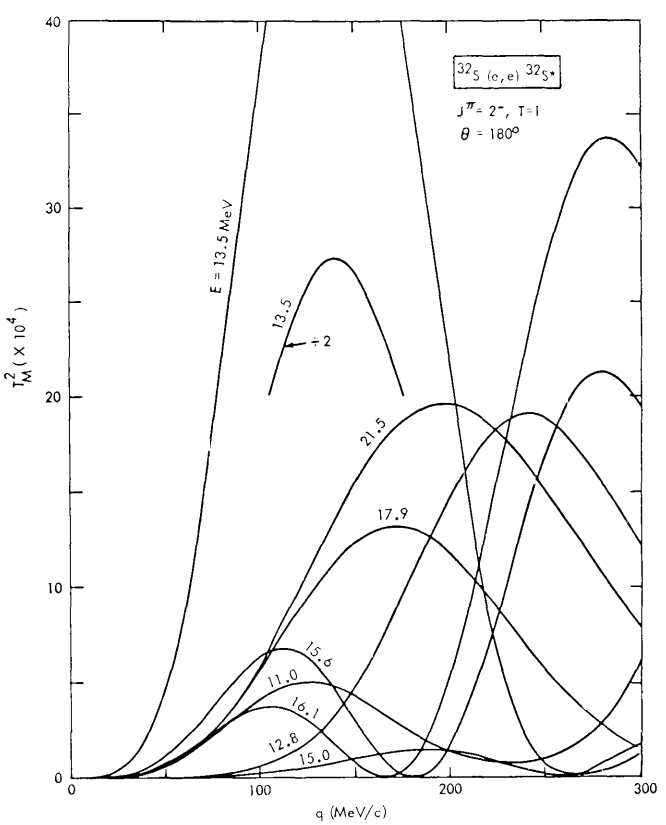

Fig. 48 - Transverse magnetic form factors (squared) vs momentum transfer, for the $0^+ \rightarrow 2^-$ giant resonance transitions in ^{32}S, based on the particle-hole model (91)

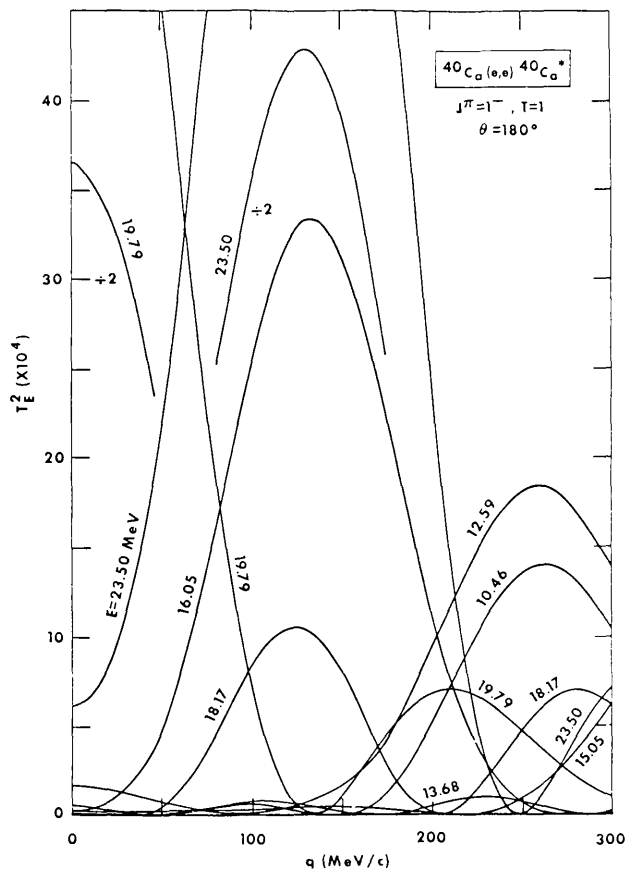

Fig. 49 - Transverse electric form factors (squared) vs momentum transfer, for the $0^+ \rightarrow 1^-$ giant dipole transitions in ^{40}Ca, based on the particle-hole model (92)

Helm's Model and its Generalization

Helm (95) has given an expression for the Coulomb matrix element by assuming the transition charge density to be concentrated on a shell about the nuclear radius, in the form of a δ function smeared out by a convolution,

$$\rho(\boldsymbol{r}) = \int \rho_0(\boldsymbol{r}-\boldsymbol{r}')\,\rho_1(\boldsymbol{r}')\,d^3r' . \tag{92a}$$

The charged shell is given by

$$\rho_0(\boldsymbol{r}) = Z\,\delta(\boldsymbol{r}-\boldsymbol{R}) , \tag{92b}$$

with $\boldsymbol{R}$ a position vector of length equal to the charge radius, over whose direction we will average later. The smearing is taken as

$$\rho_1(\boldsymbol{r}) = (2\pi g^2)^{-3/2}\, e^{-r^2/2g^2} , \tag{92c}$$

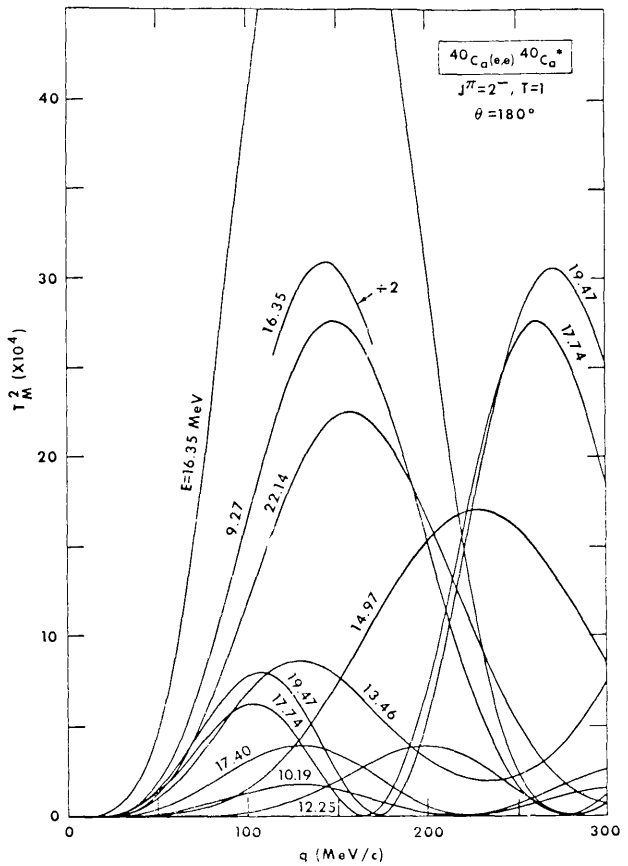

Fig. 50 - Transverse magnetic form factors (squared) vs momentum transfer, for the $0^+ \to 2^-$ giant resonance transitions in ^{40}Ca, based on the particle-hole model (92)

with some surface thickness g. By the convolution theorem, the Fourier transform of $\rho(\mathbf{r})$ is just the product of the Fourier transforms of ρ_0 and ρ_1,

$$F(q) \equiv \int d^3r\, e^{i\mathbf{q}\cdot\mathbf{r}}\, \rho(\mathbf{r}) = f_0(\mathbf{q})\, f_1(q), \tag{93a}$$

where

$$f_0(\mathbf{q}) = Z e^{i\mathbf{q}\cdot\mathbf{R}} \tag{93b}$$

and

$$f_1(q) = e^{-g^2 q^2/2}. \tag{93c}$$

The Coulomb matrix element, Eq. (16a), can easily be shown to be given by

$$M_{LM}(q) = (4\pi i^L)^{-1} \int F(\mathbf{q})\, Y_{LM}(\hat{q})\, d\hat{q} \tag{94a}$$

($\hat{q} = \mathbf{q}/q$), and inserting from Eq. (93a), one has

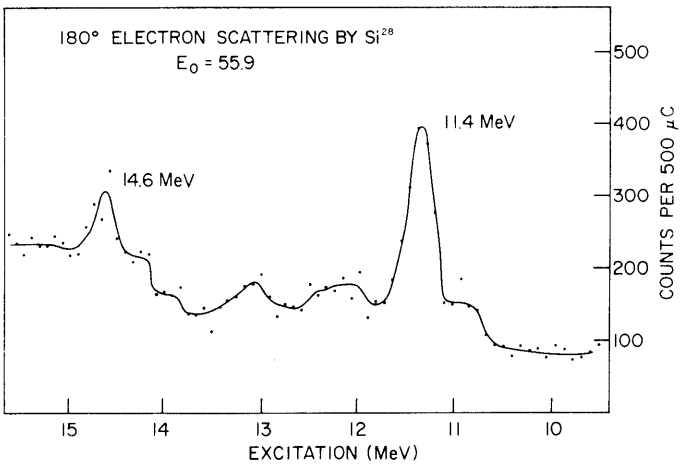

Fig. 51 - Spectrum of electrons scattered at 180° from ^{28}Si (L. W. Fagg, W. Bendel, R. A. Tobin, and H. F. Kaiser, NRL, to be published)

$$M_{LM}(q) = Z f_1(q)\ j_L(qR)\ Y_{LM}(\hat{R}). \tag{94b}$$

This gives for the reduced matrix element

$$\hat{J}_0^{-1} \langle J \| M_L(q) \| J_0 \rangle = \beta_L^{J_0 J} f_1(q)\ j_L(qR), \tag{95a}$$

with a parameter to be fitted to experiment,

$$\beta_L^{J_0 J} = \hat{J}_0^{-1} Z \langle J \| Y_L(\hat{R}) \| J_0 \rangle_{\mathrm{av}}. \tag{95b}$$

This is the result of Helm.

We now extend this procedure (37) to the calculation of $T_{LM}^{e,m}$; for this purpose, we need corresponding expressions for $\boldsymbol{j}(\boldsymbol{r})$ and $\boldsymbol{\mu}(\boldsymbol{r})$. The current can be found by solving the continuity equation, Eq. (15), which we show can be done in a unique way. First, we note that with $\rho(\boldsymbol{r})$ written as in Eq. (92a), we also have

$$\boldsymbol{j}(\boldsymbol{r}) = \int \boldsymbol{j}_0(\boldsymbol{r} - \boldsymbol{r}')\ \rho_1(\boldsymbol{r}')\ d^3r', \tag{96}$$

which follows from Eq. (10c) by taking Fourier transforms. At the same time, $\boldsymbol{j}_0(\boldsymbol{r})$ must satisfy

$$\nabla \cdot \boldsymbol{j}_0(\boldsymbol{r}) = i\omega\rho_0(\boldsymbol{r}), \tag{97a}$$

and using Eq. (92b), we have

$$\nabla \cdot \boldsymbol{j}_0(\boldsymbol{r}) = i\omega Z r^{-2}\ \delta(r - R) \sum_{LM} Y_{LM}^*(\hat{R})\ Y_{LM}(\hat{r}). \tag{97b}$$

The basic assumption will be that $\boldsymbol{j}_0$ is of the form

$$\boldsymbol{j}_0(\boldsymbol{r}) = \rho_2(r)\boldsymbol{v}, \tag{98a}$$

with

$$\rho_2(r) = \begin{cases} 3Z/4\pi R^3 , & r < R , \\ 0 , & r > R , \end{cases} \tag{98b}$$

and with the flow of nuclear matter being irrotational,

$$\nabla \times \mathbf{v} = 0 , \tag{98c}$$

which is an assumption that is commonly made (70,72). In Eq. (97b), we have to treat the monopole separately from the higher multiples,

$$\mathbf{j}_0(\mathbf{r}) = \mathbf{j}_0^{(0)}(\mathbf{r}) + \mathbf{j}_0^{(1)}(\mathbf{r}), \tag{98}$$

where $\mathbf{j}_0^{(0)}$ satisfies

$$\begin{aligned} \nabla \cdot \mathbf{j}_0^{(0)} &= i\omega Z\, \delta(r-R)/4\pi r^2 \\ &= -\frac{1}{3}\, i\omega r\, \frac{d\rho_2}{dr} . \end{aligned} \tag{99a}$$

It was shown in a paper (34) that for the monopole, conservation of matter requires a modification of the right-hand-side expression, namely

$$\nabla \cdot \mathbf{j}_0^{(0)} = -\frac{1}{3}\, i\omega\, \frac{1}{r^2}\, \frac{d}{dr}\left[r^3\, \rho_2(r)\right]. \tag{99b}$$

Further, only a radial velocity is possible (which is curl-free), and the solution is uniquely

$$\mathbf{j}_0^{(0)}(\mathbf{r}) = -\frac{1}{3}\, i\omega \mathbf{r}\, \rho_2(r). \tag{100}$$

For the higher multipoles $L \geq 1$, one makes the ansatz

$$j_0^{(1)}(\mathbf{r}) = \rho_2(r) \sum_{L\geq 1,\, M} Y^*_{LM}(\hat{R}) \left[Af(r)\, \mathbf{Y}^M_{L,\,L+1}(\hat{r}) + Bg(r)\, \mathbf{Y}^M_{L,\,L-1}(\hat{r})\right] , \tag{101}$$

being also a multipole expansion in $\hat{R}$, as required by Eq. (97b). The only other multipole term in $\hat{r}$, $\mathbf{Y}^M_{LL}(\hat{r})$, is then ruled out by parity. The corresponding velocity is essentially the bracket in Eq. (101), and if one requires its curl to vanish, one obtains one equation for A and B (taking f and g to be known for the moment); two further equations arise from inserting Eq. (101) into Eq. (97b) and comparing the coefficients of ρ_2 and ρ_2'. These three equations for two unknowns are soluble only if the rank of the three-by-three matrix of coefficients (including the column of absolute terms) is less than three, and it turns out that this is not the case unless one of the unknowns vanishes. If $B = 0$, one finds further that

$$f(r) = Cr^{-L-2},$$

which gives a singularity at $r = 0$ and is thus not permissible. With $A = 0$, one finds

$$g(r) = Cr^{L-1},$$

which is the permissible case. The expansion of the current thus contains $r^{L-1}\, \mathbf{Y}^M_{L,\,L-1}(\hat{r})$

only; this choice has also been made in a paper (58) on giant multipoles in the generalized Goldhaber-Teller model. The final solution is then

$$\boldsymbol{j}_0^{(1)}(\boldsymbol{r}) = -i\omega R\,\frac{4\pi}{3}\,\rho_2(r)\sum_{L\geq 1,M}\left(\frac{2L+1}{L}\right)^{1/2}\left(\frac{r}{R}\right)^{L-1} Y^*_{LM}(\hat{R})\;\mathbf{Y}^M_{L,\,L-1}(\hat{r})\,. \tag{102}$$

As for the magnetization density, this can simply be assumed to be of the form

$$\boldsymbol{\mu}(\boldsymbol{r}) = \boldsymbol{\mu}_0\int\bar{\rho}_0(\boldsymbol{r}-\boldsymbol{r}')\;\bar{\rho}_1(\boldsymbol{r}')\;d^3r'\,, \tag{103a}$$

with $\boldsymbol{\mu}_0$ being some constant vector containing the nucleon spins and anomalous moments, and with

$$\bar{\rho}_0(\boldsymbol{r}) = A\,\delta(\boldsymbol{r}-\bar{\boldsymbol{R}}) \tag{103b}$$

and

$$\bar{\rho}_1(\boldsymbol{r}) = (2\pi\bar{g}^2)^{-3/2}\;e^{-r^2/2\bar{g}^2}\,. \tag{103c}$$

A different nuclear radius $\bar{R}$ and surface thickness $\bar{g}$ will in general be needed here, since the magnetization density is based on the nucleon distribution rather than on the proton distribution, and it is well known that these two differ.

With the current and magnetization density of Eqs. (96) and (103), one may then calculate the transverse matrix elements of Eqs. (16d) through (16g) in a straightforward manner, and one can factor out again the functions $f_1(q)$ and

$$\bar{f}_1(q) = e^{-\bar{g}^2q^2/2}\,, \tag{104}$$

respectively, by using the relation

$$j_L(qr)\,Y_{LM}(\hat{r}) = (4\pi i^L)^{-1}\int e^{i\boldsymbol{q}\cdot\boldsymbol{r}}\,Y_{LM}(\hat{q})\;d\hat{q}\,. \tag{105}$$

The monopole does not contribute to any transverse matrix elements. We find

$$T^{mj}_{LM}(q) \equiv 0\,, \tag{106}$$

due to the absence of the term $\mathbf{Y}^M_{LL}(\hat{r})$ in the current. This operator also vanishes in the Goldhaber-Teller model (8,62). For the other reduced matrix elements, one obtains

$$\hat{J}_0^{-1}\,\langle J\|T^e_L(q)\|J_0\rangle = \left(\frac{L+1}{L}\right)^{1/2}\beta^{J_0J}\,\frac{\omega}{q}\,f_1(q)\,j_L(qR) + \gamma^{J_0J}_{L0}\,\frac{q}{2m}\,\bar{f}_1(q)\;j_L(q\bar{R})\,, \tag{107a}$$

and

$$\hat{J}_0^{-1}\,\langle J\|T^m_L(q)\|J_0\rangle = -\frac{q}{2m}\,\bar{f}_1(q)\left\{\left(\frac{L}{2L+1}\right)^{1/2}\gamma^{J_0J}_{L+}\,j_{L+1}(q\bar{R}) + \left(\frac{L+1}{2L+1}\right)^{1/2}\gamma^{J_0J}_{L-}\,j_{L-1}(q\bar{R})\right\}, \tag{107b}$$

with m = nucleon mass, where we introduced the parameters

$$\gamma^{J_0J}_{L\lambda} = 2mi^{\lambda}A\,\hat{J}_0^{-1}\,\langle J\|\boldsymbol{\mu}_0\cdot\mathbf{Y}_{L,\,L+\lambda}(\hat{R})\|J_0\rangle_{\rm av}\,, \tag{108}$$

($\lambda = 0, \pm 1$). Since the reduced matrix elements, when multiplied by i^L, are real (26), and since different multipoles do not interfere, all our (dimensionless) parameters β_L and $\gamma_{L\lambda}$ are real.

Equations (107) represent our generalization of the original Helm model of Eq. (95a). Both transverse matrix elements depend on two parameters which can in principle be obtained by fitting to the "photon point" at $q = \omega$ (this is determined by β_L or γ_{L-}, respectively) and to the experimental slope of the data vs q^2 (this will fix γ_{L0} or γ_{L+}, respectively), whereas R, $\bar{R}$, g, and $\bar{g}$ can be taken from the known ground state charge and matter distribution. In any case, the latter four parameters should not vary from level to level, whereas β_L and $\gamma_{L\lambda}$ are characteristic for a given level. Equations (107) then predict the q dependence of the form factors for higher values of q. In the transverse electric case, however, one can do better, since the first parameter β_L, due to the Siegert theorem, is the same one appearing already in the Coulomb matrix element, Eq. (95a), and can be independently obtained there, as one can experimentally separate (24) $B(CL, q)$ from $B(EL, q)$. The second term containing γ_{L0} is called "electric spin flip transition" and has no longitudinal counterpart.

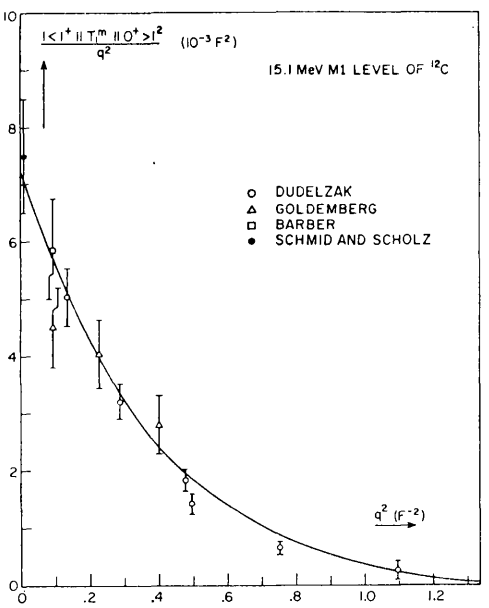

Fig. 52 - Momentum transfer dependence of the transverse $M1$ form factor for the 15.1-MeV 1^+ level in ^{12}C, fitted by the generalized Helm model (37)

We have used the generalized Helm model for a description of the 15.1-MeV $M1$ level in ^{12}C. Figure 52 shows the results. A satisfactory fit to the experiments was obtained for the squared matrix element T_1^m, with the following parameters used: $\bar{g}^2 = 1.04\ F^2$, $\bar{R} = 1.25A^{1/3}F$; $|\gamma_{1-}| = 0.995$, and $|\gamma_{1+}| = 1.37$, γ_{1-} and γ_{1+} being relatively positive.

The Helm model, as applied here and in the original papers (95, 96), is successful because in practically every model the transition densities representing the overlap of ground state and excited state wave functions are large only in the vicinity of the nuclear radius. (In the Goldhaber-Teller model, for example, this is clear from the fact that the transition density is given by the derivative of the ground state density.) All the Helm model does is to state in a phenomenological manner that the transition densities are large near the nuclear radius. But as said before, this is sufficient for providing us with the simple formulas of Eqs. (95a) and (107), suitable for rapid fitting to experimental points. They may also be useful for determining multipolarities in such a way that a good fit may be obtained for one value of L only if R should come out with a reasonable value.

Tassie's Model

A phenomenological model, somewhat less crude than Helm's, was proposed by Tassie (97), based on the hydrodynamic model of the nucleus. It will here be discussed for only the charge vibrations.

The charge density is assumed to undergo oscillations as an incompressible, irrotational fluid. An element of charge (and mass) moves from r_0 to r without alteration of the volume it occupies, i.e.,

$$\rho(\mathbf{r}) = \rho_0(\mathbf{r}_0) \ . \tag{109a}$$

This means that from the assumption of incompressibility the total time derivative of the charge density vanishes:

$$\frac{d\rho}{dt} = \frac{\rho(\mathbf{r}) - \rho_0(\mathbf{r}_0)}{dt} = 0 \ . \tag{109b}$$

Since hydrodynamically, the total time derivative is

$$\frac{d\rho}{dt} = \frac{\partial\rho}{\partial t} + \mathbf{v}\cdot\nabla\rho \ , \tag{109c}$$

we have

$$\frac{\partial\rho}{\partial t} = -\mathbf{v}\cdot\nabla\rho \ . \tag{109d}$$

The second assumption is that of irrotationality,

$$\nabla\times\mathbf{v} = 0 \ , \tag{110a}$$

which implies

$$\mathbf{v} = \nabla\Phi \ . \tag{110b}$$

Considering the continuity equation

$$\nabla\cdot(\rho\mathbf{v}) + \frac{\partial\rho}{\partial t} = 0 \ , \tag{111}$$

and using Eqs. (109d) and (110b), we find

$$\nabla^2\Phi = 0 \ ; \tag{112a}$$

i.e., the velocity potential Φ is a solution of Laplace's equation, which is given by

$$\Phi(\mathbf{r}) = \sum_{lm} \frac{r^l}{l} \beta_{lm} Y^*_{lm}(\mathbf{r}) \ . \tag{112b}$$

The meaning of the expansion parameter is simply $\beta_{lm} = \dot{\alpha}_{lm} = -i\omega\alpha_{lm}$, where α_{lm} is the harmonically varying expansion parameter of a surface,

$$r = r_0\left[1 + \sum_{lm} \alpha_{lm} r_0^{l-2} Y^*_{lm}(\hat{r}_0)\right] , \tag{112c}$$

which is generated out of an originally spherical surface in the course of the hydrodynamic collective oscillation.

The transition density for charge oscillations may now be obtained using the continuity equation, Eq. (111). We have

$$\rho^{tr}(\mathbf{r}) = \frac{1}{i\omega}\nabla\cdot[\rho(\mathbf{r})\mathbf{v}] \ , \tag{113a}$$

where on the right-hand side the ground state charge distribution $\rho(\mathbf{r})$ may be used, since v itself already contains β_{lm} to first order. Inserting Eqs. (110b) and (112b), we finally obtain

$$\rho^{tr}(\mathbf{r}) = -\sum_{lm} \frac{\alpha_{lm}}{l} \nabla\left[r^l Y^*_{lm}(\hat{r})\right] \cdot \nabla\rho(\mathbf{r}). \tag{113b}$$

This transition charge may then be used for obtaining the Coulomb matrix element, Eq. (16a). Tassie has applied the model to the excitation of the 2^+, 4.43-MeV level in ^{12}C; the satisfactory fit is shown in Fig. 53. The model was used extensively later on, especially by the Duke group (19).

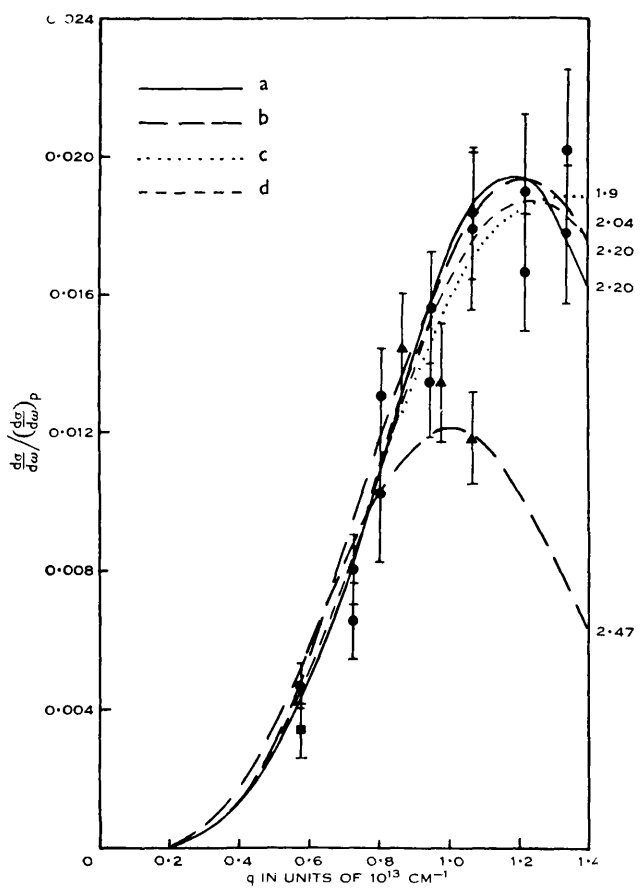

Fig. 53 - Ratio of cross section for the $0^+ \rightarrow 2^+$ excitation of the 4.43-MeV level to point charge scattering cross section of ^{12}C. The theoretical curves (for different choices of parameters) are from the model by Tassie (97); the data points are those of Fregeau and Hofstadter (Phys. Rev. 99:1503 (1955)).

CONCLUSION

In the preceding review, we have discussed a variety of topics covering, fairly broadly, electron scattering and, partly, photoabsorption by atomic nuclei. We have tried to present a picture of the excitation of nuclear levels by electrons (and photons); we have pointed out what information can be obtained from this process, and we have described a number of models for the excited states whose validity may be established by the electron scattering experiments. It will have become clear that the technique of electron scattering represents a new, powerful tool for the study of nuclear states, both ground and excited, which at present, in spite of considerable work already done, still stands only at the beginning of its application. Important developments are expected to proceed rapidly with the completion of more and better high-intensity electron linacs. At the same time, the theory of excited nuclear states, both giant resonance and lower levels, also rests in a quite preliminary stage and will undoubtedly be advanced speedily in the near future as the experimental electron scattering data come in. Thus in the years ahead, an exciting development of this subject may be expected which, with the help of electron scattering techniques, will far surpass the original advances of photonuclear physics.

REFERENCES

1. Willey, R.S., Nucl. Phys. 40:529 (1963)
2. Alder, K., Bohr, A., Huus, T., Mottelson, B., and Winther, A., Revs. Mod. Phys. 28: 432 (1956)
3. deForest, T., Jr., and Walecka, J.D., Advances in Physics 15:1 (1966)
4. Barber, W.C., Ann. Rev. Nuc. Sci. 12:1 (1962)
5. Goldemberg, J., and Pratt, R.H., Revs. Mod. Phys. 38:311 (1966)
6. Walecka, J.D., Lecture Notes, Enrico Fermi International School of Physics, Varenna, Italy, 1966
7. Schiff, L.I., Phys. Rev. 96:765 (1954)
8. Eisenberg, J.M., and Rose, M.E., Phys. Rev. 131:848 (1963)
9. Blatt, J.M., and Weisskopf, V.F., "Theoretical Nuclear Physics," New York:Wiley, 1952
10. Schwinger, J., Phys. Rev. 75:898 (1949)
11. Tsai, Y.S., Phys. Rev. 122:1898 (1961)
12. Bernheim, M., Thesis, University of Paris (Orsay), 1965
13. Isabelle, D.B., and Bishop, G.R., Nuclear Phys. 45:209 (1963)
14. Lacoste, F., Thesis, University of Paris (Orsay), 1962
15. Lombard, R., Thesis, University of Paris (Orsay), 1964
16. Hand, L.N., Phys. Rev. 129:1834 (1963)

17. Ginsberg, E.S., and Pratt, R.H., Phys. Rev. 134:B773 (1964); 137:B1500 (1965)

18. Maximon, L.C., and Isabelle, D.B., Phys. Rev. 133:B1344 (1964); 136:B674 (1964)

19. Griffy, T.A., Onley, D.S., Reynolds, J.T., and Biedenharn, L.C., Phys. Rev. 128:833 (1962); Onley, D.S., Griffy, T.A., and Reynolds, J.T., Phys. Rev. 129:1689 (1963); Onley, D.S., Reynolds, J.T., and Wright, L.E., Phys. Rev. 134:B945 (1964); see also Ziegler, J.F., Yale University Report Yale 2726E-49, 1967

20. Drechsel, D., Nucl. Phys. 78:465 (1966); also to be published

21. Bottino, A., Ciocchetti, G., and Molinari, A., Nucl. Phys. 89:192 (1966); Toepffer, C. (preprint); Onley, D. (preprint)

22. Lewis, F.H., and Walecka, J.D., Phys. Rev. 133:B849 (1964)

23. Edmonds, A.R., "Angular Momentum in Quantum Mechanics," Princeton:Princeton University Press (1960)

24. Spamer, E., Z. Physik 191:24 (1966)

25. Raphael, R., and Überall, H., Phys. Rev. 143:671 (1966)

26. Pratt, R.H., Walecka, J.D., and Griffy, T.A., Nucl. Phys. 64:677 (1965)

27. Griffy, T.A., and Yu, D.U.L., Phys. Rev. 139:B880 (1965); Rand, R.E., Frosch, R., and Yearian, M.R., Phys. Rev. 144:859 (1966); Isabelle, D.B., Orsay Report LAL 1152, Jan. 1966

28. Stovall, T., Goldemberg, J., and Isabelle, D.B., Nucl. Phys. 86:225 (1966)

29. Goldemberg, J., Isabelle, D.B., Vinciguerra, D., Stovall, T., and Bottino, A., Phys. Lett. 16:141 (1965)

30. Czyz, W., and Gottfried, K., Ann. Phys. (N.Y.) 21:47 (1963)

31. Leiss, J. and Taylor, R.E., unpublished (quoted in Ref. 3)

32. McVoy, K.W., and Van Hove, L., Phys. Rev. 125:1034 (1962)

33. Amaldi, U., Jr., Venuti, G.C., Cortellessa, G., de Sanctis, E., Frullani, S., Lombard, R., and Salvadori, P., Phys. Lett. 22:593 (1966)

34. Werntz, C., and Überall, H., Phys. Rev. 149:762 (1966)

35. Frosch, R., Rand, R.E., Yearian, M.R., Crannell, H.L., and Suelzle, L.R., Phys. Lett. 19:155 (1965)

36. Clerc, H.G., Wetzel, K.J., and Spamer, E., Phys. Lett. 20:667 (1966)

37. Rosen, M., Raphael, R., and Überall, H., Phys. Rev. 163:927 (1967)

38. Tobin, R.A., Phys. Rev. 120:175 (1960)

39. Titze, O., and Spamer, E., Zeits. f. Naturforsch. 21a:1504 (1966)

40. Kurath, D., Phys. Rev. 130:1525 (1963)

41. Kurath, D., Phys. Rev. 101:216 (1956); 106:975 (1957)

42. Sachs, R.G., and Austern, N., Phys. Rev. 81:705 (1951)

43. Goldemberg, J., Barber, W.C., Lewis, F.H., Jr., and Walecka, J.D., Phys. Rev. 134: B1022 (1964)

44. Dudelzak, B., and Taylor, R.E., J. Phys. Radium 22:544 (1961)

45. Gudden, F., Phys. Letters 10:313 (1964)

46. Kurath, D., Phys. Rev. 134:B1025 (1964)

47. Hayward, E., Rev. Mod. Phys. 35:324 (1963); Danos, M., and Fuller, E.G., Ann. Rev. Nuc. Sci. 15:29 (1965)

48. Caldwell, J.T., Bramblett, R.L., Berman, B.L., Harvey, R.R., and Fultz, S.C., Phys. Rev. Letters 15:976 (1965)

49. Thompson, M.N., and Baglin, J.E.E., Phys. Letters 25B:256 (1967)

50. Wyckoff, J.M., Ziegler, B., Koch, H.W., and Uhlig, R., Phys. Rev. 137:B576 (1965)

51. Gell-Mann, M., and Telegdi, V.L., Phys. Rev. 91:169 (1953)

52. Überall, H., Suppl. Nuovo Cimento 4:781 (1966)

53. Goldhaber, M., and Teller, E., Phys. Rev. 74:1046 (1948)

54. Goldemberg, J., Torizuka, Y., Barber, W.C., and Walecka, J.D., Nucl. Phys. 43:242 (1963)

55. Wild, W., Bayr. Akad. Wiss. Math.-Naturw. Klasse 18:371 (1956)

56. Fallieros, S., Ferrell, R.A., and Pal, M.K., Nucl. Phys. 15:363 (1960)

57. Glassgold, A.E., Heckrotte, W., and Watson, K.M., Ann. Phys. (N.Y.) 6:1 (1959)

58. Raphael, R., Überall, H., and Werntz, C., Phys. Rev. 152:899 (1966)

59. Foldy, L.L., and Walecka, J.D., Nuovo Cimento 34:1026 (1964)

60. Wigner, E., Phys. Rev. 51:106 (1937)

61. deForest, T., Jr., Walecka, J.D., Vanpraet, G., and Barber, W.C., Phys. Lett. 16: 311 (1965)

62. Überall, H., Nuovo Cimento 41:25 (1966)

63. Gillet, V., and Vinh-Mau, N., Nucl. Phys. 54:321 (1964)

64. Drake, T.E., Hutcheon, R.M., Stobie, V.W., Beer, G.A., and Caplan, H.S., Phys. Rev. 163:947 (1967)

65. Vanpraet, G.J., Nucl. Phys. 74:219 (1965)

66. Drechsel, D., Seaborn, J.B., and Greiner, W., Phys. Rev. Letters 17:488 (1966)

67. Kamimura, M., Ikeda, K., and Arima, A., Nucl. Phys. A95:129 (1967)

68. Überall, H., Phys. Rev. Letters 17:1292 (1966); Kelly, F.J., and Überall, H., to be published

69. Spicer, B.M., and Eisenberg, J.M., Nucl. Phys. 63:520 (1965)

70. Steinwedel, H., and Jensen, J.H.D., Z. Naturforsch. 5a:413 (1950)

71. Bach, R., and Werntz, C., Bull. of the American Physical Society Ser. II, 13:100 (1968)

72. Lewis, F.H., Jr., and Walecka, J.D., Phys. Rev. 133:B849 (1964)

73. Danos, M., Nucl. Phys. 5:23 (1958)

74. Le Tourneux, J., Physics Letters 13:325 (1964)

75. Danos, M., and Greiner, W., Phys. Rev. 134:B284 (1964); 138:B1055 (1965)

76. Weber, H.J., Huber, M.G., and Greiner, W., Zeits. f. Physik 192:182 (1966); 192:223 (1966)

77. Bohr, A., and Mottelson, B.R., Kgl. Danske Vid. Selsk. Mat. Fys. Medd. 27, No. 16 (1953)

78. Preston, M.A., "Physics of the Nucleus," Reading, Mass.:Addison-Wesley, 1962, p. 235

79. Urbas, T., Thesis, Univ. Frankfurt, 1965; Urbas, T.D., and Greiner, W., Z. Physik 196:44 (1966)

80. Elliott, J.P., and Flowers, B.H., Proc. Roy. Soc. (London) A242:57 (1957)

81. Nilsson, S.G., Sawicki, J., and Glendenning, N.K., Nucl. Phys. 33:239 (1962)

82. Bassichis, W.H., and Scheck, F., Phys. Rev. 145:771 (1966)

83. Wilkinson, D.H., Physica 22:1039 (1956)

84. Brown, G.E., and Bolsterli, M., Phys. Rev. Letters 3:472 (1959)

85. Hayward, E., p. 141 in "Nuclear Structure and Electromagnetic Interactions," N. MacDonald, editor, Edinburgh and London:Oliver and Boyd, 1965

86. Gillet, V., Thesis, University of Paris, 1962

87. Burgov, N.A., Danilyan, G.V., Dolbilkin, B.S., Lazareva, L.E., and Nikolaev, F.A., Soviet Physics JETP 16:50 (1963)

88. deForest, T., Jr., Phys. Rev. 139:B1217 (1965)

89. Czyz, W., Lesniak, L., and Malecki, A., Ann. Phys. (N.Y.) 42:97 (1967)

90. Rose, M.E., p. 85 in "Perspectives in Modern Physics," R.E. Marshak, and J.W. Blaker, editors, New York:John Wiley-Interscience, 1966

91. Hill, L.L., and Überall, H., Phys. Letters 24B:364 (1967)

92. Hill, L.L., Phys. Letters 25B:169 (1967)

93. Hill, L.L., Naval Ordnance Laboratory Report NOLTR 67-88, 1967

94. Fagg, L.W., Naval Research Laboratory, private communication

95. Helm, R.H., Phys. Rev. 104:1466 (1956)

96. Crannell, H., Helm, R., Kendall, H., Oeser, J., and Yearian, M., Phys. Rev. 121:283 (1961)

97. Tassie, L.J., Austral. J. Phys. 9:407 (1956)

This page intentionally left blank.

Security Classification

DOCUMENT CONTROL DATA - R & D

(Security classification of title, body of abstract and indexing annotation must be entered when the overall report is classified)

1. ORIGINATING ACTIVITY (Corporate author) U.S. Naval Research Laboratory Washington, D.C. 20390	2a. REPORT SECURITY CLASSIFICATION Unclassified 2b. GROUP

3. REPORT TITLE

TOPICS IN ELECTRON SCATTERING AND NUCLEAR MODELS: NOTES ON LECTURES GIVEN AT NRL IN THE FALL OF 1966

4. DESCRIPTIVE NOTES (Type of report and inclusive dates)
Interim report on a continuing NRL Problem.

5. AUTHOR(S) (First name, middle initial, last name)
H. Überall (Consultant to NRL Linac Branch; permanent address is The Catholic University, Washington, D.C. 20017)

6. REPORT DATE July 31, 1968	7a. TOTAL NO. OF PAGES 81	7b. NO. OF REFS 97
8a. CONTRACT OR GRANT NO. NRL Problem H01-09 b. PROJECT NO. RR 002-06-41-5005 c. d.	9a. ORIGINATOR'S REPORT NUMBER(S) NRL Report 6729 9b. OTHER REPORT NO(S) (Any other numbers that may be assigned this report)	

10. DISTRIBUTION STATEMENT

This document has been approved for public release and sale; its distribution is unlimited.

11. SUPPLEMENTARY NOTES	12. SPONSORING MILITARY ACTIVITY Department of the Navy (Office of Naval Research), Washington, D.C. 20360

13. ABSTRACT

We present a review of the basic theory of electron scattering from nuclei and of photonuclear processes, as well as a discussion of the analysis of electron scattering experiments. This includes cross sections in Born approximation, elastic scattering from nuclei for the study of nuclear moments, and continuum scattering. Particular attention is given to inelastic electron scattering with excitation of nuclear levels, both below and in the giant resonance region. A variety of theoretical models is discussed that describe excitations of nuclear states.

DD FORM 1 NOV 65 1473 (PAGE 1)

S/N 0101-807-6801

Security Classification

Security Classification

14. KEY WORDS	LINK A ROLE	LINK A WT	LINK B ROLE	LINK B WT	LINK C ROLE	LINK C WT
Nuclear models						
Electron scattering						
Elastic						
Inelastic						
Photonuclear reactions						
Nuclear excited states						
Theory						
Review						

DD FORM 1 NOV 65 1473 (BACK)
(PAGE 2)

Security Classification